



**Politecnico
di Torino**

Politecnico di Torino

MASTER OF SCIENCE IN CIVIL ENGINEERING – STRUCTURES

A.Y. 2024/2025

GRADUATION PERIOD: MARCH 2025

Buckling resistance of laminated glass members in compression

Supervisors:

Prof. Mauro Corrado

Eng. Diogo Manuel Gonçalves Dias

Student:

Giammichele Gesualdi

ACKNOWLEDGMENTS

I would like to wholeheartedly thank my supervisors, Prof. *Mauro Corrado* and Eng. *Diogo Manuel Gonçalves Dias*, for their precious support and mentorship throughout the entire process of development of my master's thesis. Your interest and dedication in the subject of the thesis gave me one more reason to be more curious about the world of structural glass.

I am grateful to my mother, *Maria*, my father *Mario*, and my brother *Tiziano* for their constant and ongoing support at any stage of my life. Without your encouragement and care for me, I probably wouldn't have started and completed this long journey. I love you.

Thank you - *Lucia* and *Valerio* - for always being there for me, for the countless conversations, valuable insights and jokes. Thank you, *Michele*, for supporting me in this path morally and also literally, by welcoming into your home without any hesitation.

I would like to thank my uncles and cousins, for their interest and support they have shown me, for their words of wisdom, and for being a part of this journey.

To my classmates - *Noe, Samu, Ema, Fra, Carla and Lavi* - for sharing lots of joyful and light-hearted moments together, thank you. I couldn't have asked for anything better. It is really true that in life, it doesn't matter so much where you are going, but rather who travels next to you. Bukowski used to say that the human race has many weaknesses, among which the incapacity to arrive on time and to keep promises. I hope to be more punctual one day.

Thanks to my lifelong friends - *Fra, Anto, Juliet, Nadia, Leta and Fede* - we have known each other since we were kids, and I know I can always count on you. I will not promise you punctuality since, it is something which does not belong to (almost) any of us.

I wish to thank my housemates - *Fra, Carlo* - and *Chiara* for filling the house with happiness and serenity, for your companionship and your constant support over these years.

Thank you, *Virginia*, for your constant presence, your empathy ever since high school. Our friendship does not need constant confirmations, there is the certainty of always being there for each other.

Last but not least, I would also thank the great Loncar family - *Patricia, Daniela and Piero* - you welcomed me when I was a child, as if I were your own, and helped me realize that dance is a life lesson, based on passion, discipline, and pleasure. Thank you for all the love, encouragement, and indelible memories at the dance studio.

ABSTRACT

Glass is one of the oldest materials known to humankind, and currently, the demand for its use in the modern construction field is steadily increasing due to its aesthetic, design versatility and energy efficiency. With the advancement of scientific and technological knowledge about this material, glass has now the opportunity to be employed for structural elements, such as stairs, walls, façades, and even floors.

Since glass exhibits brittle behaviour, in view of enhancing its structural performance, certain specialized glass types are used, among which laminated glass. Laminated glass consists of a stack of glass panes held together by thermoplastic interlayers and the resultant laminated glass unit, as is the case for glass fins and columns, is typically very slender such that it could be subjected to buckling phenomena.

This thesis is aimed at investigating the buckling behaviour of laminated glass panels subjected to in-plane compressive loads by means of a parametric analysis, wherein different variables, among which, the interlayer shear modulus and geometrical parameters of the panes, have been included and varied in pre-established ranges. *2D* and *3D* models are built up in the commercial Finite Element (*FE*) software *LUSAS*, and eigenvalue buckling and geometric nonlinear analyses are carried out. In addition to that, some relevant features such as the effective thickness for calculating out-of-plane bending deflection and bending stress, and the initial geometric imperfection of the panels are considered in the development of numerical models, in compliance with the Technical Specifications for glass structures *CEN/TS 19100:2021*.

The critical buckling loads and critical buckling stresses coming from parametric analyses are analysed to understand the buckling response of slender laminated glass elements. Also, the dependency on the slenderness ratio and on the stiffness of the interlayer are investigated.

It was found that *2D* models, having effective thickness for bending deflection and characterised by geometric nonlinearity, provide critical buckling loads which are lower than those of *2D*, having no initial imperfections. *3D* models, representing laminated glass by way of the real thickness of each layer, show buckling loads that are in between those of *2D*, with and without initial imperfections, for low values of slenderness ratio. Conversely, for large slenderness values, nonlinear analyses on *3D* models provide buckling loads similar to those provided by *2D* models with initial imperfections. To achieve more accurate results, by limiting transversal displacements and considering the effective thickness for bending stress, additional nonlinear analyses are performed on *2D* models with initial imperfections, resulting in the lowest buckling loads compared to all the others.

Lastly, *FE*-models show that critical buckling load in laminated glass elements strongly depends on the interlayer shear modulus, whose value must be carefully chosen during the design process.

KEYWORDS: Laminated glass, Buckling, Glass columns, Equivalent thickness, Finite Element Method, Parametric analysis, Geometric nonlinear analysis.

TABLE OF CONTENTS

ACKNOWLEDGMENTS	III
ABSTRACT	V
INDEX OF FIGURES	XI
INDEX OF TABLES	XIII
SYMBOLS, ACRONYMS AND ABBREVIATIONS	XVII
1 INTRODUCTION	1
1.1 PREFACE	1
1.2 OBJECTIVE AND METHODOLOGY	1
1.3 OVERVIEW	1
2 LITERATURE REVIEW	3
2.1 INTRODUCTION	3
2.2 HISTORY AND ARCHITECTURAL CONTEXT	3
2.3 GLASS PROPERTIES	10
2.4 GLASS BEHAVIOUR	12
2.5 FLOAT GLASS PRODUCTION PROCESS	13
2.6 GLASS TYPES	14
2.6.1 ANNEALED GLASS	14
2.6.2 HEAT STRENGTHENED GLASS	14
2.6.3 FULLY TEMPERED GLASS	15
2.6.4 CHEMICALLY TOUGHENED GLASS	16
2.7 LAMINATED GLASS	17
2.7.1 TYPOLOGY AND PROPERTIES OF POLYMERIC INTERLAYERS	18
2.7.2 STRUCTURAL BEHAVIOUR OF LAMINATED GLASS	19
2.8 MATERIAL PROPERTIES	20
2.9 GLASS STANDARDS	21
2.10 GLOBAL INSTABILITY OF IN-PLANE LOADED SLENDER ELEMENTS: FLEXURAL BUCKLING PHENOMENA	22
2.10.1 EULER'S BUCKLING THEORY	23
3 GLASS DESIGN AND BUCKLING CALCULATION	26
3.1 DESIGN BENDING STRENGTH OF GLASS	26
3.2 ENHANCED EFFECTIVE THICKNESS THEORY	26

3.3	BUCKLING LOAD FOR LAMINATED GLASS	28
------------	--	-----------

4	SECOND-ORDER THEORY AND BUCKLING ANALYSIS	30
----------	--	-----------

4.1	EFFECT OF INITIAL IMPERFECTIONS	30
4.2	GEOMETRIC NONLINEARITY	31
4.3	LINEAR BUCKLING ANALYSIS (LBA)	31
4.4	GEOMETRICALLY NONLINEAR BUCKLING ANALYSIS (GNA)	33
4.4.1	GEOMETRICALLY NONLINEAR PROBLEM IN MONOLITHIC GLASS	34
4.4.2	GEOMETRICALLY NONLINEAR ANALYSIS IN FEA	35

5	METHODOLOGY	37
----------	--------------------	-----------

5.1	BASICS OF FINITE ELEMENT METHOD (FEM)	37
5.2	2D FINITE ELEMENT MODELS	38
5.2.1	2D MODELS: ELEMENT TYPES	38
5.2.2	GEOMETRIC CHARACTERISTICS OF FLAT AND CURVED 2D MODELS	39
5.2.3	EFFECTIVE THICKNESS CALCULATION FOR FLAT AND CURVED 2D MODELS	40
5.2.4	2D MODELS: MATERIAL PARAMETERS	40
5.2.5	MESHING PROCESS	41
5.2.6	BOUNDARY CONDITIONS AND LOADING	42
5.2.7	OVERVIEW OF 2D FLAT MODELS	43
5.2.8	2D CURVED MODELS: INITIAL GEOMETRIC IMPERFECTION	44
5.2.9	OVERVIEW OF 2D CURVED MODELS	45
5.3	3D+SHELL FINITE ELEMENT MODELS	47
5.3.1	3D+SHELL MODEL: ELEMENT TYPES	47
5.3.2	GEOMETRIC CHARACTERISTICS OF 3D+SHELL MODELS	47
5.3.3	MESHING PROCESS	49
5.3.4	3D+SHELL MODELS: INITIAL GEOMETRIC IMPERFECTIONS	50
5.3.5	3D+SHELL MODELS: BOUNDARY CONDITIONS AND LOADING	51
5.3.6	3D MODELS: MATERIAL PARAMETERS	52
5.3.7	OVERVIEW OF 3D MODELS	53

6	RESULTS AND DISCUSSION	55
----------	-------------------------------	-----------

6.1	OVERVIEW OF NUMERICAL ANALYSIS	55
6.1.1	SOLUTION STRATEGIES	55
6.1.2	2D AND 3D MODELS: DETAILING ON ANALYSIS RESULTS	56
6.1.3	INTRODUCTION TO BUCKLING CURVES	56
6.2	EFFECT OF SLENDERNESS RATIO ON CRITICAL BUCKLING STRESS (1ST SOLUTION STRATEGY)	58
6.3	EFFECT OF SHEAR MODULUS ON CRITICAL BUCKLING LOAD	61
6.4	2D CURVED MODELS: GEOMETRICALLY NONLINEAR BUCKLING ANALYSIS RESULTS (2ND SOLUTION STRATEGY)	64
6.4.1	EFFECT OF SLENDERNESS RATIO ON CRITICAL BUCKLING STRESS (2 ND SOLUTION STRATEGY)	65
6.5	BUCKLING LOAD -DISPLACEMENT CURVES	68
6.6	DESIGN BUCKLING CURVES FOR IN-PLANE COMPRESSED LG PANELS	69

6.7	DESIGN BUCKLING CURVES FOR IN-PLANE COMPRESSED LG PANELS BASED ON EUROCODE APPROACH	71
6.7.1	PRACTICAL IMPLEMENTATION OF EC-BASED DESIGN BUCKLING CURVE FOR LAMINATED GLASS	76
7	FINAL CONCLUSIONS	79
7.1	GENERAL CONCLUSIONS	79
7.2	LIMITATIONS OF THE WORK	80
7.3	FUTURE DEVELOPMENTS	80
	REFERENCES	81
	ANNEXES	85
A.	DESIGN BENDING STRENGTH OF GLASS: FACTORS	87
B.	COUPLING PARAMETER FOR BEAMS	91
C.	2D FLAT AND CURVED MODELS: EFFECTIVE THICKNESS FOR OUT-OF-PLANE BENDING DEFLECTION	92
D.	2D (1ST SOLUTION STRATEGY) AND 3D MODELS: NUMERICAL RESULTS	96
E.	2D-FE CURVED MODELS: PRELIMINARY CALCULATIONS AND NUMERICAL RESULTS (2ND SOLUTION STRATEGY)	111
F.	DESIGN BUCKLING CURVES BASED ON EC3: CALCULATIONS	124

INDEX OF FIGURES

FIGURE 2-1: CORE-FORMING TECHNIQUE	4
FIGURE 2-2: CASTING TECHNIQUE	4
FIGURE 2-3: GLASSBLOWING TECHNIQUE	4
FIGURE 2-4: CHARTRES' BELLE-VERRIÈRE, EXAMPLE OF STAINED-GLASS WINDOW IN NOTRE-DAME DE CHARTRES CATHEDRAL	5
FIGURE 2-5: ON THE LEFT THE CYLINDER PROCESS AND ON THE RIGHT THE PLATE PROCESS	6
FIGURE 2-6: ILLUSTRATION OF THE TRANSEPT OF THE CRYSTAL PALACE ON THE LEFT AND THE EXTERIOR OF THE CRYSTAL PALACE AT SYDENHAM IN 1854 ON THE RIGHT '	7
FIGURE 2-7: EXTERIOR OF THE NEUE NATIONALGALERIE IN BERLIN	8
FIGURE 2-8: DETAILS OF THE GLASS FAÇADE AND THE SUSPENDED ROOF OF THE NEUE NATIONALGALERIE	9
FIGURE 2-9: THE HANGZHOU'S APPLE STORE. ON THE LEFT, THE FAÇADE AND ON THE RIGHT THE "FLOATING" GLASS STAIRCASE	9
FIGURE 2-10: IRREGULAR CRYSTAL LATTICE OF SODA LIME SILICA GLASS	10
FIGURE 2-11: COMPARISON BETWEEN STEEL AND GLASS CONSTITUTIVE LAWS	12
FIGURE 2-12: GLASS PRODUCTION PROCESSES, TREATMENTS AND CORRESPONDING FINAL PRODUCTS	13
FIGURE 2-13: MAIN STAGES OF THE FLOAT PROCESS	13
FIGURE 2-14: RESIDUAL STRESS PROFILE THROUGH THE THICKNESS OF HEAT STRENGTHENED GLASS	15
FIGURE 2-15: COMPARISON OF THE FRACTURE PATTERN FOR DIFFERENT GLASS TYPES: ON THE LEFT ANNEALED GLASS, IN THE MIDDLE HEAT STRENGTHENED GLASS AND, ON THE RIGHT, FULLY TEMPERED GLASS	15
FIGURE 2-16: STRESS DISTRIBUTION IN FULLY TEMPERED GLASS	16
FIGURE 2-17: COMPARISON BETWEEN THERMAL TEMPERING STRESSES AND CHEMICAL TEMPERING ONE	17
FIGURE 2-18: CROSS SECTION OF LAMINATED GLASS	17
FIGURE 2-19: SHEAR MODULUS VARIATION AS FUNCTION OF THE LOAD DURATION FOR PVB (BUTACITE®) AND IONOPLAST (SENTRYGLAS®) INTERLAYERS	19
FIGURE 2-20: STRESS PROFILE DUE TO BENDING STRESSES IN CASE OF MONOLITHIC LIMIT	19
FIGURE 2-21: STRESS PROFILE DUE TO BENDING STRESSES IN CASE OF LAYERED LIMIT	20
FIGURE 2-22: STRESS PROFILE DUE TO BENDING STRESSES IN CASE OF PARTIAL COMPOSITE EFFECT	20
FIGURE 2-23: GENERAL VIEW OF CURRENT EUROPEAN STANDARDS RELATED TO GLASS IN BUILDINGS	22
FIGURE 2-24: BEHAVIOUR OF PERFECT AND IMPERFECT MEMBERS UNDER COMPRESSIVE LOADS. BASED ON [34].	23
FIGURE 2-25: NON-LINEAR BEHAVIOUR OF A REAL MEMBER IN COMPRESSION (SOLID CURVE)	23
FIGURE 2-26: FREE LENGTH OF DEFLECTION FOR DIFFERENT STATIC SCHEMES	24
FIGURE 2-27: EULER'S BUCKLING CURVE AND FAILURE ZONES	25
FIGURE 2-28: BUCKLING BEHAVIOUR OF IMPERFECT MEMBERS	25
FIGURE 3-1: GEOMETRICAL PARAMETERS OF A LAMINATED GLASS CROSS-SECTION	27
FIGURE 3-2: BUCKLING LENGTH OF A SIMPLY SUPPORTED GLASS ELEMENT IN COMPRESSION	28
FIGURE 3-3: GEOMETRICAL PARAMETERS OF A DOUBLE-LAYERED LAMINATED GLASS CROSS-SECTION	29
FIGURE 4-1: TYPES OF INITIAL IMPERFECTIONS AFFECTING GLASS ELEMENTS	30
FIGURE 4-2: LINEAR VS NONLINEAR BUCKLING	33
FIGURE 4-3: SECOND ORDER BENDING MOMENTS IN A COMPRESSED CANTILEVER BEAM	33
FIGURE 4-4: SIMPLY SUPPORTED COLUMN WITH INITIAL IMPERFECTION AND SUBJECTED TO COMPRESSIVE FORCE	34
FIGURE 4-5: NEWTON-RAPHSON ITERATION METHOD	36
FIGURE 5-1: MESHING PROCESS OF A FINITE ELEMENT MODEL	37
FIGURE 5-2: SEMILOOF CURVED THIN SHELL ELEMENTS (QSL8).....	38
FIGURE 5-3: DIFFERENT ARRANGEMENT OF LAMINATED GLASS UNITS UNDER ANALYSIS. FROM THE LEFT TO THE RIGHT: CASE A, B AND C ...	39
FIGURE 5-4: MESH (0,1M X 0,13M) OF A 4-METER LENGTH 2D MODEL.....	41
FIGURE 5-5: SIMPLY SUPPORTED BOUNDARY CONDITIONS ALONG THE SHORTER EDGE ON WHICH THE COMPRESSIVE LOAD IS APPLIED.....	42
FIGURE 5-6: SIMPLY SUPPORTED BOUNDARY CONDITIONS ALONG THE OPPOSITE SHORTER EDGE.	42
FIGURE 5-7: APPLIED COMPRESSIVE LOAD $P_0 = 5 \text{ kN/M}$	43
FIGURE 5-8: 2D FLAT MODEL HAVING LENGTH $L_b = 2\text{M}$ (CASE C).	43
FIGURE 5-9: 2D FLAT MODEL HAVING LENGTH $L_b = 4\text{M}$ (CASE C).	43
FIGURE 5-10: 2D FLAT MODEL HAVING LENGTH $L_b = 6\text{M}$ (CASE C).	44

FIGURE 5-11: 2D FLAT MODEL HAVING LENGTH $L_B = 8M$ (CASE C).	44
FIGURE 5-12: 2D CURVED MODEL HAVING LENGTH $L_B = 2M$ (CASE B $E_0 = 14,10$ MM).	45
FIGURE 5-13: 2D CURVED MODEL HAVING LENGTH $L_B = 4M$ (CASE B $E_0 = 17,52$ MM).	46
FIGURE 5-14: 2D CURVED MODEL HAVING LENGTH $L_B = 6M$ (CASE B $E_0 = 22,08$ MM).	46
FIGURE 5-15: 2D CURVED MODEL HAVING LENGTH $L_B = 8M$ (CASE B $E_0 = 27,20$ MM).	46
FIGURE 5-16: 3D SOLID CONTINUUM ELEMENT WITH ENHANCED STRAINS (HXM8).	47
FIGURE 5-17: CROSS-SECTION OF 3D+SHELL MODELS.	48
FIGURE 5-18: ASSIGNMENT OF THE ECCENTRICITY TO THE TOP GLASS PLY ON THE LEFT AND TO THE BOTTOM PLY ON THE RIGHT, FOR CASE A. (UNITS OF MEASUREMENT ARE IN METERS IN THIS FIGURE).....	48
FIGURE 5-19: "VERTICAL" PLATES LOCATED AT THE SHORTER EDGES OF THE MODEL.....	49
FIGURE 5-20: THICKNESS OF VERTICAL PLATES FOR CASE A. (UNITS OF MEASUREMENT ARE IN METERS IN THIS FIGURE).	49
FIGURE 5-21: SIMPLY SUPPORTED BOUNDARY CONDITIONS ALONG THE SHORTER EDGE, ON WHICH THE COMPRESSIVE LOAD IS APPLIED.	51
FIGURE 5-22: SYMMETRY BOUNDARY CONDITIONS (SLIDER) ALONG THE OPPOSITE SHORTER EDGE.	52
FIGURE 5-23: APPLIED COMPRESSIVE LOADS $P_{0,1} = P_{0,2} = 2,5$ kN/M ON 3D MODELS.	52
FIGURE 5-24: 3D MODEL HAVING LENGTH $L_B = 2M$ (CASE A $E_0 = 12,32$ MM).	53
FIGURE 5-25: 3D MODEL HAVING LENGTH $L_B = 4M$ (CASE A $E_0 = 16,13$ MM).	53
FIGURE 5-26: 3D MODEL HAVING LENGTH $L_B = 6M$ (CASE A $E_0 = 20,99$ MM).	54
FIGURE 5-27: 3D MODEL HAVING LENGTH $L_B = 8M$ (CASE A $E_0 = 26,32$ MM).	54
FIGURE 6-1: BUCKLING CURVES FOR CASE STUDY A (1 ST SOLUTION STRATEGY).	58
FIGURE 6-2: BUCKLING CURVES FOR CASE STUDY B (1 ST SOLUTION STRATEGY).	59
FIGURE 6-3: BUCKLING CURVES FOR CASE STUDY C (1 ST SOLUTION STRATEGY).....	60
FIGURE 6-4: EFFECT OF SHEAR MODULUS G ON THE CRITICAL BUCKLING LOAD $N_{cr,FEA}$ (CASE A).	61
FIGURE 6-5: EFFECT OF SHEAR MODULUS G ON THE CRITICAL BUCKLING LOAD $N_{cr,FEA}$ (CASE B).....	62
FIGURE 6-6: EFFECT OF SHEAR MODULUS G ON THE CRITICAL BUCKLING LOAD $N_{cr,FEA}$ (CASE C).....	63
FIGURE 6-7: BUCKLING CURVES FOR CASE STUDY A (2 ND SOLUTION STRATEGY).....	65
FIGURE 6-8: BUCKLING CURVES FOR CASE STUDY B (2 ND SOLUTION STRATEGY).....	66
FIGURE 6-9: BUCKLING CURVES FOR CASE STUDY C (2 ND SOLUTION STRATEGY).....	67
FIGURE 6-10: BUCKLING LOAD VS DISPLACEMENT CURVES FOR DIFFERENT LENGTHS L_B (CASE A).....	68
FIGURE 6-11: DESIGN BUCKLING CURVES FOR IN-PLANE LOADED LG ELEMENTS	70
FIGURE 6-12: DESIGN BUCKLING CURVES FOR IN-PLANE LOADED LG ELEMENTS IN BI-LOGARITHMIC SCALE	70
FIGURE 6-13: DESIGN BUCKLING CURVES BASED ON EUROCODE FOR ANNEALED GLASS (ANG).	73
FIGURE 6-14: DESIGN BUCKLING CURVES BASED ON EUROCODE FOR FULLY TEMPERED GLASS (FTG).	74
FIGURE 6-15: DESIGN BUCKLING CURVES BASED ON EUROCODE FOR HEAT STRENGTHENED GLASS (HSG).	75
FIGURE 6-16: FINAL EUROCODE-BASED DESIGN BUCKLING CURVE FOR LAMINATED GLASS MEMBERS IN COMPRESSION	75
FIGURE 6-17: PRACTICAL IMPLEMENTATION OF EC-BASED DESIGN BUCKLING CURVE FOR GLASS.....	77
FIGURE B-1: COUPLING PARAMETER FOR BEAMS Ψ_B FOR DIFFERENT LOADING AND BOUNDARY CONDITIONS.	91

INDEX OF TABLES

TABLE 2-1: CHEMICAL COMPOSITION OF SODA LIME SILICA GLASS AND BOROSILICATE GLASS	10
TABLE 2-2: VISCOSITY OF GLASS AT DIFFERENT STATES AND RESPECTIVE TEMPERATURES FOR SLSG AND BSG	11
TABLE 2-3: SLSG AND BSG PHYSICAL PROPERTIES	11
TABLE 2-4: PHYSICAL PROPERTIES OF PVB INTERLAYER	18
TABLE 2-5: PHYSICAL AND MECHANICAL PROPERTIES OF SODA LIME SILICATE GLASS	20
TABLE 2-6: CHARACTERISTIC STRENGTH OF DIFFERENT GLASS TYPES	21
TABLE 3-1: PARAMETERS NECESSARY TO COMPUTE THE EFFECTIVE MOMENT OF INERTIA $I_{z,EFF}$	29
TABLE 4-1: CALCULATION OF BASIC IMPERFECTION PARAMETER E_0	31
TABLE 4-2: BUCKLING VERIFICATION.	35
TABLE 5-1: DIFFERENT THICKNESSES OF LAMINATED GLASS PLIES UNDER CONSIDERATION IN MODELLING STAGE.....	39
TABLE 5-2: MATERIAL PROPERTIES OF ANNEALED GLASS FOR 2D-FE MODELS.....	40
TABLE 5-3: MATERIAL PROPERTIES OF PVB FOR 2D-FE MODELS.	40
TABLE 5-4: MESH SIZE SELECTED FOR EACH 2D MODEL.....	41
TABLE 5-5: BOUNDARY CONDITIONS FOR 2D MODELS.	42
TABLE 5-6: BASIC IMPERFECTION E_0 FOR CASE A.....	44
TABLE 5-7: BASIC IMPERFECTION E_0 FOR CASE B.....	45
TABLE 5-8: BASIC IMPERFECTION E_0 FOR CASE C.....	45
TABLE 5-9: DIFFERENT THICKNESSES OF GLASS PLIES TO BE CONSIDERED IN MODELLING PROCESS.	48
TABLE 5-10: MESH SIZE FOR EACH ELEMENT CONSTITUTING 3D+SHELL MODELS.....	50
TABLE 5-11: BASIC IMPERFECTION E_0 FOR CASE A.....	50
TABLE 5-12: BASIC IMPERFECTION E_0 FOR CASE B.....	51
TABLE 5-13: BASIC IMPERFECTION E_0 FOR CASE C.....	51
TABLE 5-14: BOUNDARY CONDITIONS FOR 3D MODELS.	52
TABLE 5-15: GLASS PARAMETERS USED IN 3D MODELS.....	53
TABLE 5-16: PVB PARAMETERS USED IN 3D MODELS.....	53
TABLE 6-1: CALCULATION OF THE SLENDERNESS RATIO OF EACH LAMINATED GLASS PANEL (CASE A).	57
TABLE 6-2: CALCULATION OF THE SLENDERNESS RATIO OF EACH LAMINATED GLASS PANEL (CASE B).....	57
TABLE 6-3: CALCULATION OF THE SLENDERNESS RATIO OF EACH LAMINATED GLASS PANEL (CASE C).....	57
TABLE A-1: VALUES FOR EDGE OR HOLE FINISHING FACTOR FOR VERIFICATIONS NEAR EDGES AND HOLES UNDER TENSION.	87
TABLE A-2: VALUES FOR SURFACE PROFILE FACTOR FOR VARIOUS SURFACE CONDITIONS.....	87
TABLE A-3: VALUES FOR MODIFICATION FACTOR FOR ANNEALED GLASS.	88
TABLE A-4: VALUES FOR PRE-STRESSING PROCESS FACTOR.	89
TABLE A-5: VALUES FOR THE EDGE PRE-STRESSING FACTOR FOR VERIFICATIONS NEAR EDGES AND HOLES UNDER TENSION.....	89
TABLE A-6: CLASS OF CONSEQUENCES: DESCRIPTION AND EXAMPLES.....	90
TABLE A-7: PARTIAL SAFETY FACTORS Γ_M AND Γ_P FOR GLASS.....	90
TABLE C-1: EFFECTIVE THICKNESS FOR BENDING DEFLECTION FOR $G = 0,01$ MPA (CASE A).	92
TABLE C-2: EFFECTIVE THICKNESS FOR BENDING DEFLECTION FOR $G = 0,1$ MPA (CASE A).	92
TABLE C-3: EFFECTIVE THICKNESS FOR BENDING DEFLECTION FOR $G = 1$ MPA (CASE A).	92
TABLE C-4: EFFECTIVE THICKNESS FOR BENDING DEFLECTION FOR $G = 10$ MPA (CASE A).	93
TABLE C-5: EFFECTIVE THICKNESS FOR BENDING DEFLECTION FOR $G = 0,01$ MPA (CASE B).	93
TABLE C-6: EFFECTIVE THICKNESS FOR BENDING DEFLECTION FOR $G = 0,1$ MPA (CASE B).	93
TABLE C-7: EFFECTIVE THICKNESS FOR BENDING DEFLECTION FOR $G = 1$ MPA (CASE B).	94
TABLE C-8: EFFECTIVE THICKNESS FOR BENDING DEFLECTION FOR $G = 10$ MPA (CASE B).	94
TABLE C-9: EFFECTIVE THICKNESS FOR BENDING DEFLECTION FOR $G = 0,01$ MPA (CASE C).	94
TABLE C-10: EFFECTIVE THICKNESS FOR BENDING DEFLECTION FOR $G = 0,1$ MPA (CASE C).	95
TABLE C-11: EFFECTIVE THICKNESS FOR BENDING DEFLECTION FOR $G = 1$ MPA (CASE C).	95
TABLE C-12: EFFECTIVE THICKNESS FOR BENDING DEFLECTION FOR $G = 10$ MPA (CASE C).	95
TABLE D-1: CRITICAL BUCKLING LOADS AND STRESSES FOR 2D FLAT MODELS WITH $G = 0,01$ MPA (CASE A – 1 ST SOLUTION STRATEGY).	96
TABLE D-2: CRITICAL BUCKLING LOADS AND STRESSES FOR 2D FLAT MODELS WITH $G = 0,1$ MPA (CASE A – 1 ST SOLUTION STRATEGY).	96

TABLE D-3: CRITICAL BUCKLING LOADS AND STRESSES FOR 2D FLAT MODELS WITH $G = 1$ MPa (CASE A – 1 ST SOLUTION STRATEGY).....	97
TABLE D-4: CRITICAL BUCKLING LOADS AND STRESSES FOR 2D FLAT MODELS WITH $G = 10$ MPa (CASE A – 1 ST SOLUTION STRATEGY).....	97
TABLE D-5: CRITICAL BUCKLING LOADS AND STRESSES FOR 2D FLAT MODELS WITH $G = 0,01$ MPa (CASE B – 1 ST SOLUTION STRATEGY).....	97
TABLE D-6: CRITICAL BUCKLING LOADS AND STRESSES FOR 2D FLAT MODELS WITH $G = 0,1$ MPa (CASE B – 1 ST SOLUTION STRATEGY).....	98
TABLE D-7: CRITICAL BUCKLING LOADS AND STRESSES FOR 2D FLAT MODELS WITH $G = 1$ MPa (CASE B – 1 ST SOLUTION STRATEGY).....	98
TABLE D-8: CRITICAL BUCKLING LOADS AND STRESSES FOR 2D FLAT MODELS WITH $G = 10$ MPa (CASE B – 1 ST SOLUTION).....	98
TABLE D-9: CRITICAL BUCKLING LOADS AND STRESSES FOR 2D FLAT MODELS WITH $G = 0,01$ MPa (CASE C – 1 ST SOLUTION STRATEGY).....	99
TABLE D-10: CRITICAL BUCKLING LOADS AND STRESSES FOR 2D FLAT MODELS WITH $G = 0,1$ MPa (CASE C – 1 ST SOLUTION STRATEGY).....	99
TABLE D-11: CRITICAL BUCKLING LOADS AND STRESSES FOR 2D FLAT MODELS WITH $G = 1$ MPa (CASE C – 1 ST SOLUTION STRATEGY).....	99
TABLE D-12: CRITICAL BUCKLING LOADS AND STRESSES FOR 2D FLAT MODELS WITH $G = 10$ MPa (CASE C – 1 ST SOLUTION STRATEGY).....	100
TABLE D-13: CRITICAL BUCKLING LOADS AND STRESSES FOR 2D CURVED MODELS WITH $G = 0,01$ MPa (CASE A – 1 ST SOLUTION STRATEGY).....	100
TABLE D-14: CRITICAL BUCKLING LOADS AND STRESSES FOR 2D CURVED MODELS WITH $G = 0,1$ MPa (CASE A – 1 ST SOLUTION STRATEGY).....	100
TABLE D-15: CRITICAL BUCKLING LOADS AND STRESSES FOR 2D CURVED MODELS WITH $G = 1$ MPa (CASE A – 1 ST SOLUTION STRATEGY).....	101
TABLE D-16: CRITICAL BUCKLING LOADS AND STRESSES FOR 2D CURVED MODELS WITH $G = 10$ MPa (CASE A – 1 ST SOLUTION STRATEGY).....	101
TABLE D-17: CRITICAL BUCKLING LOADS AND STRESSES FOR 2D CURVED MODELS WITH $G = 0,01$ MPa (CASE B – 1 ST SOLUTION STRATEGY).....	101
TABLE D-18: CRITICAL BUCKLING LOADS AND STRESSES FOR 2D CURVED MODELS WITH $G = 0,1$ MPa (CASE B – 1 ST SOLUTION STRATEGY).....	102
TABLE D-19: CRITICAL BUCKLING LOADS AND STRESSES FOR 2D CURVED MODELS WITH $G = 1$ MPa (CASE B – 1 ST SOLUTION STRATEGY).....	102
TABLE D-20: CRITICAL BUCKLING LOADS AND STRESSES FOR 2D CURVED MODELS WITH $G = 10$ MPa (CASE B – 1 ST SOLUTION STRATEGY).....	102
TABLE D-21: CRITICAL BUCKLING LOADS AND STRESSES FOR 2D CURVED MODELS WITH $G = 0,01$ MPa (CASE C – 1 ST SOLUTION STRATEGY).....	103
TABLE D-22: CRITICAL BUCKLING LOADS AND STRESSES FOR 2D CURVED MODELS WITH $G = 0,1$ MPa (CASE C – 1 ST SOLUTION STRATEGY).....	103
TABLE D-23: CRITICAL BUCKLING LOADS AND STRESSES FOR 2D CURVED MODELS WITH $G = 1$ MPa (CASE C – 1 ST SOLUTION STRATEGY).....	103
TABLE D-24: CRITICAL BUCKLING LOADS AND STRESSES FOR 2D CURVED MODELS WITH $G = 10$ MPa (CASE C – 1 ST SOLUTION STRATEGY).....	104
TABLE D-25: CRITICAL BUCKLING LOADS AND STRESSES FOR 3D MODELS WITH $G = 0,01$ MPa (CASE A).....	104
TABLE D-26: CRITICAL BUCKLING LOADS AND STRESSES FOR 3D MODELS WITH $G = 0,1$ MPa (CASE A).....	105
TABLE D-27: CRITICAL BUCKLING LOADS AND STRESSES FOR 3D MODELS WITH $G = 1$ MPa (CASE A).....	105
TABLE D-28: CRITICAL BUCKLING LOADS AND STRESSES FOR 3D MODELS WITH $G = 10$ MPa (CASE A).....	106
TABLE D-29: CRITICAL BUCKLING LOADS AND STRESSES FOR 3D MODELS WITH $G = 0,01$ MPa (CASE B).....	106
TABLE D-30: CRITICAL BUCKLING LOADS AND STRESSES FOR 3D MODELS WITH $G = 0,1$ MPa (CASE B).....	107
TABLE D-31: CRITICAL BUCKLING LOADS AND STRESSES FOR 3D MODELS WITH $G = 1$ MPa (CASE B).....	107
TABLE D-32: CRITICAL BUCKLING LOADS AND STRESSES FOR 3D MODELS WITH $G = 10$ MPa (CASE B).....	108
TABLE D-33: CRITICAL BUCKLING LOADS AND STRESSES FOR 3D MODELS WITH $G = 0,01$ MPa (CASE C).....	108
TABLE D-34: CRITICAL BUCKLING LOADS AND STRESSES FOR 3D MODELS WITH $G = 0,1$ MPa (CASE C).....	109
TABLE D-35: CRITICAL BUCKLING LOADS AND STRESSES FOR 3D MODELS WITH $G = 1$ MPa (CASE C).....	109
TABLE D-36: CRITICAL BUCKLING LOADS AND STRESSES FOR 3D MODELS WITH $G = 10$ MPa (CASE C).....	110
TABLE E-1: SECTION MODULUS AND EFFECTIVE THICKNESS FOR BENDING STRESS FOR 2D CURVED MODELS WITH $G = 0,01$ MPa (CASE A).....	111
TABLE E-2: SECTION MODULUS AND EFFECTIVE THICKNESS FOR BENDING STRESS FOR 2D CURVED MODELS WITH $G = 0,1$ MPa (CASE A).....	111
TABLE E-3: SECTION MODULUS AND EFFECTIVE THICKNESS FOR BENDING STRESS FOR 2D CURVED MODELS WITH $G = 1$ MPa (CASE A).....	112
TABLE E-4: SECTION MODULUS AND EFFECTIVE THICKNESS FOR BENDING STRESS FOR 2D CURVED MODELS WITH $G = 10$ MPa (CASE A).....	112
TABLE E-5: CALCULATION OF TRUE BUCKLING STRESS FOR 2D CURVED MODELS WITH $G = 0,01$ MPa (CASE A).....	113
TABLE E-6: CALCULATION OF TRUE BUCKLING STRESS FOR 2D CURVED MODELS WITH $G = 0,1$ MPa (CASE A).....	113
TABLE E-7: CALCULATION OF TRUE BUCKLING STRESS FOR 2D CURVED MODELS WITH $G = 1$ MPa (CASE A).....	113
TABLE E-8: CALCULATION OF TRUE BUCKLING STRESS FOR 2D CURVED MODELS WITH $G = 10$ MPa (CASE A).....	114
TABLE E-9: CRITICAL BUCKLING LOADS AND STRESSES FOR 2D CURVED MODELS WITH $G = 0,01$ MPa (CASE A – 2 ND SOLUTION STRATEGY).....	114

TABLE E-10: CRITICAL BUCKLING LOADS AND STRESSES FOR 2D CURVED MODELS WITH $G = 0,1$ MPA (CASE A – 2 ND SOLUTION STRATEGY).	114
TABLE E-11: CRITICAL BUCKLING LOADS AND STRESSES FOR 2D CURVED MODELS WITH $G = 1$ MPA (CASE A – 2 ND SOLUTION STRATEGY).	115
TABLE E-12: CRITICAL BUCKLING LOADS AND STRESSES FOR 2D CURVED MODELS WITH $G = 10$ MPA (CASE A – 2 ND SOLUTION STRATEGY).	115
TABLE E-13: SECTION MODULUS AND EFFECTIVE THICKNESS FOR BENDING STRESS FOR 2D CURVED MODELS WITH $G = 0,01$ MPA (CASE B).	115
TABLE E-14: SECTION MODULUS AND EFFECTIVE THICKNESS FOR BENDING STRESS FOR 2D CURVED MODELS WITH $G = 0,1$ MPA (CASE B).	116
TABLE E-15: SECTION MODULUS AND EFFECTIVE THICKNESS FOR BENDING STRESS FOR 2D CURVED MODELS WITH $G = 1$ MPA (CASE B).	116
TABLE E-16: SECTION MODULUS AND EFFECTIVE THICKNESS FOR BENDING STRESS FOR 2D CURVED MODELS WITH $G = 10$ MPA (CASE B).	116
TABLE E-17: CALCULATION OF TRUE BUCKLING STRESS FOR 2D CURVED MODELS WITH $G = 0,01$ MPA (CASE B).	117
TABLE E-18: CALCULATION OF TRUE BUCKLING STRESS FOR 2D CURVED MODELS WITH $G = 0,1$ MPA (CASE B).	117
TABLE E-19: CALCULATION OF TRUE BUCKLING STRESS FOR 2D CURVED MODELS WITH $G = 1$ MPA (CASE B).	117
TABLE E-20: CALCULATION OF TRUE BUCKLING STRESS FOR 2D CURVED MODELS WITH $G = 10$ MPA (CASE B).	118
TABLE E-21: CRITICAL BUCKLING LOADS AND STRESSES FOR 2D CURVED MODELS WITH $G = 0,01$ MPA (CASE B – 2 ND SOLUTION STRATEGY).	118
TABLE E-22: CRITICAL BUCKLING LOADS AND STRESSES FOR 2D CURVED MODELS WITH $G = 0,1$ MPA (CASE B – 2 ND SOLUTION STRATEGY).	118
TABLE E-23: CRITICAL BUCKLING LOADS AND STRESSES FOR 2D CURVED MODELS WITH $G = 1$ MPA (CASE B – 2 ND SOLUTION STRATEGY).	119
TABLE E-24: CRITICAL BUCKLING LOADS AND STRESSES FOR 2D CURVED MODELS WITH $G = 10$ MPA (CASE B – 2 ND SOLUTION STRATEGY).	119
TABLE E-25: SECTION MODULUS AND EFFECTIVE THICKNESS FOR BENDING STRESS FOR 2D CURVED MODELS WITH $G = 0,01$ MPA (CASE C).	119
TABLE E-26: SECTION MODULUS AND EFFECTIVE THICKNESS FOR BENDING STRESS FOR 2D CURVED MODELS WITH $G = 0,1$ MPA (CASE C).	120
TABLE E-27: SECTION MODULUS AND EFFECTIVE THICKNESS FOR BENDING STRESS FOR 2D CURVED MODELS WITH $G = 1$ MPA (CASE C).	120
TABLE E-28: SECTION MODULUS AND EFFECTIVE THICKNESS FOR BENDING STRESS FOR 2D CURVED MODELS WITH $G = 10$ MPA (CASE C).	120
TABLE E-29: CALCULATION OF TRUE BUCKLING STRESS FOR 2D CURVED MODELS WITH $G = 0,01$ MPA (CASE C).	121
TABLE E-30: CALCULATION OF TRUE BUCKLING STRESS FOR 2D CURVED MODELS WITH $G = 0,1$ MPA (CASE C).	121
TABLE E-31: CALCULATION OF TRUE BUCKLING STRESS FOR 2D CURVED MODELS WITH $G = 1$ MPA (CASE C).	121
TABLE E-32: CALCULATION OF TRUE BUCKLING STRESS FOR 2D CURVED MODELS WITH $G = 10$ MPA (CASE C).	122
TABLE E-33: CRITICAL BUCKLING LOADS AND STRESSES FOR 2D CURVED MODELS WITH $G = 0,01$ MPA (CASE C – 2 ND SOLUTION STRATEGY).	122
TABLE E-34: CRITICAL BUCKLING LOADS AND STRESSES FOR 2D CURVED MODELS WITH $G = 0,1$ MPA (CASE C – 2 ND SOLUTION STRATEGY).	122
TABLE E-35: CRITICAL BUCKLING LOADS AND STRESSES FOR 2D CURVED MODELS WITH $G = 1$ MPA (CASE C – 2 ND SOLUTION STRATEGY).	123
TABLE E-36: CRITICAL BUCKLING LOADS AND STRESSES FOR 2D CURVED MODELS WITH $G = 10$ MPA (CASE C – 2 ND SOLUTION STRATEGY).	123
TABLE F-1: NONDIMENSIONAL SLENDERNESS AND BUCKLING REDUCTION FACTORS FOR ANNEALED GLASS (CASE A).	124
TABLE F-2: NONDIMENSIONAL SLENDERNESS AND BUCKLING REDUCTION FACTORS FOR ANNEALED GLASS (CASE A).	124
TABLE F-3: NONDIMENSIONAL SLENDERNESS AND BUCKLING REDUCTION FACTORS FOR ANNEALED GLASS (CASE A).	125
TABLE F-4: NONDIMENSIONAL SLENDERNESS AND BUCKLING REDUCTION FACTORS FOR ANNEALED GLASS (CASE A).	125
TABLE F-5: NONDIMENSIONAL SLENDERNESS AND BUCKLING REDUCTION FACTORS FOR ANNEALED GLASS (CASE B).	125
TABLE F-6: NONDIMENSIONAL SLENDERNESS AND BUCKLING REDUCTION FACTORS FOR ANNEALED GLASS (CASE B).	126
TABLE F-7: NONDIMENSIONAL SLENDERNESS AND BUCKLING REDUCTION FACTORS FOR ANNEALED GLASS (CASE B).	126
TABLE F-8: NONDIMENSIONAL SLENDERNESS AND BUCKLING REDUCTION FACTORS FOR ANNEALED GLASS (CASE B).	126
TABLE F-9: NONDIMENSIONAL SLENDERNESS AND BUCKLING REDUCTION FACTORS FOR ANNEALED GLASS (CASE C).	127
TABLE F-10: NONDIMENSIONAL SLENDERNESS AND BUCKLING REDUCTION FACTORS FOR ANNEALED GLASS (CASE C).	127
TABLE F-11: NONDIMENSIONAL SLENDERNESS AND BUCKLING REDUCTION FACTORS FOR ANNEALED GLASS (CASE C).	127
TABLE F-12: NONDIMENSIONAL SLENDERNESS AND BUCKLING REDUCTION FACTORS FOR ANNEALED GLASS (CASE C).	128
TABLE F-13: NONDIMENSIONAL SLENDERNESS AND BUCKLING REDUCTION FACTORS FOR FULLY TEMPERED GLASS (CASE A).	128
TABLE F-14: NONDIMENSIONAL SLENDERNESS AND BUCKLING REDUCTION FACTORS FOR FULLY TEMPERED GLASS (CASE A).	128
TABLE F-15: NONDIMENSIONAL SLENDERNESS AND BUCKLING REDUCTION FACTORS FOR FULLY TEMPERED GLASS (CASE A).	129
TABLE F-16: NONDIMENSIONAL SLENDERNESS AND BUCKLING REDUCTION FACTORS FOR FULLY TEMPERED GLASS (CASE A).	129

TABLE F-17: NONDIMENSIONAL SLENDERNESS AND BUCKLING REDUCTION FACTORS FOR FULLY TEMPERED GLASS (CASE B). 129

TABLE F-18: NONDIMENSIONAL SLENDERNESS AND BUCKLING REDUCTION FACTORS FOR FULLY TEMPERED GLASS (CASE B). 130

TABLE F-19: NONDIMENSIONAL SLENDERNESS AND BUCKLING REDUCTION FACTORS FOR FULLY TEMPERED GLASS (CASE B). 130

TABLE F-20: NONDIMENSIONAL SLENDERNESS AND BUCKLING REDUCTION FACTORS FOR FULLY TEMPERED GLASS (CASE B). 130

TABLE F-21: NONDIMENSIONAL SLENDERNESS AND BUCKLING REDUCTION FACTORS FOR FULLY TEMPERED GLASS (CASE C). 131

TABLE F-22: NONDIMENSIONAL SLENDERNESS AND BUCKLING REDUCTION FACTORS FOR FULLY TEMPERED GLASS (CASE C). 131

TABLE F-23: NONDIMENSIONAL SLENDERNESS AND BUCKLING REDUCTION FACTORS FOR FULLY TEMPERED GLASS (CASE C). 131

TABLE F-24: NONDIMENSIONAL SLENDERNESS AND BUCKLING REDUCTION FACTORS FOR FULLY TEMPERED GLASS (CASE C). 132

TABLE F-25: NONDIMENSIONAL SLENDERNESS AND BUCKLING REDUCTION FACTORS FOR HEAT STRENGTHENED GLASS (CASE A). 132

TABLE F-26: NONDIMENSIONAL SLENDERNESS AND BUCKLING REDUCTION FACTORS FOR HEAT STRENGTHENED GLASS (CASE A). 133

TABLE F-27: NONDIMENSIONAL SLENDERNESS AND BUCKLING REDUCTION FACTORS FOR HEAT STRENGTHENED GLASS (CASE A). 133

TABLE F-28: NONDIMENSIONAL SLENDERNESS AND BUCKLING REDUCTION FACTORS FOR HEAT STRENGTHENED GLASS (CASE A). 133

TABLE F-29: NONDIMENSIONAL SLENDERNESS AND BUCKLING REDUCTION FACTORS FOR HEAT STRENGTHENED GLASS (CASE B). 134

TABLE F-30: NONDIMENSIONAL SLENDERNESS AND BUCKLING REDUCTION FACTORS FOR HEAT STRENGTHENED GLASS (CASE B). 134

TABLE F-31: NONDIMENSIONAL SLENDERNESS AND BUCKLING REDUCTION FACTORS FOR HEAT STRENGTHENED GLASS (CASE B). 134

TABLE F-32: NONDIMENSIONAL SLENDERNESS AND BUCKLING REDUCTION FACTORS FOR HEAT STRENGTHENED GLASS (CASE B). 135

TABLE F-33: NONDIMENSIONAL SLENDERNESS AND BUCKLING REDUCTION FACTORS FOR HEAT STRENGTHENED GLASS (CASE C). 135

TABLE F-34: NONDIMENSIONAL SLENDERNESS AND BUCKLING REDUCTION FACTORS FOR HEAT STRENGTHENED GLASS (CASE C). 135

TABLE F-35: NONDIMENSIONAL SLENDERNESS AND BUCKLING REDUCTION FACTORS FOR HEAT STRENGTHENED GLASS (CASE C). 136

TABLE F-36: NONDIMENSIONAL SLENDERNESS AND BUCKLING REDUCTION FACTORS FOR HEAT STRENGTHENED GLASS (CASE C). 136

SYMBOLS, ACRONYMS AND ABBREVIATIONS

$[K]$	Stiffness matrix.
$[K_g]$	Stress stiffness matrix.
$\{\Phi_i\}$	Eigenmode or buckling mode shape.
A	Cross-sectional area of the element.
A_1	Cross-sectional area of glass ply 1.
A_2	Cross-sectional area of glass ply 2.
A_{full}	Cross-sectional area of the entire laminated glass pane (also including PVB interlayer).
A_{MG}	Area of the monolithic glass cross-section.
b	Width of the laminated glass pane.
BLF	Eigenvalue, also named, buckling load factor multiplier.
d_i	Distance of the mid-plane of the i -th glass ply from the mid-plane of the laminated glass.
E	Young's modulus.
E_g	Young's modulus of glass.
$e(x)$	Initial imperfection along the length of glass column.
e_0	Basic imperfection.
$e_{0,installation}$	Imperfection concerning the deviation of glass pane from unexpected eccentric loads.
$e_{0,length}$	Imperfection concerning the length of the element.
$e_{initial}$	Initial imperfection in the middle of glass column.
e_z	Eccentricity of the load.
$f_{b,k}$	Characteristic value of glass strength after a strengthening treatment.
$f_{g,d}$	Design value of glass bending strength.
$f_{g,k}$	Characteristic bending strength of annealed glass.
$f_{t,PVB}$	Tensile strength of the interlayer.
$f_{u,c}$	Compressive glass strength.
f_y	Yielding stress.
G	Interlayer shear modulus.
h_1	Thickness of top glass ply.
h_2	Thickness of bottom glass ply.
h_e	Total thickness of laminated glass pane obtained by summing up h_1 , h_2 and h_{int} .
$h_{ef,w}$	Equivalent thickness for calculating out-of-plane bending deflection.
$h_{ef,\sigma,i}$	Equivalent thickness for calculating out-of-plane bending stress of ply " i ".
h_i	Nominal thickness of the i -th glass ply.
h_{int}	Thickness of the interlayer.
I	Moment of inertia of the member.
I_1	Moment of inertia of glass ply 1.
I_2	Moment of inertia of glass ply 2.
I_{MG}	Moment of inertia of monolithic glass.
$I_{z,eff}$	Effective moment of inertia of laminated glass about the minor or weak axis (z -axis).
J_{full}	Moment of inertia of the entire laminated glass cross-section (also including PVB interlayer).
k_e	Edge or hole finishing factor.
$k_{e,p}$	Edge or hole pre-stressing factor.
k_{mod}	Modification factor.
k_p	Pre-stressing process factor.
K_s	First parameter necessary to compute the effective moment of inertia of laminated glass.
k_{sp}	Surface profile factor.
K_T	Tangent stiffness.
L	Length of the element.
L_b	Buckling length of the member.

N	Applied compressive load.
n	Number of glass plies.
$N_{b,Rd}$	Design buckling resistance of laminated glass member.
$N_{cr,EU}$	Elastic critical buckling load.
$N_{cr,FEA}$	Critical buckling load obtained from Finite Element Analysis.
$N_{cr,LG}$	Elastic buckling load for laminated glass.
$N_{cr,MG}$	Elastic buckling load for monolithic glass elements.
N_{Ed}	Design compressive load.
P_0	Initial applied load on <i>FE</i> -models.
R	Given external load.
T_g	Glass transition temperature between liquid and solid state.
T_s	Glass melting temperature.
u	Displacement of the panel.
$w(x)$	Bending deflection along the length of glass column due to the axial force.
W_{MG}	Elastic section modulus of the monolithic glass cross-section.
$W(h_{ef,\sigma,i})$	Section modulus of laminated glass cross-section using stress-equivalent effective thickness.
$w_{total}(x)$	Total deflection along the length of glass column.
x	Coordinate along length of glass column.
z_1	Distance of the mid-plane of the glass ply 1 from the mid-plane of the laminated glass.
z_2	Distance of the mid-plane of the glass ply 2 from the mid-plane of the laminated glass.
α^2	Second parameter necessary to compute the effective moment of inertia of laminated glass.
α_0	First imperfection coefficient (Eurocode approach).
α_{imp}	Second imperfection coefficient (Eurocode approach).
α_T	Glass thermal expansion coefficient.
β	Third parameter necessary to compute the effective moment of inertia of laminated glass.
γ_M	Material partial safety factor.
γ_{M1}	Buckling safety factor.
γ_p	Partial factor for pre-stress on the surface.
δ_{max}	Maximum transversal displacement in the midspan of the <i>FE</i> -model.
δ_{lim}	Limit transversal displacement.
Δa	Incremental displacement.
ε_t	Elongation at failure of the interlayer.
η	Coupling parameter coefficient.
η_b	Coupling parameter for beams.
λ	Slenderness ratio.
$\bar{\lambda}$	Non-dimensional slenderness.
λ_{lim}	Slenderness ratio threshold between failure by yielding and failure by buckling.
λ_1	Second factor which considers size effect.
λ_A	First factor which considers size effect.
λ_{panel}	Slenderness ratio of the laminated glass panel.
ν	Poisson's ratio.
ρ	Radius of gyration of the cross-section.
ρ_{full}	Radius of gyration of the entire laminated glass cross-section.
ρ_g	Glass density.
ρ_{PVB}	PVB density.
σ	Negative normal stress (compressive stress).
$\sigma(x)$	Normal stress.
$\bar{\sigma}$	True stress.
σ^+	Positive normal stress (tensile stress).
$\sigma_{cr,EU}$	Euler's critical pressure or critical stress.
$\sigma_{cr,FEA}$	Critical buckling stress obtained from Finite Element Analysis.

φ	Rotation of the panel.
Φ	Buckling parameter (Eurocode approach).
χ	Buckling reduction factor (Eurocode approach).
χ_{FEM}	Buckling reduction factor for numerical results.
Ψ	Fourth parameter necessary to compute the effective moment of inertia of laminated glass.
Ψ_a	Out-of-balance residual force.
Ψ_b	Boundary coefficient for beams.
<i>1D</i>	One-dimensional.
<i>2D</i>	Two-dimensional.
<i>3D</i>	Three-dimensional.
<i>ANG</i>	Annealed glass.
<i>BCs</i>	Boundary conditions.
<i>BSG</i>	Borosilicate glass.
<i>CaO</i>	Calcium oxide or lime.
<i>CC</i>	Class of consequence.
<i>DoF(s)</i>	Degree of freedom(s).
<i>EC</i>	Eurocode.
<i>EET</i>	Effective thickness theory for laminated glass.
<i>EVA</i>	Ethylene Vinyl Acetate.
<i>FEA</i>	Finite Element Analysis.
<i>FEM</i>	Finite Element model.
<i>FE</i>	Finite Element.
<i>FTG</i>	Fully tempered glass.
<i>GNA</i>	Geometrically nonlinear buckling analysis.
<i>HSG</i>	Heat strengthened glass.
<i>HXM8</i>	Three-dimensional finite elements with eight nodes.
<i>LBA</i>	Linear buckling analysis or eigenvalue analysis.
<i>LG</i>	Laminated glass.
<i>Na₂O</i>	Sodium oxide or soda.
<i>NiS</i>	Nickel-sulfide.
<i>PET</i>	Polyester.
<i>PVB</i>	Polyvinyl Butyral.
<i>QSL8</i>	Semiloof curved thin shell elements.
<i>SiO₂</i>	Silica sand.
<i>SLSG</i>	Soda lime silica glass.
<i>TPU</i>	Thermoplastic Polyurethane.

1 INTRODUCTION

1.1 Preface

Glass is a very ancient material which has been used since the very beginning from stone-age civilizations in the regions of *Egypt* and *Mesopotamia* to produce objects and weapons such as knives, cups, and jewellery. Glass production was subsequently developed in Roman times and soon it was diffused to all the countries ruled by the *Roman Empire*, but nevertheless during the *Gothic Era*, the use of colourfully and finely decorated stained glass windows grew strongly, and it created greater interest and new studies on glass technology and manufacturing processes were performed. Further applications of glass were accomplished in the *Modern Age*, during which, thanks to the knowledge and the increasing use of structural steel and then reinforced concrete technology, there was the possibility to create large floors and walls with relatively small columns. This represented a sort of turning point, since architects and engineers realized that they could close wall openings using large glass panels providing better thermal and acoustic insulation as well as natural lighting. Nowadays, glass is frequently used for many applications such as windows, façades, roof lights and in some cases floors and staircases.

However, the use and the scientific knowledge of glass in terms of structural material is fairly new, and for that reason, the following thesis is devoted to enlarging the awareness about structural glass, in particular regarding the problem of instability.

1.2 Objective and methodology

The objective of the present thesis is to investigate buckling behaviour of slender laminated glass panels, taking into account geometric nonlinearities, which could strongly affect load-carrying capacity. To this end, a parametric study is performed by varying the length of the panes, the geometric properties of the laminated cross-section and the interlayer shear modulus in pre-established ranges. To this end, 2D and 3D models, with and without initial geometric imperfections, are modelled in the Finite Element (FE) software, LUSAS, taking advantage of the *Enhanced Effective Thickness Theory (EET)* for the case of 2D. After modelling process, eigenvalue analyses (LBA) and geometrically nonlinear buckling analyses (GNA) are carried out in order to determine the critical buckling loads for each typology of model and for the two different types of analysis.

Finally, numerical findings are analysed and discussed, also through the use of graphs and diagrams.

1.3 Overview

The document is organized in seven chapters, following the next format:

Chapter 2, *Literature Review*, presents an overview regarding the use in the architectural context and the evolution of glass throughout history. Physical and mechanical properties, as well as different typologies of glass, are described. And lastly, a brief introduction on the current Standard for glass in buildings and on the buckling phenomena is presented.

Chapter 3, *Glass Design and Buckling Calculation*, describes some relevant features and formulas of glass design process according to the Standard *CEN/TS 19100:2021*.

Chapter 4, *Second-Order Theory and Buckling Analysis*, explains the different types of buckling analysis performed and the topic of initial imperfections.

Chapter 5, *Methodology*, illustrates the characteristics of the numerical models developed in the Finite Element software.

Chapter 6, *Results and Discussion*, describes the significant outcomes obtained by parametric study.

At last, Chapter 7, *Final Conclusions*, presents a summary of the numerical findings and some improvements for the analysis of buckling in laminated glass.

Six annexes are also included in this document, which illustrate supplementary calculations and tables with numerical results.

2 LITERATURE REVIEW

2.1 Introduction

Glass is one of the most versatile materials known to humankind. It has been closely associated with architectural design for centuries [1]. It offers numerous features allowing the designer to meet aesthetic and structural needs, making it attractive in buildings. Even if glass is defined as a brittle material, some types of glass, e.g. laminated glass, are characterized by a high compressive strength and are able to bear various kinds of loads. This material has been used for windows, roofs, stairs, as well as in glazing of façades, providing sufficient brightness inside the building, protection from atmospheric agents and chemical resistance.

However, Europe has implemented strategies and actions capable of reducing emissions and energy consumption. Buildings in the European Union are responsible for 40% of energy consumption and 36% of greenhouse gas emissions. One important area for improvement is the heating and cooling of buildings and domestic hot water, which account for 80% of households' energy consumption [2]. By means of certain treatments and/or coatings, glass can offer great thermal and acoustic insulation enhancing the performance of the building and reducing energy consumption [1]. Furthermore, design versatility of glass is another benefit to be considered, in fact, glass elements, thanks to the manufacturing process, can be shaped into a lot of forms, enamelled, textured and coated, meeting the needs of the client [1].

Nowadays, glass must meet high standards of safety for the users, so glass elements are made resistant to shocks and sudden temperature changes, and if they are damaged or shattered, they will not break in [3]. At last, glass can be considered as a recyclable material: when a building is refurbished, end-of-life façade glass can be crushed and used as aggregates in construction, or the most effective use is to turn glass into new glass products with a view to circular economy and sustainability [4].

At last, an important topic worth clarification is the definition of “structural glass”: structural glass is considered to be applications involving an element or system that supports other element(s) or system(s) and/or has consequences of collapse, safety or function in the event of failure other than the cost of repair/replacement. ‘Non-structural’ describes an element or system that has little or no consequence in the event of failure (other than the cost of repair/replacement) [5].

2.2 History and Architectural Context

The origin of glass has its roots in remote times. Glass objects have been found in *Syria* that date to 2500 BCE, and by 2450 BCE, glass beads were believed to be plentiful in *Mesopotamia* (situated in the valleys between the *Tigris* and *Euphrates* rivers) [6]. It is generally thought that introduction of glass technology into *Egypt* occurred during the reign of *Tuthmosis III* (1479-1425 BCE), with glass objects and ingots being imported as tribute [6]. In these early periods, two types of techniques were used to produce glass objects: core-forming or casting.

The core-forming procedure involved the shaping of a form or core onto the end of a wooden or metal rod, after which it could then be heated to help set its shape. Then, glass layers were built up around the central set core, as shown in Figure 2-1 [4].

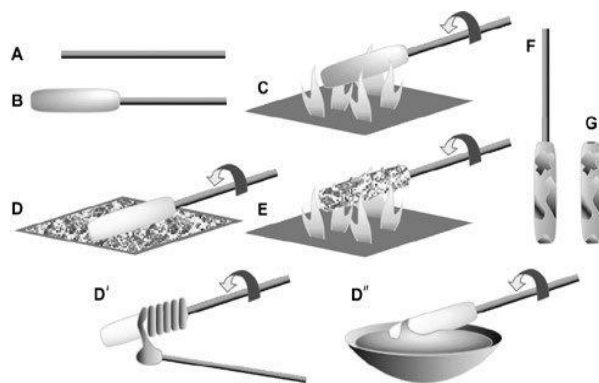


Figure 2-1: Core-forming technique ¹.

The casting involved melting glass pieces into a mold which provided the simple, crude shape of the desired object. After the glass had cooled, the mold could then be removed and carved or polished to give the final product, as shown in Figure 2-2 [6].

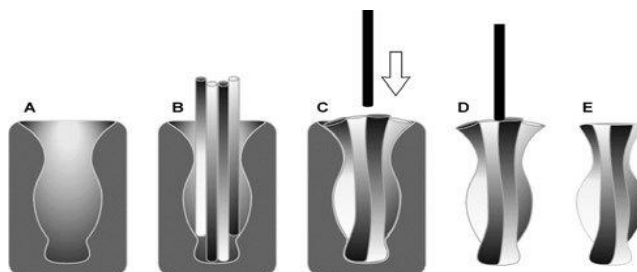


Figure 2-2: Casting technique ².

It was the Romans who introduced additional methods to create glass objects, and they were able to develop new techniques, among which the most innovative and still used today is the “glassblowing”. Invented in about 40 B.C., it was the most important innovation in Roman glassmaking technology [7]. This method consists of shaping a mass of glass that has been softened by heat by blowing air into it through a tube, i.e. the blowpipe [8], as illustrated in Figure 2-3.

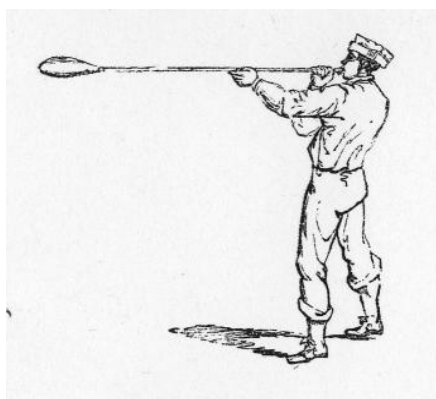


Figure 2-3: Glassblowing technique ³.

^{1,2} Figures from: Seth C Rasmussen, ‘A Brief History of Early Silica Glass: Impact on Science and Society’, *Substantia* 3(2) Suppl. 5, pages: 125-138, 2019, DOI: 10.13128/Sub-stantia-267 (Accessed Nov. 26, 2024).

³ Figure from: <https://www.classicalchandeliers.co.uk/history-of-glassworks> (Accessed Nov. 28, 2024).

In addition, the Romans were the first to use glass for windows: early window panes were fabricated via a variety of different processes, the oldest of which was the production of cast glass. This process produces panes of uneven thickness, with one side exhibiting a smooth texture and the other side a pitted, rough finish [6].

Then, with the coming of Gothic style- born in *France* in the middle of the 12th century- stained glass began to be more used in Gothic cathedrals and churches, that could be coloured. The production method was a complex process, that required the addition of various metal oxides during the melting process; for example, cobalt oxide gave the glass a blue tint, while copper oxide coloured it green [9]. Stained-glass windows illustrated the stories of the bible and the lives of saints. But since the size of glass panes was limited, artists were able to develop a new system to cover large areas with small glass panes: to assemble the window, pieces of coloured and painted glass are laid out on the design board, with the edges of each piece fitted into H-shaped strips of lead (also called cames). These cames were soldered to one another so that the panel was secure. When a panel was completed, putty was inserted between the glass and the lead cames for waterproofing. The entire composition was then stabilized with an iron frame (armature) and mounted in the space for window [10].

For illustration, *Notre-Dame de Chartres* Cathedral, in France, is a good example. Built and decorated between 1134 and 1260, registered by *UNESCO* as a World Heritage Site, it is the most complete and best preserved of the Gothic cathedrals [11]. *Chartres* Cathedral is renowned for its large number of stained-glass windows aimed at telling the story of the *Virgin Mary* and one of the most stunning windows inside the Cathedral is presented in Figure 2-4.

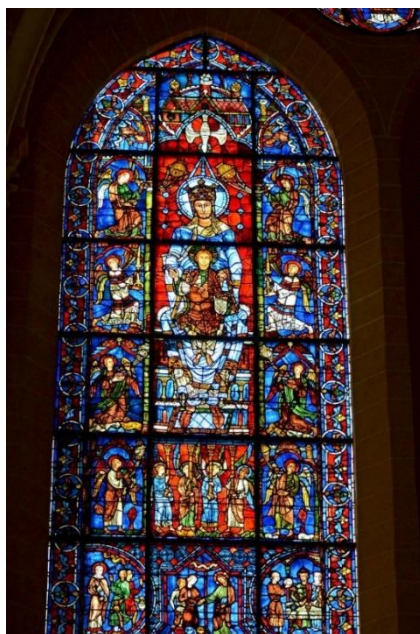


Figure 2-4: Chartres' Belle-Verrière, example of stained-glass window in Notre-Dame de Chartres Cathedral ⁴.

In the 18th and 19th centuries, some innovative glass production techniques such as the plate process and the cylinder process were introduced, making it possible to produce large and transparent glass panes. The cylinder process can be seen as the evolution of the glass blowing technique, and indeed a blowing technique was in fact used in the first version of the method. But since it may take some time and effort at the hands of the glassmakers, then, a machine was designed by *William Pilkington*, and a later version was mechanized and could create cylinders 13 meters high.

⁴ Figure from: <https://www.britannica.com/topic/Chartres-Cathedral> (Accessed Dec. 2,2024).

This was done by dipping a round metal bait into a bath of molten glass which was then raised to create a long cylinder of clear glass. An advantage of this version of the process was that bigger panes could be made, and less human energy went into it [12].

In the plate process, molten glass is rolled to create a flat plate of glass. At this stage, it could be done on a table with a mobile roller, but the rollers would leave the surface of the glass rough and marked, so would be opaque after this phase. The plate of glass is then ground to create two parallel and smooth surfaces, and in the final stage the glass plate is polished at one surface at a time, in order to leave glass transparent and distortion-free [12]. Both processes are shown in Figure 2-5.

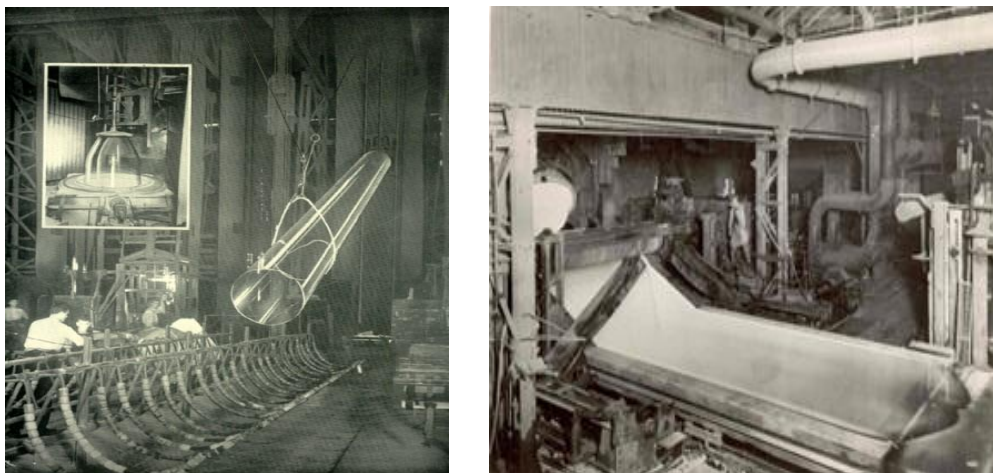


Figure 2-5: On the left the Cylinder process and on the right the Plate process ⁵.

In the late 19th and early 20th centuries, glass became more widely available and affordable, leading to its widespread use in buildings. This period marked the beginning of the modern era of glass in building design. Architects began experimenting with different shapes and sizes of glass, and the use of metal frames and connectors allowed for larger, more intricate window designs [13].

Evidence of the 19th century is represented by the iconic *Crystal Palace* designed by the architect *Joseph Paxton* and built in London in 1851 to host in a temporary international exhibition of industry. It was also called the Great Exhibition of the Works of Industry of All Nations.

At the time, the Royal Commission set up to oversee the announced project agreed that the building to house the exhibition should have a target net area of 800'000 square feet and the upper limit of the contract budget for construction was set at £100,000. The complexity of the building was set: not only it would have to be the largest building ever constructed, it would also have to be cheaper than any building previously built [14]. The Commission received 245 entries but none of them were approved, and the time to build it was running out. So, *Sir Joseph Paxton* took a step forward showing interest in this challenging project. Paxton' design was based on a 0,25 m x 1,24 m module, the size of the largest glass sheet available at the time. The modular system consisted of right-angled triangles, mirrored and multiplied, supported by a grid of cast iron beams and pillars [15].

The building, as shown in Figure 2-6, was rectangular in plan, with some minor single-story additions along the south front. At ground floor level it was laid out as 77 × 17 bays, with columns at 7,3-meter centres. The overall length of the building, depending on how you measure it, was between 563,58 meters and 563,88 meters.

⁵ Figures from: <https://www.pilkington.com/en-gb/uk/about/heritage/cylinder-process> (Accessed Dec. 3,2024).

The second tier of the building was 11 bays wide and the third tier, just 5 bays [16]. The structure, covering approximately an exhibition area of 70'000 m² and using nearly 84'000 m² of glass, is made of cast iron columns, cast iron girders, walls composed of timber and glass, laminated timber arches and glazing. To speed up the construction process, all the structural elements were precast, ready to be simply assembled on site and the construction was concluded within only five months.



Figure 2-6: Illustration of the transept of the Crystal Palace on the left and the exterior of the Crystal Palace at Sydenham in 1854 on the right ^{6,7}.

The 20th century came across great innovations in glass field, when, in 1900 the patent for toughened glass was filed by the Austrian chemist *Rudolph A. Seiden* and in the mid-20th century *Pilkington* developed the float glass process [17] – both are going to be more broadly discussed in the following sections. The float process is still used and also the most commonly used today to produce a large variety of specialized glass products, including safety laminated glass, toughened glass, acoustic glass etc.

Always in the same century other pioneering developments occurred in glass sheet drawing manufacturing processes, such as the *American Colburn Process* and the Belgian *Fourcault Process*, which made it possible to produce glass windows in large quantities.

The *Fourcault procedure* was developed in Belgium by the homonymous inventor *Émile Fourcault* (1862-1919) and it can be defined as a vertical drawn process. In this process molten glass is “pulled” through a ceramic extrusion die in the upward direction, against gravity, to form a rectangular ribbon of glass which is immediately after cooled to preserve the rectangular section. The novelty of this process lies in the fact that molten glass is not pulled in the literal sense, but the pressure is obtained thanks to the difference of pressure in height during the process.

Regarding the *American Colburn Process*, *Irving W. Colburn* was an experienced machinist really interested in developing a mechanized continuous process to produce glass sheets. In September 1909, *Colburn* produced the world’s first glass sheet using his revolutionary new horizontal sheet draw process [18]. This process is very similar to the previous one and the only difference is that molten glass is drawn vertically and then is actually pulled through rollers in the horizontal direction to produce a glass sheet.

As a consequence, large glass panes were used in buildings, and in fact modernist architects made extensive use of glass in their projects.

⁶ Figure from: <https://www.britannica.com/topic/Crystal-Palace-building-London> (Accessed Dec. 3,2024).

⁷Figure from: <https://www.paul-mellon-centre.ac.uk/whats-on/past/the-crystal-palace-at-sydenham/year/2004> (Accessed Dec. 3,2024).

The use of glass in modern buildings comes from the architectural philosophy that questions how we integrate the interior and exterior of a building to create spaces that best reflect natural states of work, rest and play [19].

The modernist movement is an architectural and artistic style that emerged in the early 20th century as expression of a renewed society and new technologies in opposition to classicism. In 1927, the pioneer of modern architecture *Le Corbusier* conceived his “*Five Points of a New Architecture*” which are the fundamental ideological principles to be followed during the design of a structure: pilotis, free design of the ground plan, free design of the façade, horizontal windows and roof garden.

Furthermore, functionalism was another founding idea of the movement, implying that every element designed in a building must be firstly functional, only secondarily aesthetic. In addition, modernist architects widely employed reinforced concrete and steel as structural materials and glass for large glass windows.

Ludwig Mies van der Rohe (1886-1969) was a German architect and a leading exponent of the modern architecture in the *USA*. Fundamental to Mies’s design philosophy and one of the driving forces behind his use of glass was the concept of fluid space. He believed that architecture should embody a continuous flow of space, blurring the lines between interior and exterior. Glass was seen as a quintessentially modern material that also had the ability to reconnect humans to nature and even change how we perceive it [20].

One remarkable example of his works is the *Neue Nationalgalerie*, an iconic modern art museum located in Berlin that was designed and built from 1963 to 1968. *Mies van der Rohe* realized a minimalist two-story temple of steel and glass which rests on a 105x110 meters granite basement, in accordance with his “*skin and bone*” philosophy. To create wide open spaces, eight cruciform steel columns were used along the façade and large single glazed panes to enclose the room between the columns, establishing a seamless visual experience. Around the perimeter of the building, eight massive steel columns carry a cantilevered suspended roof with coffer ceiling which spans 18 meters, resulting in a large space between the façade and the external columns. The building does not require any additional wall or partition thanks to the presence of the steel columns, which allows for a large open space, creating a flexible and adaptable environment.



Figure 2-7: Exterior of the *Neue Nationalgalerie* in Berlin ⁸.

⁸ Figure from: <https://www.theplan.it/architettura/lintervento-di-ripristino-e-ristrutturazione-della-neue-nationalgalerie-di-berlino> (Accessed Dec. 28,2024).



Figure 2-8: Details of the glass façade and the suspended roof of the Neue Nationalgalerie ⁹.

As the research and knowledge in the use of glass has been proceeded, glass to be used as a structural material has been more recently employed in creating almost invisible walls, stunning staircases and floors, and even bridges. One example could be the *Hangzhou's Apple Store in China* designed by the British *Foster+Partners Studio*, whose team conceived a 15-metre-high volume creates a sense of space and calm within the busy store and city. It is divided horizontally by a dramatic cantilevered floor, which extends 12 meters from the rear wall like a diving board to create a 9-metre-high piano nobile. The façade comprises 11 double-glazed panels, each rising 15 meters [21]. In addition, inside the building an impressive, laminated glass staircase is present. In Figure 2-9 it is possible to look at these ingenious designs.

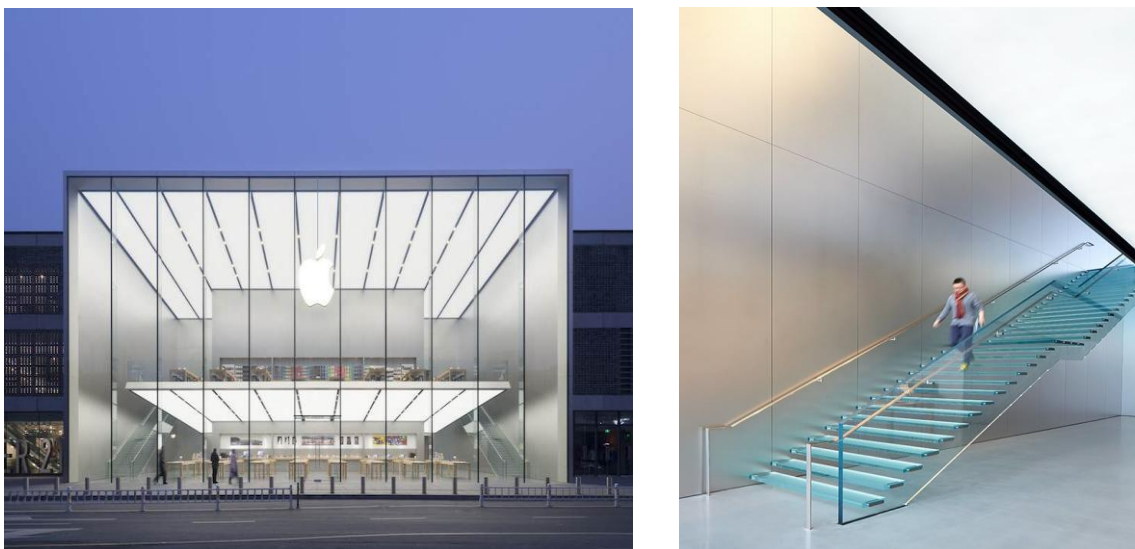


Figure 2-9: The Hangzhou's Apple Store. On the left, the façade and on the right the “floating” glass staircase ¹⁰.

⁹ Figure from: <https://architectuul.com/architecture/new-national-gallery> (Accessed Dec. 28,2024).

¹⁰ Figure from: <https://www.archipanic.com/hangzhous-apple-store/> (Accessed Jan. 3,2025).

2.3 Glass properties

Glass is an inorganic product of fusion, that was cooled to a rigid condition without crystallization [22]. Depending on the chemical composition, it is possible to obtain a broad range of glass types, but generally they have in common some basic chemical compounds such as silica sand (SiO_2), calcium oxide or lime (CaO) and sodium oxide or soda (Na_2O). Usually some specific glass families- soda lime silica glass (*SLSG*) and borosilicate glass (*BSG*)- are commonly available on the market.

Most of the glass used in construction is soda lime silica glass (*SLSG*). For some special applications , e.g. scientific lenses, reagent vials and lighting, borosilicate glass (*BSG*) is used, since it offers very high resistance to temperature changes as well as a very high hydrolytic and acid resistance [22]. Table 2-1 shows the chemical compositions, in terms of mass percentage, of *SLSG* and *BSG* according to the European specifications *EN 1748-1-1:2004 Part 1-1* [23] regarding *BSG* properties and *EN 572-1:2004 Part 1* [24] regarding *SLSG* properties.

Table 2-1: Chemical composition of soda lime silica glass and borosilicate glass ¹¹.

Components	Notation	Soda lime silica glass	Borosilicate glass
Silica sand	SiO_2	69-74 %	70-87 %
Lime (calcium oxide)	CaO	5-14 %	/
Soda	Na_2O	10-16 %	0-8 %
Boron-oxide	B_2O_3	/	7-15 %
Potassium oxide	K_2O	/	0-8 %
Magnesia	MgO	0-6 %	/
Alumina	Al_2O_3	0-3 %	0-8 %
Others	/	0-5 %	0-8 %

Since glass is an amorphous solid, it implies that the atoms are not arranged in an orderly and regular manner. In fact, glasses do not consist of a geometrically regular network of crystals, but of an irregular network of silicon and oxygen atoms with alkaline parts in between (Figure 2-10) [22].

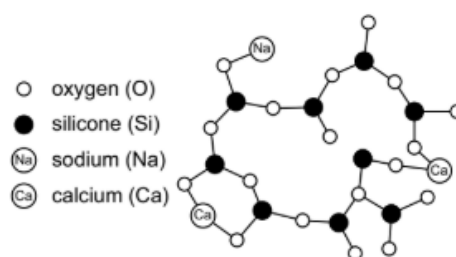


Figure 2-10: Irregular crystal lattice of soda lime silica glass ¹².

^{11, 12} Table and Figure from: M. Haldimann, A. Luible, M. Overend, 'Structural Use of Glass', IABSE- AIPC – IVBH, 2008.

The chemical composition has an important influence on the viscosity, the melting temperature T_s and the thermal expansion coefficient of glass α_T [22]. Generally, since the melting temperature of pure silica oxide is approximately 1710 °C, it is convenient to introduce alkaline molecules to reduce the melting temperature that will be about 1300-1600 °C.

Another important parameter which characterizes glass and its processes is viscosity. In this regard, four standard temperature points are used to define its viscosity: the working point is the viscosity at which a melt is delivered to a forming device [25]. The Softening point, which is the minimum viscosity, can prevent the glass from deforming under its own weight [25]. The Annealing point is defined as the temperature where stress is substantially relieved within a few minutes [25]. Finally, the temperature at solidification is called glass transition temperature T_g and is about 530 °C for SLSG [22] and it represents the transition between liquid and solid states.

Table 2-2: Viscosity of glass at different states and respective temperatures for SLSG and BSG ¹³.

Viscosity (dPa s)	State	Temperature SLSG (°C)	Temperature BSG (°C)
10^5	Working point	1040	1280
$10^{8.6}$	Softening point	720	830
10^{14}	Annealing point	540	570
$10^{14.3}$	Transition temperature T_g	530	560
$10^{15.5}$	Strain point	506	530

Table 2-3 shows glass physical properties according to the European specifications [23] regarding BSG properties and [24] regarding SLSG properties.

Table 2-3: SLSG and BSG physical properties ¹⁴.

Property	Notation	Unit of measurement	Soda lime silica glass	Borosilicate glass
Density	ρ_g	kg/m ³	2500	2200-2500
Young's modulus	E_g	MPa	70000	4,5-6
Poisson's ratio	ν	/	0,23	0,2
Coefficient of thermal expansion	α_T	$10^{-6} K^{-1}$	9	Class 1: 3,1-4,0 Class 2: 4,1-5,0 Class 3: 5,1-6,0

¹³ Table from: M. Haldimann, A. Luible, M. Overend, 'Structural Use of Glass', IABSE- AIPC – IVBH, 2008.

¹⁴ Table adapted from: M. Haldimann, A. Luible, M. Overend, 'Structural Use of Glass', IABSE- AIPC – IVBH, 2008.

2.4 Glass behaviour

Glass shows an almost perfectly elastic, isotropic behaviour and exhibits brittle fracture. It does not yield plastically, which is why local stress concentrations are not reduced through stress redistribution as in the case for other construction materials like steel [22]. Since glass lacks plasticity, when tensile strength is reached, cracks will start to fastly propagate and then it will suddenly break without prior notices.

In this context, one disadvantage of glass is represented by the significant discrepancy between glass compressive strength and its tensile strength. The theoretical tensile strength (based on molecular forces) of glass is exceptionally high and may reach 32 GPa [22]; the reason why it is so high could be found in silica-oxygen bonds which are very strong. But the actual tensile strength, used in engineering, is lower and is about one tenth of the compressive one because in brittle materials the tensile strength depends on many factors such as load duration, concentration of stresses, size of the element and mechanical defects on the surface. While the surface of glass panes generally contains a large number of relatively severe flaws, the surface of glass fibres contains less and less deep surface flaws; this explains the much higher strength of glass fibres when compared to glass panes [22].

Steel can be defined as an isotropic, linear elastic material characterized by a symmetrical behaviour in tension and compression. Its constitutive law, i.e. the relationship between stress σ and strain ϵ , for engineering purposes can be schematized with an elastic perfectly plastic model, not considering a possible hardening effect. Since steel is characterized by a large plastic branch, entailing an ability in the redistribution of stresses, it is able to withstand large forces and deformations going beyond its elastic limit. Structural engineers, designing steel structures, have typically concentrated their attention on limiting stresses at places of maximum bending and shear. However, localised yielding is rarely considered during design of steel elements [17]. Glass lacks plasticity and is not able to redistribute stresses, therefore it is not possible to neglect possible stress concentrations. For this reason, connection design is a core component when designing structures made from glass (see Figure 2-11) [17].

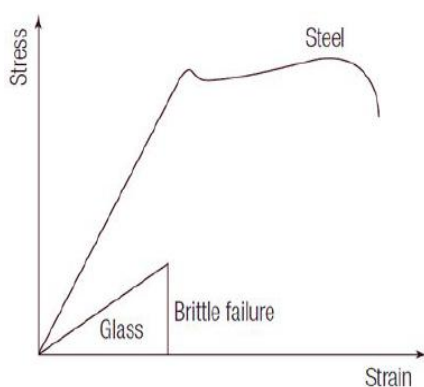


Figure 2-11: Comparison between steel and glass constitutive laws ¹⁵.

¹⁵ Figure from: C. O' Regan and Institution of Structural Engineers, 'Structural Use of Glass in Buildings (2nd edition)', IStructE Ltd, 2015.

2.5 Float glass production process

Glass elements can be produced by means of several processes nevertheless the main production steps are always similar: firstly, the raw material is melted at a temperature of about 1600-1800 °C, then the melted material is formed at a temperature range of 800-1600 °C and, lastly, glass is cooled at temperatures between 100-800 °C. In Figure 2-12, the main glass production processes are shown together with the possible treatments, post-processing methods and finished products.

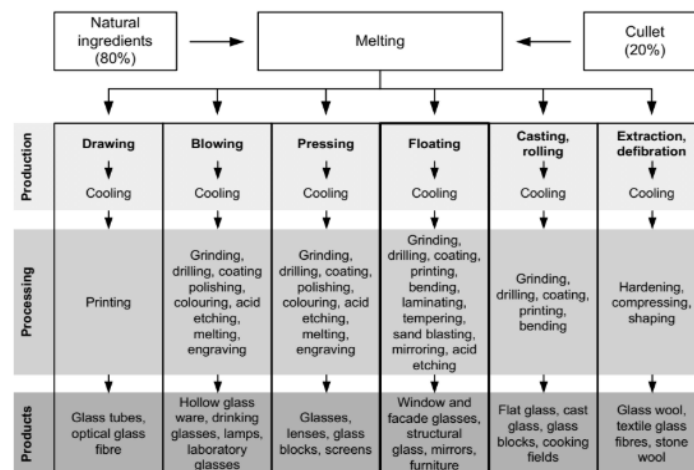


Figure 2-12: Glass production processes, treatments and corresponding final products ¹⁶.

Currently the *Float process* is the most popular primary manufacturing process and accounts for about 90% of today's flat glass production worldwide [22].

Sir Alastair Pilkington (1920-1995) was a British engineer and inventor who conceived in the early 1950s the innovative *Float Process* which deeply transformed glass industry, so much that it is still the most widely used process for producing high-quality glass elements. Sir Pilkington's final purpose was to get flat glass sheets which must also be translucent and without optical imperfections. When he started work on his process, the target was to make, more economically, the high-quality glass essential for shop windows, cars, mirrors and other applications where distortion free glass was necessary. At that time this quality of glass could only be made by the costly and wasteful plate process and because of glass-to-roller contact, surfaces were marked [26].

The *Float Process* basically consists of three main stages which are: melting, float bath in tin and cooling (annealing). In Figure 2-13, the principal stages of the *Float Process* are depicted in a schematic way:

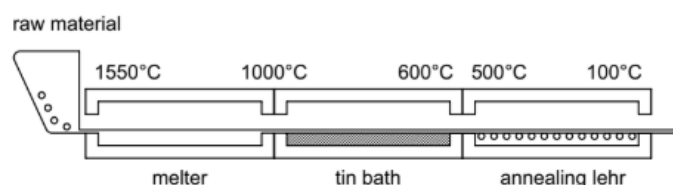


Figure 2-13: Main stages of the float process ¹⁷.

^{16, 17} Figures from: M. Haldimann, A. Luible, M. Overend, 'Structural Use of Glass', IABSE- AIPC – IVBH, 2008.

First, raw materials (mainly *silica sand*, *soda* and *lime*) are mixed and heated inside a furnace which can melt them at temperatures up to 1550 °C. The molten glass is then poured onto the mirror-like surface of molten tin bath in an inert atmosphere consisting of hydrogen and nitrogen. During this phase, due to the higher tin melting temperature compared to the glass one, glass can float above the tin bath surface and a flat surface of thickness between 6 and 7 mm will be formed [22].

In the last phase, in order to relieve the stresses, the rigid glass ribbon enters inside the, so called, annealing lehr in which the glass temperature gradually decreases and in the meanwhile the glass ribbon is flattened through the presence of rollers. By acting on the speed of rollers, it is possible to regulate the thickness of the glass plate. After annealing and a subsequent inspection, the glass edges are trimmed to give a constant width to the emerging sheet, which is then cut into jumbo sheets that are normally 3m x 6m in size [17].

Because of this production process, and in particular, as a result of floating onto the tin bath, the top and bottom glass surfaces are not identical: the upper surface in contact with the inert atmosphere (*air side*) is completely smooth with no defects whereas the bottom surface (*tin side*) that is in contact with the rollers will be flaw-free because these rollers can cause surface flaws that reduce the strength [22].

2.6 Glass types

Thanks to the *Float Process*, four glass variants can be produced and each of them are different in terms of strength. These types are, in ascending order of strength: annealed, heat strengthened, fully tempered and chemically toughened [17].

2.6.1 Annealed glass

Annealed glass (*ANG*) is also known as ordinary, or float glass and it is produced from *Float Process* without being subjected to further manufacturing processes. It is characterized by a smooth surface and no optical defects, but it is the weakest type in terms of bending strength.

It is not only impact damage that causes brittle fracture of basic annealed glass but also bending stresses, thermal stresses and imposed strains all cause elastic deformation that could also lead to fracture [17].

As regards the fracture pattern, it is a function of the energy stored inside the glass, i.e. of the residual stress and the stress due to loads [22].

Since residual stresses inside annealed glass are low, during the event of fracture, the number of cracks will be limited and then it will break into large and sharp-edged shards. Having large fragments implies a good post-failure performance and safety. Generally, the use of annealed glass as monolithic pane in buildings is restricted to small applications such as small windows, table tops and mirrors.

2.6.2 Heat strengthened glass

Heat strengthened glass (*HSG*) is also known as partially toughened or semi-tempered. It is basic annealed glass which is subjected to the tempering process: it consists of heating and a subsequent quenching phase. The tempering process, in the case of *HSG*, occurs with a lower cooling rate compared to the case of fully tempered glass, which will be discussed in the next paragraph.

The tempering has the effect of cooling and solidifying first the external surface of the pane and only after the interior part of the glass. As the interior cools it tries to shrink and then as a result, a parabolic stress profile is obtained through the thickness of the pane (see Figure 2-14).

More specifically, the external glass surfaces will be subjected to compressive stresses, where superficial flaws are present, while tensile stresses arise through the core of the glass pane. This has a beneficial effect because compressive residual stresses on the two glass surfaces can prevent the opening of superficial flaws.

Furthermore, since the cooling rate affects residual stresses- the higher is the cooling rate, the higher will be the residual stresses inside glass- it results in residual compressive stresses varying between 40 MPa and 80 MPa in HSG [22], [17].

Heat strengthened glass could be a good compromise between structural capacity, because of its tensile strength that is higher than annealed glass, and post-failure performance. The fracture pattern of heat strengthened glass is similar to annealed glass with much bigger fragments than for fully tempered glass [22].

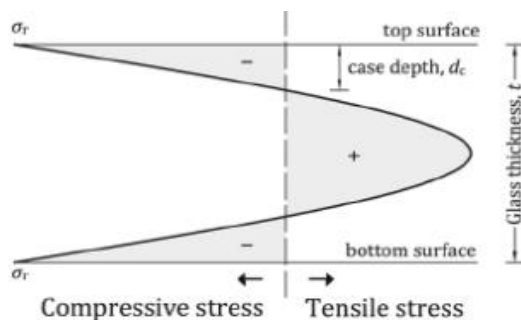


Figure 2-14: Residual stress profile through the thickness of heat strengthened glass ¹⁸.

Figure 2-15 shows the different fracture patterns of specimens loaded in a coaxial double ring test setup for different types of glass [22].

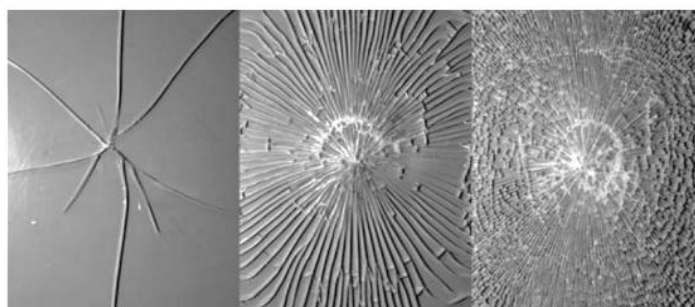


Figure 2-15: Comparison of the fracture pattern for different glass types: on the left annealed glass, in the middle heat strengthened glass and, on the right, fully tempered glass ¹⁹.

2.6.3 Fully tempered glass

The creation of fully tempered glass (FTG) follows a similar tempering process to that for heat-strengthened glass, with the major difference being that it is cooled more rapidly than heat-strengthened glass [17]. As said before, the external glass surfaces will solidify first, and only then the internal core of the pane, leading to compressive residual stresses on the external surfaces and a tensile state of stress through the thickness. In this regard, the difference with respect to heat strengthened glass lies in the compressive zone which is more extended rather than in heat strengthened glass (see Figure 2-16). The typical residual compressive surface stress varies between 80 MPa and 170 MPa for fully tempered soda lime silica glass [22].

¹⁸ Figure from: K. C. Datsiou, M. Overend, 'The Strength of Aged Glass', Glass Struct. Eng., Vol.2, pages:105–120, 2017, DOI:10.1007/s40940-017-0045-6.

¹⁹ Figure from: M. Haldimann, A. Luible, M. Overend, 'Structural Use of Glass', IABSE- AIPC – IVBH, 2008.

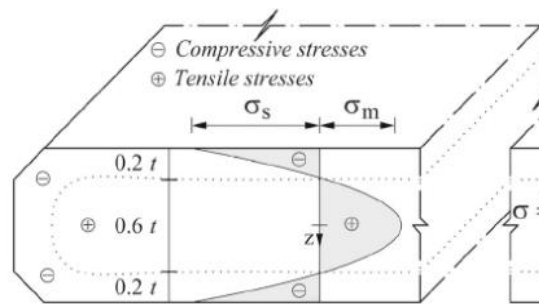


Figure 2-16: Stress distribution in fully tempered glass ²⁰.

The tempering process confers two benefits. Firstly, glass is stronger in bending because, both the thermally induced compressive stress and the inherent strength of basic annealed glass, must be overcome before failure occurs. Secondly, due to a higher cooling rate with respect to heat strengthened glass, fully tempered glass can store more elastic energy. So, in case of fracture, the high amount of stored energy is released in the form of many cracks, which can rapidly progress and repeatedly bifurcate, causing complete fragmentation in small and rounded pieces [17]. Own for such reason, fully tempered glass is also called “*safety glass*”, meaning that the small fragments could be theoretically less dangerous for people. Even small glass fragments falling from great heights can actually cause serious injury. In conclusion, while fully tempered glass has the highest structural capacity among all glass types, its post-failure performance is inadequate due to tiny fragments.

At last, a topic worth consideration is *nickel sulfide*-induced spontaneous failure: fully tempered glass elements show a small but not negligible risk of spontaneous breaking within a few years of production. The cause of it could be attributed to *nickel-sulfide (NiS)* inclusions, which cannot be avoided during the production of glass. These particles are particularly present in the internal core of the glass pane and, by increasing the temperature, they are able to expand in volume due to a change of phase. The combination of tensile stresses in the core of the glass pane and the volume expansion of *NiS* inclusions could lead to the spontaneous failure of fully tempered glass.

The risk of spontaneous failure cannot be totally eliminated, but only reduced, by means of the heat-soak test which can show the presence of *nickel-sulfide* particles by slowly heating glass and maintaining the temperature for several hours. If *NiS* inclusions are present inside, the glass will break [22].

2.6.4 Chemically toughened glass

Chemically toughened glass is a typology of glass that is rarely used in structural applications, which has not undergone thermal tempering process but chemical tempering. This alternative process involves the use of *potassium* ions, which are 30% bigger than *sodium* ions present on the surface of the glass pane, and during this process glass is submerged in a bath of *potassium salt* or *potassium nitrate* at 300°C. The bath is not hot enough to melt the glass, but the relatively high temperature allows the potassium nitrate to react with the surface of the glass, causing an exchange on the surface of sodium ions by potassium ions.

²⁰ Figure from: N. Pourmoghaddam, M. A. Kraus, J. Schneider, G. Siebert, ‘Relationship between strain energy and fracture pattern morphology of thermally tempered glass for the prediction of the 2D macroscale fragmentation of glass’, *Glass Struct. Eng.*, Vol.4, pages:257-275, 2019, DOI:10.1007/s40940-018-00091-1

As previously said, since potassium ions are bigger in volume than sodium ions, they are able to “compact” the crystal lattice, thereby strengthening the glass and creating large compressive stresses on both the surfaces [27].

The compressive state in chemical tempering affects only a very thin depth zone near the glass surface compared to thermal tempering process, as shown in Figure 2-17 [22]. This also implies that superficial microcracks can easily reach the glass zone subjected to tensile stresses, leading to failure.

Since the compressive state of stress affects only a very shallow zone through the thickness, the contribution of strain energy that could be stored is scarce. Considering that, rather than shattering into many small pieces, chemically toughened glass will break into larger shards that are not as sharp as untreated glass [27].

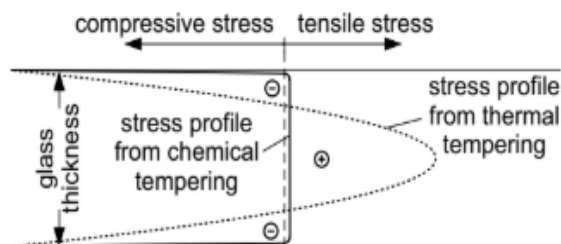


Figure 2-17: Comparison between thermal tempering stresses and chemical tempering one ²¹.

2.7 Laminated glass

Monolithic glass panes, due to their brittle behaviour after failure, cannot be used to make structural elements [28]. So, to improve post-breakage performance, the idea behind laminated glass is to take advantage of an assembly of glass panes and some polymeric interlayers which, in case of glass failure, are still able to keep together the glass fragments without spreading. Another advantage is related to the presence of several glass plies: if one ply were to break, there would be at least another one to carry the loads, still ensuring sufficient load-carrying capacity.

Laminated glass (LG) consists of two or more glass panes of equal or unequal thickness bonded together by some transparent plastic interlayer (see Figure 2-18) [22]. A particular manufacturing process, called lamination process, is needed to produce it. Glass panes and interlayers are introduced in an autoclave which can create vacuum, allowing it to develop a perfect adhesion between glass and interlayer. Then, the laminate is heated and pressed, achieving an edge seal, in order to prevent ambient air to enter again into the laminate [29].

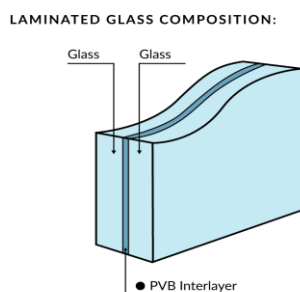


Figure 2-18: Cross section of laminated glass ²².

²¹ Figure from: M. Haldimann, A. Luible, M. Overend, 'Structural Use of Glass', IABSE- AIPC – IVBH, 2008.

²² Figure from: <https://dynamicfenestration.com/laminated-glass-benefits/> (Accessed Jan. 12,2024).

2.7.1 Typology and properties of polymeric interlayers

Six types of polymeric material are typically used to produce interlayers: *Polyvinyl Butyral (PVB)* which is the most common for laminated glass, *Ionoplastic polymers*, *Thermoplastic Polyurethane (TPU)*, *Ethylene Vinyl Acetate (EVA)* and *Polyester (PET)*.

Regarding *PVB*, the thickness of a single foil is 0,38 mm but, normally, two (0,76 mm) or four (1,52 mm) foils form one *PVB* interlayer [22]. In addition, in case of heat strengthened glass, it is possible to use even more than four *PVB* foils because of the non-perfectly flatness of the glass surface.

As mentioned before, polymeric interlayers can be categorized as a viscoelastic material. This type of material exhibits mechanical properties intermediate between those of viscous liquid and those of elastic solid. When a viscoelastic material is subjected to an applied stress, the response is composed of an elastic deformation (which stores energy) and a viscous flow (which dissipates energy) [30]. The physical properties of viscoelastic materials are not constant over the time, but they could strongly vary according to the load duration and the temperature. For instance, at room temperature, *PVB* is comparatively soft with an elongation at breakage of more than 200% [22].

Some typical physical properties of *PVB* interlayer can be read in Table 2-4.

Table 2-4: Physical properties of *PVB* interlayer²³.

Property	Notation	Unit of measurement	PVB
Density	ρ_{PVB}	kg/m ³	1070
Shear modulus	G	GPa	0-4
Poisson's ratio	ν	-	≈ 0,50
Coefficient of thermal expansion	α_T	10 ⁻⁶ K ⁻¹	80
Tensile strength	$f_{t,PVB}$	MPa	≥ 20
Elongation at failure	ϵ_t	%	≥ 300

The most important mechanical parameter characterizing *PVB* interlayer is undoubtedly its shear modulus G , which varies within a range between 0 GPa and 4 GPa. The large variability of shear modulus is attributable to the physical properties, which in turn, depend on load duration and temperature. Figure 2-19 shows the evident dependency of the shear modulus G from the load duration time for two different temperatures, in the case of *PVB* and *ionoplast* interlayers.

The knowledge of the shear modulus is fundamental in the design of laminated glass, since it affects the bonding between the layers, and consequently, the stress profile through the thickness of the entire pane.

²³ Table from: M. Haldimann, A. Luible, M. Overend, 'Structural Use of Glass', IABSE- AIPC – IVBH, 2008.

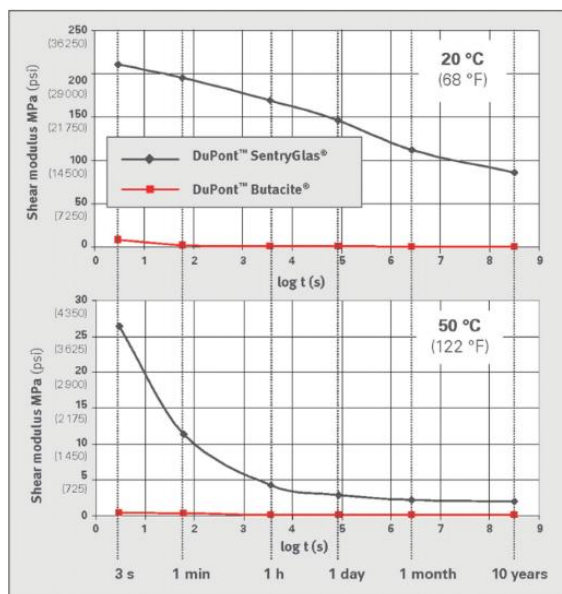


Figure 2-19: Shear modulus variation as function of the load duration for PVB (Butacite®) and ionoplast (SentryGlas®) interlayers²⁴.

2.7.2 Structural behaviour of laminated glass

The structural behaviour of laminated glass depends on the type(s) of glass used and on the properties of the interlayer [17]. Depending on the coupling degree between the glass plies, provided by the interlayer, it is possible to distinguish between two limit behaviours: monolithic limit and layered limit.

In the case of monolithic limit behaviour, the interlayer is characterized by a high- tending to infinity- value of the shear modulus G , which implies full bonding between the layers, and so the interlayer is able to completely transfer shear stresses from the top layer to the bottom one. In this case, the laminated glass element behaves as a monolithic body in which no sliding between the layers is allowed. The stress profile through the thickness of the layers will be therefore unique and bi-triangular. Generally, for PVB and resin interlayer materials, short-term out-of-plane loads can be resisted by both laminates acting compositely, achieving a monolithic behaviour [17], as shown in Figure 2-20.

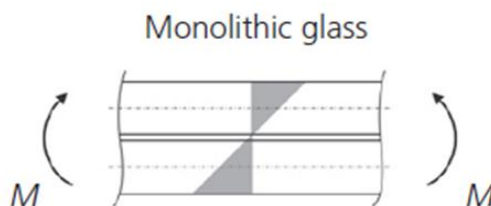


Figure 2-20: Stress profile due to bending stresses in case of monolithic limit²⁵.

In the case of layered limit behaviour, on the other hand, the shear stiffness of the interlayer is considered so low, such that, there is no connection at all between layers and interlayer, i.e. no shear coupling, thereby each glass ply behaves as if it was alone. The stress profile through the thickness of the layers is bi-triangular, but, no longer unique for the entire element: each layer is featured by its own stress profile (see Figure 2-21).

²⁴ Figure from: C. O' Regan and Institution of Structural Engineers, 'Structural Use of Glass in Buildings (2nd edition)', IStructE Ltd, 2015.

²⁵ Figure from: K. Langosch and M. Feldmann, 'Design of Pane-Like Laminated Glass Columns', Structures and Buildings Vol. 169, Jun. 2016, pages:403–415, DOI:10.1680/jstbu.13.00117.



Figure 2-21: Stress profile due to bending stresses in case of layered limit ²⁶.

The actual structural behaviour of laminated glass is however in between these two limit conditions, namely partial composite effect, since the polymeric interlayer is not able to provide a full adhesion between the layers (see Figure 2-22).



Figure 2-22: Stress profile due to bending stresses in case of partial composite effect ²⁷.

2.8 Material properties

The basic *soda lime silica* glass properties used in design process are specified in *UNI CEN/TS 19100-1: 2021*, Section 5.1 Technical Specifications [31] and are shown in Table 2-5.

Table 2-5: Physical and mechanical properties of soda lime silicate glass ²⁸.

Property	Notation	Unit of measurement	Soda lime silica glass
Glass density	ρ_g	kg/m ³	2500
Young's modulus	E	MPa	70000
Poisson's ratio	ν	-	0,23
Coefficient of linear thermal expansion	α_T	10 ⁻⁶ K ⁻¹	9

²⁷ Figure from: K. Langosch and M. Feldmann, 'Design of Pane-Like Laminated Glass Columns', Structures and Buildings Vol. 169, Jun. 2016, pages:403–415, DOI:10.1680/jstbu.13.00117.

²⁸ Table from: UNI CEN/TS 19100-1: 2021, page:18, 2021.

In addition, the Standard *UNI CEN/TS 19100-1: 2021* [31] also recommends, in the aforementioned paragraph, the values of characteristic bending strength for different typologies of glass, presented in Table 2-6.

Table 2-6: Characteristic strength of different glass types²⁹.

Type of glass	Notation	Unit of measurement	Characteristic strength
Annealed (ANG)	$f_{g,k}$	MPa	45
Heat strengthened (HSG)	$f_{b,k}$	MPa	70
Thermally toughened (FTG)	$f_{b,k}$	MPa	120
Chemically toughened	$f_{b,k}$	MPa	150

2.9 Glass Standards

In the last decades, glass has been used further and further in construction field as load-bearing element such as fins, glazing façades, walls and roofings. Structural applications of glass have led Competent Authority to initially develop and publish technical guidelines and manuals to allow engineers to perform structural verifications, but only later, some Technical Standards with the aim of guarantee certain levels of safety.

A brief overview of the glass Standard used in this thesis is presented in this section.

The European Technical Specifications *UNI CEN/TS 19100-1: 2021* – “Design of glass structures” is subdivided into three parts. The first part introduces the basis of glass design and material such as glass properties, design limit states, design bending strength resistances and general structural provisions. The second and third parts aim to address the definition of the effective thickness, resistance and verifications at limit states of glass elements, respectively for, out-of-plane and in-plane loads.

Historically, the presence of numerous national regulations about glass in buildings (see Figure 2-23) - some of which are incomplete or contradictory – has often resulted in structural glass designs which can only be realised with special approvals [32]. It encouraged a more pan-European approach in structural glass design, similar to what has existed for other construction materials since the 1990s [32]. To harmonize the Standards and the design methods about glass, the European Commission gave a mandate to create a new generation of Eurocodes, including the creation of a new Eurocode for the Design of Glass Structures named *CEN/TS 19100* [32].

²⁹ Table adapted from: *UNI CEN/TS 19100-1: 2021*, page:19, 2021.

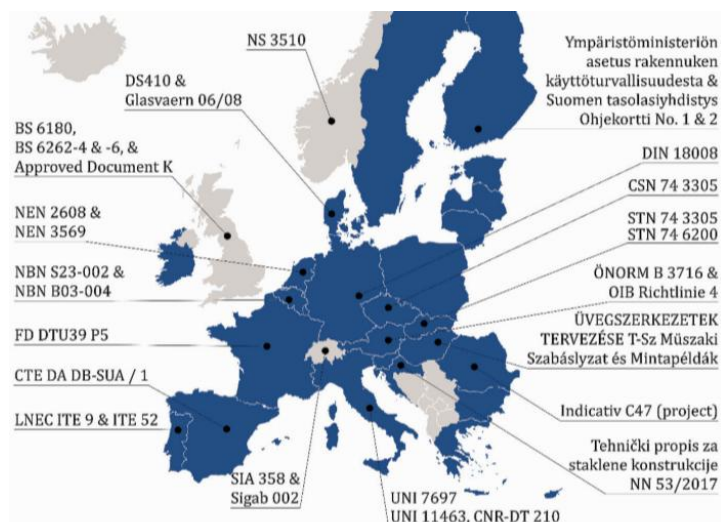


Figure 2-23: General view of current European Standards related to glass in buildings³⁰.

2.10 Global instability of in-plane loaded slender elements: flexural buckling phenomena

The compressive strength of glass, as already mentioned, is significantly higher than its tensile strength and this has paved the way for glass structural applications in being used as columns, shear panels, beams and fins. Since glass elements are generally very slender, at least in one direction, they could undergo buckling phenomena and collapse by reaching earlier tensile strength rather than compressive one.

The loss of stability of elastic equilibrium is commonly referred to as buckling and it is one of the three fundamental phenomena of structural collapse, the other two are general yielding and brittle fracturing [33].

Buckling can be defined as the behaviour in which a structure or a structural element suddenly deforms in a (buckling) plane different to the original (pre-buckling) plane of loading and response [34].

It should be emphasized that, unlike steel, in glass members buckling verification must be checked on the tension side. Buckling, in fact, can lead to failure because of tensile stresses which could overcome its bending strength. Conversely, buckling verification in steel members must be checked on the compressive side.

According to bifurcation buckling models which are based on linear elastic stability theory, a geometrically straight and perfectly elastic member subjected to an increasing in-plane load will suddenly fail when the critical load is reached. The name bifurcation model stems from the fact that, at the beginning, the element is perfectly straight (without imperfections) and by increasing the in-plane load, no lateral displacement occurs. Keeping increasing the compressive load, bifurcation suddenly occurs when the critical load is reached and, after bifurcation, an instable path, i.e. buckling, is followed (see horizontal path n° 2 in Figure 2-24).

Real members are not perfectly straight, but they are always characterized by geometric initial imperfections due to the industrial production processes. Therefore, in displacement vs axial load diagram, instead of starting from null initial deformations, the analysis of real members has to start from an initial displacement w_0 . It is possible to observe that the behaviour of a real member, in the aforementioned diagram, is non-linear, asymptotically tending to the ideal behaviour of a perfect element (Figure 2-25).

³⁰ Figure from: M. Feldmann, M. Laurs, J. Belis et al., 'The New CEN/TS 19100: Design of Glass Structures', Glass Struct. Eng., Vol.8, pages:317-337, 2023, DOI: 10.1007/s40940-023-00219-y.

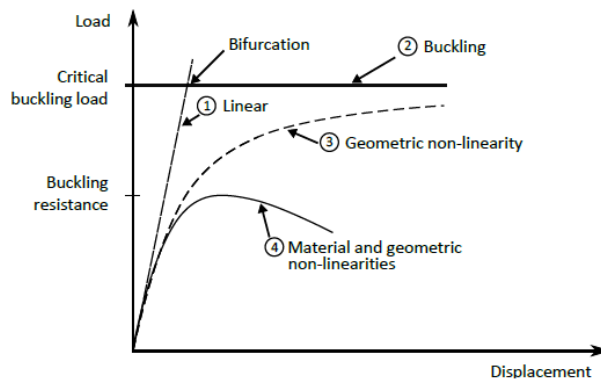


Figure 2-24: Behaviour of perfect and imperfect members under compressive loads. Based on [34]³¹.

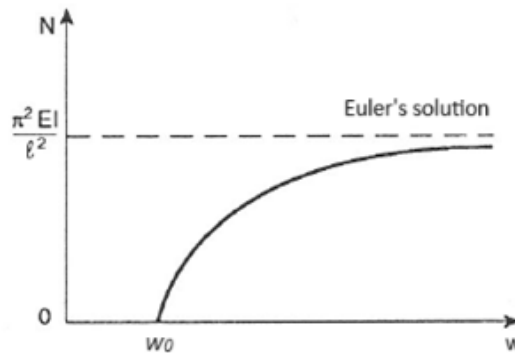


Figure 2-25: Non-linear behaviour of a real member in compression (solid curve) ³².

2.10.1 Euler's buckling theory

Historically, analysing the problem of elastic equilibrium of a perfectly straight slender beam, the solution was derived by the mathematician *Leonhard Euler* in 1744 and is the elastic critical buckling load $N_{cr,EU}$, also named *Euler's critical load*.

The Euler's critical load is the load at which a member suddenly buckles in another plane with respect to the loading one.

The Euler's theory is based on some key assumptions: the material must be isotropic, homogeneous and linear elastic; the member must be perfectly straight, and the cross-section must be very small compared to the length of the member.

Under these hypotheses, the Euler's critical load reads:

$$N_{cr,EU} = \frac{\pi^2 EI}{L_b^2} \quad (2.1)$$

³¹ Figure from: D. Sonck, 'Global Buckling of Castellated and Cellular Steel Beams and Columns', Ph.D. Thesis at Ghent University, page: 51, 2014.

³² Figure adapted from: A. Carpinteri, 'Advanced Structural Mechanics', CRC Press Taylor & Francis Group, 2016.

Where:

- $N_{cr,EU}$ is the Euler's buckling load.
- E is the Young's modulus of the member.
- I is the moment of inertia.
- L_b is the free length of deflection of the member or buckling length.

L_b is the distance between the deflection points and depends on the static scheme assumed for the member, as shown in Figure 2-26.



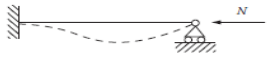

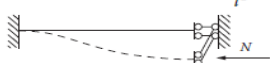

Kinematic conditions	Static conditions	Critical load (N_{cr})	Free length of deflection (L_b)
$l = \text{Beam length}$ $v(0) = 0$ $v(l) = 0$		$\pi^2 \frac{EI}{l^2}$	l
$v(0) = 0$ $v'(0) = 0$		$\pi^2 \frac{EI}{4l^2}$	$2l$
$v(0) = 0$ $v'(0) = 0$		$-2\pi^2 \frac{EI}{l^2}$	$\frac{l}{\sqrt{2}}$
$v(0) = 0$ $v'(0) = 0$		None $4\pi^2 \frac{EI}{l^2}$	$\frac{l}{2}$
$v(0) = 0$ $v'(0) = 0$		$\pi^2 \frac{EI}{l^2}$	l
$v(0) = 0$ $v'(0) = 0$		$\pi^2 \frac{EI}{4l^2}$	$2l$

Figure 2-26: Free length of deflection for different static schemes³³.

It is possible to define the Euler's critical pressure or critical stress (σ_{cr}) as:

$$\sigma_{cr} = \frac{N_{cr,EU}}{A} \quad (2.2)$$

Where A defines the cross-sectional area of the element.

Then, by substituting (2.1) in (2.2), the equation holds in other form:

$$\sigma_{cr} = \frac{\pi^2 EI}{L_b^2 A} = \pi^2 E \frac{\rho^2}{L_b^2} = \frac{\pi^2 E}{\lambda^2} \quad (2.3)$$

Where:

$\rho = \sqrt{I/A}$ is the radius of gyration of the cross-section.

$\lambda = L_b/\rho$ is the slenderness ratio.

³³ Figure from: A. Carpinteri, 'Advanced Structural Mechanics', CRC Press Taylor & Francis Group, 2016.

By plotting the Equation (2.3) for different values of slenderness ratio on a graph $\lambda - \sigma_{cr}$, the Euler's hyperbola is obtained (see Figure 2-27) and it can be observed that, for very large values of slenderness ratio, the critical stress tends to zero – as expected for slender members – whereas for very low values of slenderness ratio, the critical stress tends to infinity. The critical stress, obviously, cannot tend to infinity since there is a limit represented by the material strength, thereby a cut-off must be introduced, and it corresponds to the yielding stress (f_y).

Figure 2-27 also shows the presence of two different failure zones: in the yielding zone, failure occurs when the yielding strength is exceeded whereas, in the buckling zone, failure occurs only if the slenderness ratio of the member is larger than the critical one, i.e. λ_{lim} , and at the same time, the critical pressure is smaller than the yielding stress.

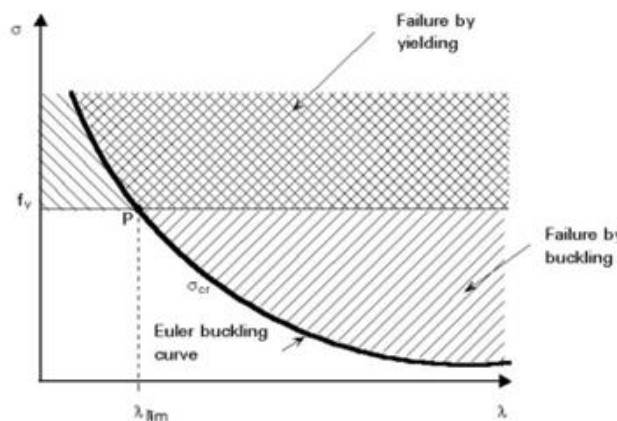


Figure 2-27: Euler's buckling curve and failure zones ³⁴.

As already stated, Euler's hyperbola provides the theoretical behaviour of an element which is perfectly straight, without any initial geometric imperfection. But the effect of the imperfections has a relevant impact on the critical load, since real members buckle before reaching the Euler's critical load. So, the actual behaviour of imperfect members is provided by the Johnson's parabola, which represents a smooth transition between the two critical curves: Euler's hyperbola and cut-off. Figure 2-28 shows the Johnson's parabola (dotted curve) and the Euler's buckling curve (solid curve).

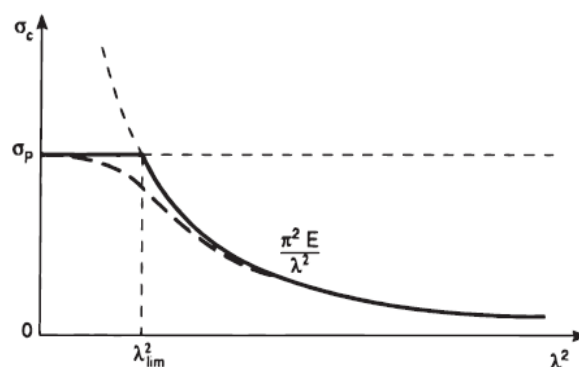


Figure 2-28: Buckling behaviour of imperfect members ³⁵.

³⁴ Figure adapted from: <https://fgg-web.fgg.uni-lj.si/~pmoze/esdep/master/wg07/I0510.htm> (Accessed Jan.30, 2025)

³⁵ Figure from: A. Carpinteri, 'Advanced Structural Mechanics', CRC Press Taylor & Francis Group, 2016.

3 GLASS DESIGN AND BUCKLING CALCULATION

In this chapter, some peculiar features of glass design, such as the design strength and the concept of effective thickness are outlined, and subsequently, the problem of buckling for laminated glass.

3.1 Design bending strength of glass

According to the Standard *UNI CEN/TS 19100-1* [31], the determination of glass bending strength ($f_{g,d}$) is through a stress-based criterion and not applying fracture mechanics failure criteria, since the latter one is complex, and the size of the most critical cracks is currently unknown.

The design value of glass strength $f_{g,d}$ is thus defined as:

$$f_{g,d} = k_e \cdot k_{sp} \cdot \lambda_A \cdot \lambda_1 \cdot k_{mod} \cdot \frac{f_{g,k}}{\gamma_M} + k_p \cdot k_{e,p} \cdot \frac{f_{b,k} - f_{g,k}}{\gamma_p} \quad (3.1)$$

Where:

k_e	is the edge or hole finishing factor.
k_{sp}	is the surface profile factor.
λ_A	is a factor which considers size effect.
λ_1	is another factor which considers size effect.
k_{mod}	is the modification factor.
$f_{g,k}$	is the characteristic bending strength of annealed glass.
γ_M	is the material partial safety factor.
k_p	is the pre-stressing process factor.
$k_{e,p}$	is the edge or hole pre-stressing factor.
$f_{b,k}$	is the characteristic value of glass strength after a strengthening treatment.
γ_p	is the partial factor for pre-stress on the surface.

It is noteworthy that the abovementioned formula is composed of a first term that is related to the characteristic bending strength of annealed glass ($f_{g,k}$) and a second term which refers to the characteristic value of glass strength after a strengthening process ($f_{b,k}$). Furthermore, the presence of various material and surface treatment factors is due to the brittle nature of glass. All the factors and their values present in the glass design bending strength formula are available in the Annex A of this document.

3.2 Enhanced Effective Thickness Theory

With the purpose of design, at least in a preliminary design stage, it could be convenient and simple to use the *Enhanced Effective Thickness approach (EET)* which was developed by *L. Galuppi* and *G. Royer-Carfagni* [35], and suggested in the Standard *CEN/TS 19100*. The effective thickness of a laminated glass plate is defined as the (constant) thickness of a monolithic plate that, under the same boundary and load conditions, presents a similar maximum stress or maximum deflection [35].

The Standard *CEN/TS 19100-2* [36] provides two different formulas to compute the equivalent thickness for calculating out-of-plane bending stress of ply "*i*" ($h_{ef,\sigma,i}$) and the equivalent thickness for calculating out-of-plane bending deflection ($h_{ef,w}$).

The effective thickness for out-of-plane bending deflection $h_{ef,w}$ can be calculated as:

$$h_{ef,w} = \sqrt[3]{\frac{1}{\frac{\eta}{\sum_{i=1}^n h_i^3 + 12 \cdot \sum_{i=1}^n (h_i \cdot d_i^2)} + \frac{1-\eta}{\sum_{i=1}^n h_i^3}}} \quad (3.2)$$

Where:

- η is the coupling parameter coefficient.
- h_i is the nominal thickness of the i -th glass ply.
- d_i is the distance of the mid-plane of the i -th glass ply from the mid-plane of the laminated glass.

For further details concerning coupling parameter η , please refer to Annex B.

The effective thickness of the ply “ i ” of the laminated glass pane for out-of-plane bending stress calculation $h_{ef,\sigma,i}$ can be calculated as follows:

$$h_{ef,\sigma,i} = \sqrt[2]{\frac{1}{\frac{2 \cdot \eta \cdot |d_i|}{\sum_{i=1}^n h_i^3 + 12 \cdot \sum_{i=1}^n (h_i \cdot d_i^2)} + \frac{h_i}{h_{ef,w}^3}}} \quad (3.3)$$

Where all the parameters have been already defined above.

The geometrical parameters (h_i and d_i) presented in the effective thickness formulas are shown in Figure 3-1:

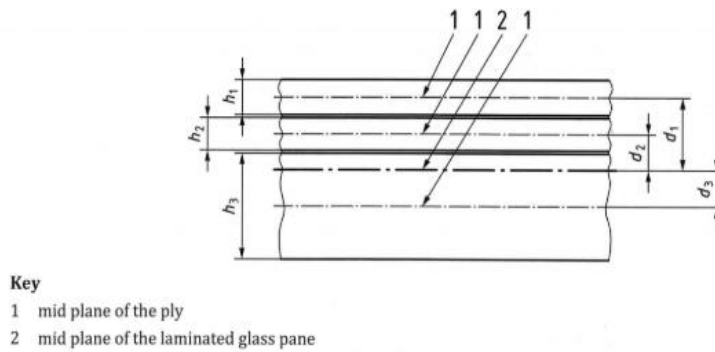


Figure 3-1: Geometrical parameters of a laminated glass cross-section ³⁶.

³⁶ Figure from: UNI CEN/TS 19100-2: 2021, page:19, 2021.

3.3 Buckling load for laminated glass

The elastic buckling load for laminated glass ($N_{cr,LG}$), as stated in Annex A of the Standard *CEN/TS 19100-3* [37], can be computed using the Euler's formula as:

$$N_{cr,LG} = \frac{\pi^2 E_g I_{z,eff}}{L_b^2} \quad (3.4)$$

Where:

- $N_{cr,LG}$ is elastic critical buckling load for laminated glass.
- E_g is the Young's modulus of glass.
- $I_{z,eff}$ is the effective moment of inertia about the minor or weak axis (z-axis).
- L_b is the buckling length.

The buckling length (L_b) depends on the restraints of the glass element, e.g. for a simply supported static scheme, the buckling length corresponds to the entire length of the element itself, as shown in Figure 3-2:

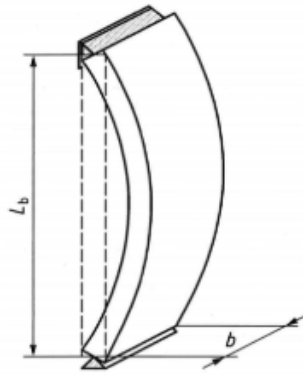


Figure 3-2: Buckling length of a simply supported glass element in compression ³⁷.

It is also necessary to compute the effective moment of inertia about the minor axis ($I_{z,eff}$), whose formula is presented in Annex B of the Standard *CEN/TS 19100-3* [37].

If the shape of the lateral deflection component is sinusoidal, the effective moment of inertia may be calculated for a symmetric double or triple layered laminated cross-section as follows [37]:

$$I_{z,eff} = \frac{\sum I_i}{1 - \frac{\Psi \cdot \beta \cdot K_s}{\left(\frac{\pi}{L}\right)^2 + \alpha^2}} \quad (3.5)$$

³⁷ Figure from: UNI CEN/TS 19100-3: 2021, Annex A, page:29, 2021.

All the parameters inside equation (3.5) are given in Table 3-1.

Table 3-1: Parameters necessary to compute the effective moment of inertia $I_{z,eff}$ ³⁸.

Parameter	Formula
K_s	$\frac{G_L}{t} B$
α^2	$\frac{K_s}{E} \left(\frac{(z_1 + z_2)^2}{I_1 + I_2} + \frac{1}{A_1} + \frac{1}{A_2} \right)$
β	$\frac{(z_1 + z_2)}{E_g(I_1 + I_2)}$
ψ	$(z_1 + z_2)$

Finally, the parameters z_1 and z_2 can be seen in Figure 3-3:

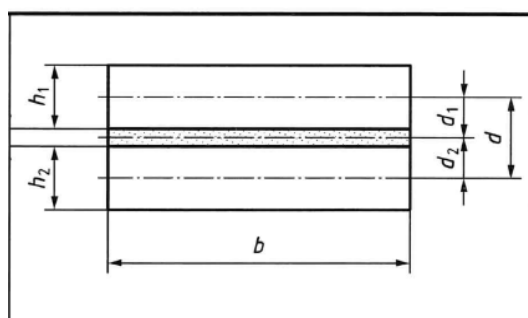


Figure 3-3: Geometrical parameters of a double-layered laminated glass cross-section³⁹.

It is worth pointing out that, in the Standard UNI CEN/TS 19100, there are sometimes some inconsistencies between symbols used in formulas and those used in figures. To dispel the doubts, the parameters contained in Table 3-1 are the following:

- G_L is the shear modulus of the interlayer and corresponds to G in this document.
- t is the thickness of the interlayer (most frequently it is denoted as h_{int}).
- B is the width of the glass pane and corresponds to the symbol “ b ” of Table 3-1.
- E_g is the Young’s modulus of glass.
- z_1 is the distance of the mid-plane of the glass ply 1 from the mid-plane of the laminated glass and corresponds to the symbol “ d_1 ” of Table 3-1.
- z_2 is the distance of the mid-plane of the glass ply 2 from the mid-plane of the laminated glass and corresponds to the symbol “ d_2 ” of Table 3-1.
- I_1 is the moment of inertia of glass ply 1.
- I_2 is the moment of inertia of glass ply 2.
- A_1 is the cross-sectional area of glass ply 1.
- A_2 is the cross-sectional area of glass ply 2.

³⁸ Table from: UNI CEN/TS 19100-3: 2021, Annex B, page:31, 2021.

³⁹ Figure from: UNI CEN/TS 19100-3: 2021, Annex B, page:31, 2021.

4 SECOND-ORDER THEORY AND BUCKLING ANALYSIS

This chapter is devoted to provide notions regarding initial imperfections of glass members, geometric nonlinearity and buckling analysis.

4.1 Effect of initial imperfections

Glass, similar to other materials, is characterized by having initial imperfections due to manufacturing processes. For this reason, some specific tolerances, in terms of thickness of the pane, must be respected. For instance, the tempering process used to produce heat strengthened and fully tempered glass induces a small curvature of the external surface of the plate. The size of deformations depends on type of glass (coated glass, patterned glass etc.), on glass dimensions and aspect ratio, on nominal thickness and on type of tempering process (vertical or horizontal) [38]. As shown in Figure 4-1, thermal treatments can result in four types of imperfections: global bow that is the overall curvature of the pane (a), roller wave distortion in which the surface is not perfectly flat, but some “waves” are present (b), deformation of edges (c) and local bow (d).

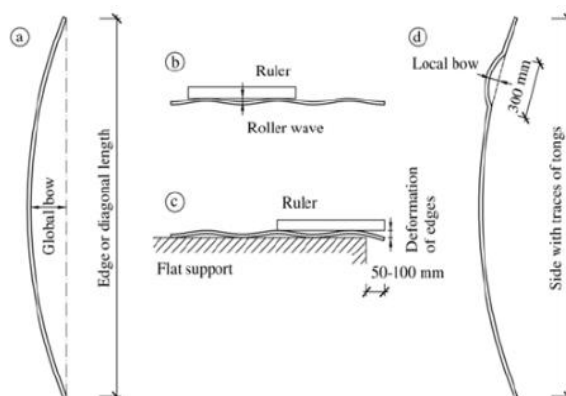


Figure 4-1: Types of initial imperfections affecting glass elements ⁴⁰.

Furthermore, an extended experimental campaign performed by *Belis et al.* [39] on 312 glass beams with variable length, height, thickness and glass type highlighted that the sinusoidal shape describes the initial imperfection in monolithic or laminated glass beams with a good level of accuracy [40].

The Standard for glass structures *CEN/TS 19100-3:2021* requires that for in-plane loaded glass components, in the structural analysis, the effects of imperfections must be considered since the buckling behaviour may be influenced by geometrical and material imperfections [37]. So, according to the aforementioned Standard, initial imperfections can be replaced by one basic imperfection e_0 , whose formula reads:

$$e_0 = \sqrt{e_{0,length}^2 + e_{0,installation}^2} \quad (4.1)$$

Where:

- $e_{0,length}$ considers the imperfection concerning the length of the element.
- $e_{0,installation}$ considers the deviation of the glass pane from unexpected eccentric loads.

⁴⁰ Figure from: Ondrej Pesek et al., ‘On the Problem of the Imperfections of the Structural Glass Members Made of Flat Glass’, IOP Conf. Ser.: Mater. Sci. Eng. 471 052042, pages:2-3, 2019, DOI: 10.1088/1757-899X/471/5/052042.

The two parameters $e_{0,length}$ and $e_{0,installation}$ assume different values according to the type of buckling phenomena, and for flexural buckling, it holds:

Table 4-1: Calculation of basic imperfection parameter e_0 ⁴¹.

Type	Buckling length L_b	$e_{0,length}$	$e_{0,installation}$
Flexural buckling and plate buckling	Distance of inflexion points in the relevant critical mode in direction of the applied load	$\frac{L_b}{333}$	$\frac{h_e}{2}$

4.2 Geometric nonlinearity

As basic assumption, Technical Specifications *UNI CEN/TS 19100-1* states that the structural analysis of a glass element must be performed using an appropriate structural model with adequate boundary conditions and loads and that is able to reflect glass structural behaviour [31]. One relevant aspect characterizing glass behaviour is geometric nonlinearity (also called *second-order effects*), which could affect its structural performance.

Three different forms of nonlinearity exist: material, geometric and finally boundary (or contact) nonlinearity. In this paragraph, only geometric nonlinearity is going to be explained, as it is of interest regarding the problem of global instability affecting structural glass. The term geometric nonlinearity refers to the deviation from linearity in the geometry of a structure when subjected to significant loads or displacements, and this deviation arises due to the large rotations, translations, and strains experienced by the structure [41]. This is the case of glass, in fact, glass elements are generally slender, at least in one dimension, and the polymeric interlayer is quite compliant such that they can undergo large deflections.

4.3 Linear buckling analysis (LBA)

Linear buckling analysis (*LBA*) or Eigenvalue analysis is a technique that can be applied to relatively "stiff" structures to estimate the maximum load that can be supported prior to structural instability or collapse [42]. It is indeed defined as materially linear to mean that the stress-strain law is linear and also geometrically linear, i.e. no imperfections.

In this kind of analysis, it is only possible to predict the theoretical value of the elastic buckling load, which will coincide with that obtained by means of Euler's formula, as it does not take into consideration any sort of material and geometric imperfection or nonlinear behaviour.

A benefit of using linear buckling analysis consists in lower computational costs compared to nonlinear analysis. However, on the other hand, it must be recalled that *LBA* is less conservative, as it will overestimate the overall structural capacity by not accounting for imperfections.

⁴¹ Table from: UNI CEN/TS 19100-3: 2021, page:17, 2021.

Linear buckling analysis is an eigenvalue problem which can be stated as:

$$([K] + BLF_i[K_g])\{\Phi_i\} = \{0\} \quad (4.2)$$

Where:

- $[K]$ is the stiffness matrix.
- BLF_i is the eigenvalue, also named buckling load factor multiplier.
- $[K_g]$ is the stress stiffness matrix.
- $\{\Phi_i\}$ is the eigenmode or buckling mode shape, i.e. normalised displacement.

The basic assumptions of linear buckling analysis are the following: the linear stiffness matrix $[K]$, which relates the applied forces to the nodal displacements, does not change prior to buckling and the stress stiffness matrix $[K_g]$ is simply a multiple of its initial value. Accordingly, *LBA* can only be used to predict the load level at which a structure becomes unstable, considering that pre-buckling displacements have negligible influence on the structural response (i.e. hypothesis of small displacements is still valid) [42]. Since displacements are small, changes in the geometry can be considered negligible, and therefore it is possible to impose equilibrium equations considering the undeformed configuration of the element.

In every buckling analysis on a *FE* software, both linear and nonlinear, an iterative algorithm is used to extract eigenvalues and eigenmodes [43], and so, the critical buckling load $N_{cr,FEA}$ can be also defined as follows:

$$N_{cr,FEA} = P_0 \cdot BLF \quad (4.3)$$

Where:

- $N_{cr,FEA}$ is the buckling load obtained from *FE* analysis.
- P_0 is the initial applied compressive load.
- BLF is the eigenvalue or buckling load factor multiplier.

The eigenvalue is, in effect, a safety factor for the structure against buckling. An eigenvalue less than 1,0 indicates that a structure has buckled under the applied loads, conversely an eigenvalue greater than 1,0 indicates that the structure will not buckle [43].

4.4 Geometrically nonlinear buckling analysis (GNA)

In nonlinear analysis there is the possibility of accounting for material and/or geometric nonlinearity (second-order effects), which are always present in reality. In real and slender members, due to nonlinearity, buckling occurs earlier than classic Euler's buckling load predicts because the strength of the member is reduced (see Figure 4-2).

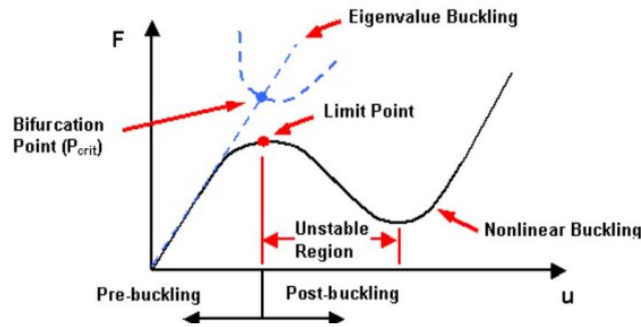


Figure 4-2: Linear vs nonlinear buckling ⁴².

In nonlinear problems the relationship between load and displacement is usually nonlinear and the stiffness matrix is not constant, but it is continuously updated at each step. Since displacements, in nonlinear analysis, may be large- the assumption of small displacements or similarly small rotations is no longer valid- then equilibrium equations must be imposed in the deformed state and by doing so, additional bending moments, called *second-order moments*, will arise with the effect of reducing internal stresses (see Figure 4-3). This is beneficial, since the actual stress will be less if compared to the one computed with linear analysis and also allows to optimize the design, avoiding being too overly conservative.

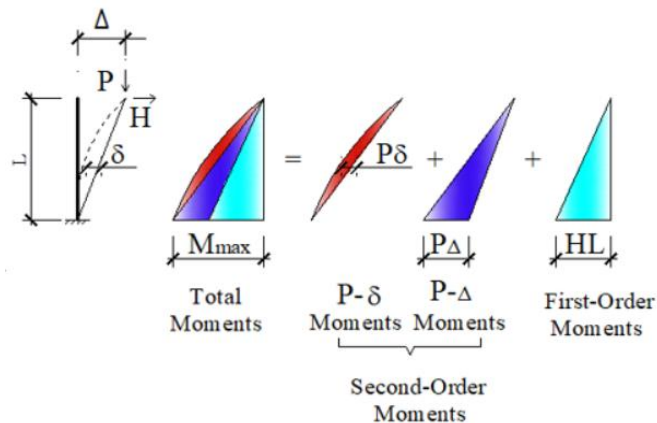


Figure 4-3: Second order bending moments in a compressed cantilever beam ⁴³.

⁴² Figure from: <https://www.researchgate.net/post/Arc-length-method-for-non-linear-buckling-Nonlin-FEM-in-ANSYS-Is-there-any-way-I-can-continue-the-Simulation-beyond-the-critical-point> (Accessed Jan. 28, 2025).

⁴³ Figure from: <https://axisvm.eu/docs/sources-of-non-linearity/> (Accessed Jan. 19,2025).

4.4.1 Geometrically nonlinear problem in monolithic glass

Let's consider the problem of buckling in monolithic glass columns (1D element) introducing second-order effects, as illustrated in Figure 4-4.

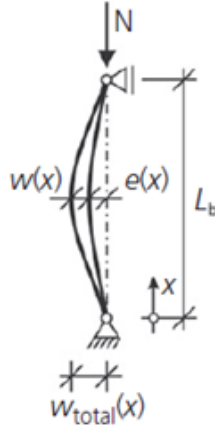


Figure 4-4: Simply supported column with initial imperfection and subjected to compressive force ⁴⁴.

The total deflection in the middle of a bar of length L_b pinned at both ends, with an initial sinusoidal imperfection at midspan $e_{initial}$ and axial compressive load N , can be written as:

$$w_{total}(x) = w(x) + e(x) = e_{initial} \cdot \frac{1}{1 - \frac{N}{N_{cr,MG}}} \cdot \sin\left(\frac{\pi x}{L_b}\right) \quad (4.4)$$

Where:

- $w_{total}(x)$ is the total deflection along the length of glass column.
- $w(x)$ is the bending deflection along the length of glass column due to the axial force.
- $e(x)$ is the initial (effective) imperfection along the length of glass column.
- $e_{initial}$ is the initial (effective) imperfection in the middle of glass column.
- N is the applied compressive load.
- $N_{cr,MG}$ is the Euler's critical buckling load for monolithic glass.
- L_b is the buckling length of glass column.
- x is the coordinate along length of glass column.

By enforcing the equilibrium in the deformed configuration between the reactive moment, which is the bending moment due to curvature of the glass column $w(x)$, and the external moment that considers the contributions of $e_{initial}$ and $w(x)$, a 2nd order differential equation is obtained:

$$E_g I_{MG} \frac{d^2 w(x)}{dx^2} + N \left[e_{initial} \sin \frac{\pi x}{L_b} + w(x) \right] = 0 \quad (4.5)$$

⁴⁴ Figure adapted from: K. Langosch and M. Feldmann, 'Design of Pane-Like Laminated Glass Columns', Structures and Buildings, Vol. 169 Issue SB6, pages:403–415, 2016, DOI: 10.1680/jstbu.13.00117.

Where:

- E_g is the Young's modulus of glass.
- I_{MG} is the moment of inertia of monolithic glass cross-section.

All the other parameters have been previously defined.

It is now possible to compute normal stresses $\sigma(x)$ by means of Navier's formula:

$$\sigma(x) = \frac{N}{A_{MG}} \pm \frac{N}{W_{MG}} \cdot (e_{initial} + w(x)) = \frac{N}{A_{MG}} \pm \left[\frac{N \cdot e_{initial}}{W_{MG}} \cdot \frac{1}{1 - \frac{N}{N_{cr, MG}}} \cdot \sin\left(\frac{\pi x}{L_b}\right) \right] \quad (4.6)$$

Where:

- A_{MG} is the cross-sectional area of monolithic glass.
- W_{MG} is the elastic section modulus of monolithic glass.

All the other parameters have been already defined.

Buckling verification must be then checked for both compressive and tensile cases: it is possible to compute two acting maximum stresses by means of Navier's formula: one positive (σ^+), due to the positive contribution of bending moment, and one negative (σ^-), due to the negative contribution of the compressive load. Immediately after, the two maximum stresses can be compared with respect to glass tensile strength ($f_{g,d}$) and glass compressive strength ($f_{u,c}$). If the two acting maximum stresses σ^+ and σ^- are lower than the tensile and compressive glass strength, then, buckling verification is fulfilled, as shown in Table 4-2.

Anyway, since the compressive glass strength is much higher than the tensile one, the attention is usually addressed to the buckling verification towards tensile glass strength.

Table 4-2: Buckling verification.

Buckling verification	
Tensile case	Compressive case
$\sigma^+ \leq f_{g,d}$	$ \sigma^- \leq f_{u,c}$

4.4.2 Geometrically nonlinear analysis in FEA

In the Finite Element software, *LUSAS*, four different geometrically nonlinear formulations are available: Total Lagrangian formulation, Updated Lagrangian formulation, Eulerian formulation and finally Co-rotational formulation.

In Total Lagrangian formulation all the variables are referred to the undeformed configuration while in the Updated formulation they are referred to the configuration obtained at the last converged solution. Both are based on Green-Lagrange strains which are only applicable to small strains.

A Lagrangian approach tends to be preferred in structural problems where it is required to monitor the path of a particular particle through space.

In the Eulerian formulation all variables are referred to the deformed configuration and is currently only available with 2D and 3D continuum elements. It is applicable for large direct strains but is less accurate if

large shear strains are present. In the past, this has been preferred for fluid problems where it is required to monitor the path of fluid through a particular control volume and not the path of one particle in its entirety. Finally, in the co-rotational formulation, all strains are computed in the co-rotational local coordinate system which follows the element as it deforms. This approach, used in nonlinear analyses performed in this thesis, is generally applicable but is especially useful in geometrically nonlinear problems involving large rotations. At present, this formulation is available for beam elements (1D) and for all 2D and 3D continuum elements including the solid composite elements [42].

Nonlinear analysis is defined as an iterative procedure in which, differently from linear analysis, the external load is not applied all at once but for incremental steps and this is basically attributable to the stiffness. The geometric stiffness is expressed as a function of the displacement, which is then affected by the geometric stiffness again [43]. So, the stiffness matrix may change at each load increment and must be repeatedly updated. For that reason, to comply with static equilibrium between the external load and the internal stress and strain fields, the load has to be applied gradually over a certain number of increments. Within each load increment a linear prediction of the nonlinear response is initially made and subsequent iterative corrections are performed in order to restore equilibrium by the elimination of "out of balance" forces. The iterative corrections refer to various convergence criteria and such a solution procedure is commonly referred to as an incremental-iterative (or predictor-corrector) method [44].

In nonlinear analysis, the widely used iterative procedure to reach convergence is the so-called *Newton-Raphson Iteration Method*. This procedure uses tangent stiffness (K_T) to compute for each load step the incremental displacement (Δa) and the corresponding iterative out-of-balance residual force (ψ_o) to restore the equilibrium with the given external load (R). Being an iterative process, it will end when, within each load increment, the load level remains constant. In that sense, this iteration method is also named as constant load level incrementation procedure [44]. An illustration of how this kind of iteration procedure works is given in Figure 4-5.

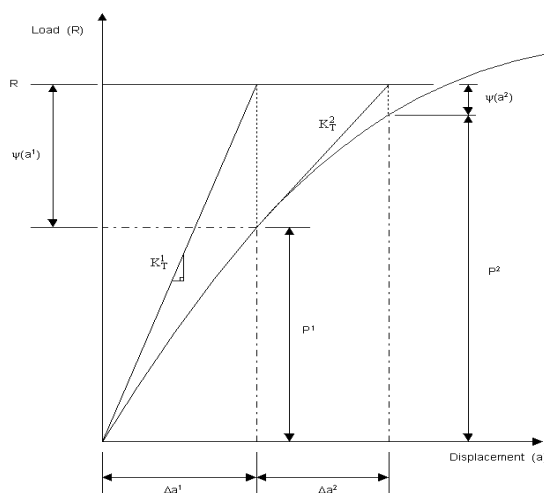


Figure 4-5: Newton-Raphson Iteration Method ⁴⁵.

⁴⁵ Figure from: https://www.lusas.com/user_area/theory/Nonlinear_Iterative_Procedures.html (Accessed Jan. 30,2025).

5 METHODOLOGY

This section presents the basics of Finite Element Method (*FEM*), and the characteristics of two-dimensional (*2D*) and three-dimensional (*3D*) glass models, built up in the Finite Element software *LUSAS*.

5.1 Basics of Finite Element Method (FEM)

Every phenomenon in nature can be described with the aid of the laws of physics, in terms of algebraic, differential or integral equations. While the derivation of governing equations for most problems is not unduly difficult, their solution by exact methods of analysis is a formidable task [45].

To simplify the problem and for the purpose of deriving approximate but at the same time accurate solutions, a numerical solution method can be used and the most frequently used in various types of engineering problems is the Finite Element Method.

The first step is to know which are the governing equations and the boundary conditions of the physical problem, then it is necessary to discretize the entire domain into smaller elements and this essential process is called *meshing* (see Figure 5-1). In fact, a continuum body is characterized by an infinite number of degrees of freedom (*DoFs*) in real life and this results in the impossibility of solving all the equations. The meshing technique allows the body to be subdivided into finite elements, each of them is connected to the others by means of specific points, called *nodes*. Each node can have different displacements, and then nodal displacements are the unknowns of the problem. While performing the meshing process, care should be taken to make sure that enough elements are included to capture the behaviour of the solution over the entire domain. Areas of particular interest and care are located where critical values are expected, locations with large gradients, locations where the geometry changes suddenly and locations where boundary conditions and loads are applied [46].

As a general rule, the more refined is the mesh size, the more the solution will be accurate but, on the other hand, by considerably increasing the mesh size it will result in longer computational time.

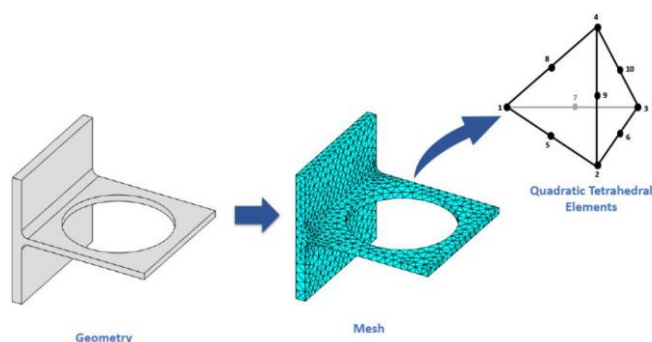


Figure 5-1: Meshing process of a Finite Element Model ⁴⁶.

⁴⁶ Figure from: <https://it.mathworks.com/discovery/finite-element-analysis.html> (Accessed Jan. 30,2025).

Another key aspect in meshing is represented by the choice of the appropriate element type depending on the type of body to be modelled (1D, 2D or 3D) and the prevalent mechanical behaviour of it.

Once the meshing process is completed, the finite equations are developed for each individual element by using a shape function which is able to approximate the value of the unknown variable in each element. The form of the algebraic equations for every element will be the same and differences from one element to the next will be due to changes in element size and properties [46].

The next step is the assemblage: it is necessary to move from element equations to global equations and to this end, element equations are assembled to form a global system of equations. Then, it is possible to enforce the boundary conditions of the problem which is helpful for reducing the assembled global equations into solvable size, since it involves substituting some known values of the parameter under consideration at some known points into the assembled global equations [46]. At the very end, the global system of equations is solved in specific points of the domain, called *Gauss points*, in which the numerical integration is performed.

5.2 2D Finite Element models

In order to simulate the buckling behaviour of laminated glass panels subjected to compressive in-plane loading, 2D Finite Element models were built in the commercial Finite Element software, *LUSAS*, in the undeformed configuration (perfectly flat) to perform eigenvalue analysis (*LBA*) and in the deformed one (with an initial geometric imperfection) to perform geometrically nonlinear buckling analysis (*GNA*).

5.2.1 2D models: element types

Each 2D model consists of semiloof curved thin shell elements (*QSL8*), which are useful in modelling the response of elements that are characterised by a thickness that is considerably smaller than the other two dimensions. Shell elements are, able to describe the real flexural stiffness of a bidimensional element and the effective thicknesses of the layers constituting the laminated glass beam [40].

QSL8 elements can be used for both flat and curved shell geometries. This type of quadrilateral elements consists of eight nodes (see Figure 5-2) and the interpolation order was selected as quadratic. The degrees of freedom (*DoF*) at the nodes are the displacements at corner nodes and the displacements and loofs at the mid-side nodes. The element formulations are based on the *Kirchhoff* hypothesis for thin shells, namely that transverse shear is negligible.

This kind of element type is also compatible with geometrically nonlinear formulations, in order to perform geometrically nonlinear buckling analysis (*GNA*).

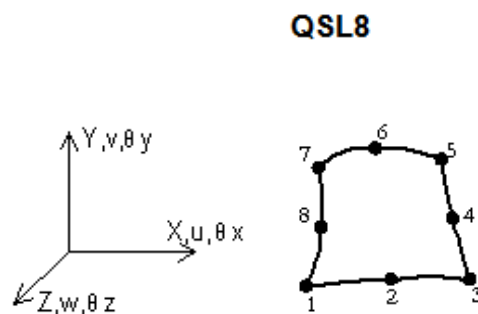


Figure 5-2: Semiloof curved thin shell elements (*QSL8*)

5.2.2 Geometric characteristics of flat and curved 2D models

The laminated glass panels to be modelled have width (b) equal to 500 mm and buckling length (L_b) which is varied within a predetermined range: $L_b = 2000$ mm, 4000 mm, 6000 mm, 8000 mm.

Also, three different thicknesses of laminated glass are considered in modelling process, as shown in Table 5-1:

Table 5-1: Different thicknesses of laminated glass plies under consideration in modelling stage.

Case	Thickness glass ply 1 h_1	Thickness PVB interlayer h_{int}	Thickness glass ply 2 h_2	Acronym
(-)	(mm)	(mm)	(mm)	(-)
A	10	1,52	10	10/1,52/10
B	12	1,52	12	12/1,52/12
C	14	1,52	14	14/1,52/14

In Figure 5-3 it is possible to observe the different geometry of each laminated glass unit under consideration:

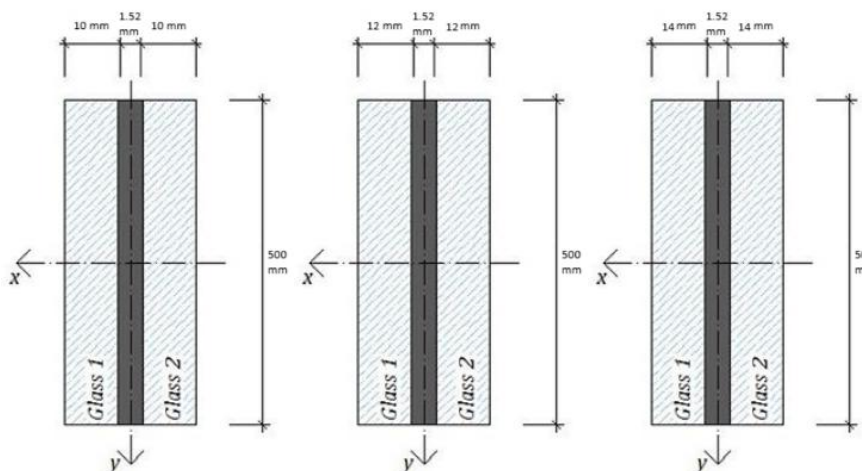


Figure 5-3: Different arrangement of laminated glass units under analysis. From the left to the right: case A, B and C⁴⁷.

Immediately after, for each case A, B and C, the shear modulus G of PVB interlayer is varied within the range: $G = 0,01$ MPa, 0,1 MPa, 1 MPa, 10 MPa.

⁴⁷ Figure adapted from: C. Amadio, C. Bedon, 'Buckling verification of laminated glass elements in compression', JCES, Vol. 1 Issue 3, pages:90-101, 2012, DOI: N/A.

5.2.3 Effective thickness calculation for flat and curved 2D models

The thickness to be assigned as attribute in 2D numerical models is precisely the effective thickness for bending deflection $h_{ef,w}$ (see Section 3.2), since it can provide an accurate description of the element flexural stiffness under analysis.

The effective thickness for calculating out-of-plane bending deflection ($h_{ef,w}$) is the same for both flat and curved 2D-FE models and can be computed, for each aforementioned case and for each shear modulus G (see Annex C).

5.2.4 2D models: material parameters

As regards material parameters, for all 2D models, glass has been considered as an isotropic material which behaves linearly elastic. So, it is characterized by a modulus of elasticity $E_g = 70000$ MPa and Poisson's ratio $\nu = 0,23$ MPa. *Poly Vinyl Butyral (PVB)* is a viscoelastic material, i.e. its shear modulus G strongly depends on many factors, such as load duration time and temperature.

Nevertheless, also *PVB* has been described as a linear elastic material, characterized by "equivalent" mechanical properties able to take into account for the degradation of its shear stiffness G . In each simulation, Poisson's ratio for *PVB* was fixed as $\nu = 0,498$ [40].

Material parameters used for all the 2D numerical simulations are summarized in Table 5-2 and Table 5-3.

Table 5-2: Material properties of annealed glass for 2D-FE models.

Parameter	Unit of measurement	Annealed Glass
Young's modulus E_g	MPa	70000
Poisson's ratio ν	-	0,23
Characteristic strength $f_{g,k}$	MPa	45

Table 5-3: Material properties of PVB for 2D-FE models.

Parameter	Unit of measurement	PVB
Shear modulus G	MPa	$0,01 \leq G \leq 10$
Poisson's ratio ν	-	0,498

5.2.5 Meshing process

As already said, mesh size is a prominent factor, because the more refined is the mesh size, the more the solution will be accurate and reliable but, at the same time, by considerably increasing the mesh density it will result in longer computational time.

To be accurate, the mesh size is varied according to the buckling length (L_b) of the model.

All data are reported in Table 5-4:

Table 5-4: Mesh size selected for each 2D model.

2D Model - Case	Width model b	Length model L_b	Mesh size (along b - along L_b)
(-)	(m)	(m)	(m x m)
2D_A	0,5	2	0,1 x 0,06
	0,5	4	0,1 x 0,13
	0,5	6	0,1 x 0,1
	0,5	8	0,1 x 0,1
2D_B	0,5	2	0,1 x 0,06
	0,5	4	0,1 x 0,13
	0,5	6	0,1 x 0,1
	0,5	8	0,1 x 0,1
2D_C	0,5	2	0,1 x 0,06
	0,5	4	0,1 x 0,13
	0,5	6	0,1 x 0,1
	0,5	8	0,1 x 0,1

As an example, in Figure 5-4 it is possible to take a look to the mesh used for a 2D model having length $L_b = 4$ m.

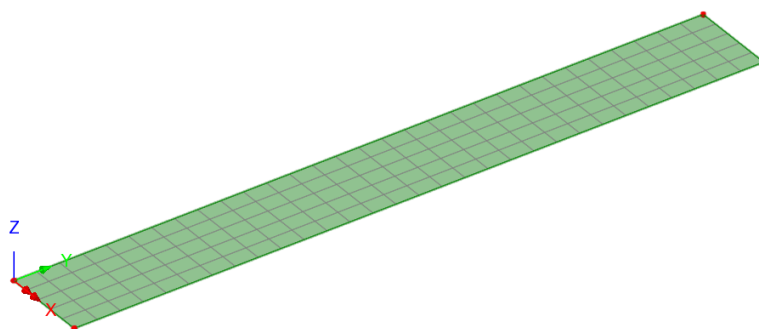


Figure 5-4: Mesh (0,1m x 0,13m) of a 4-meter length 2D model.

5.2.6 Boundary conditions and loading

2D laminated glass models has been developed in the plane X-Y, on which shorter edges are set along X-axis while longer edges along Y-axis. The thickness of the model is defined along Z-axis.

As regards boundary conditions (BCs), 2D Finite Element models are simply supported along shorter edges and free along longer edges.

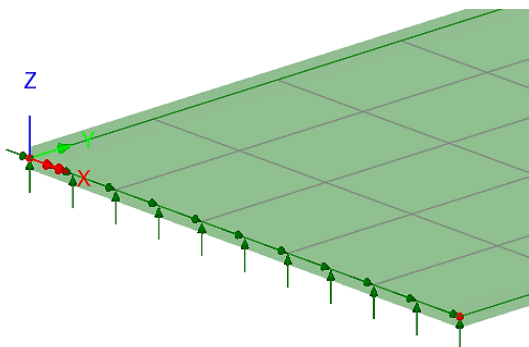


Figure 5-5: Simply supported boundary conditions along the shorter edge on which the compressive load is applied.

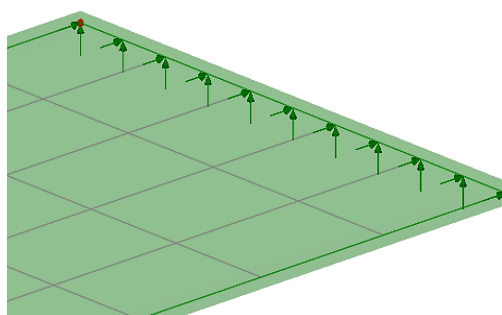


Figure 5-6: Simply supported boundary conditions along the opposite shorter edge.

A brief resume of the applied boundary conditions is available in Table 5-5:

Table 5-5: Boundary conditions for 2D models.

Edge	Boundary conditions (BCs)
Shorter (on which the load is applied)	Fix u_x , fix u_z
Shorter (the opposite one)	Fix u_y , fix u_z
Longer	Free
Longer	Free

As regards loading conditions, a compressive linear load $P_0 = 5 \text{ kN/m} = 5 \text{ N/mm}$ is applied in the midplane of the plate model, as shown in Figure 5-7.

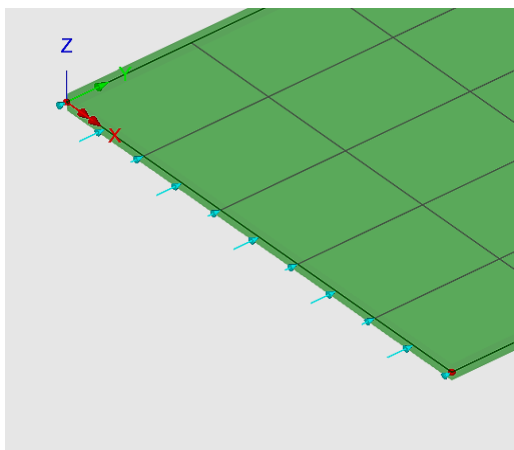


Figure 5-7: Applied compressive load $P_0 = 5 \text{ kN/m}$.

5.2.7 Overview of 2D flat models

A general overview of 2D flat models (case C), built in the FE software LUSAS, is presented from Figure 5-8 to Figure 5-11.

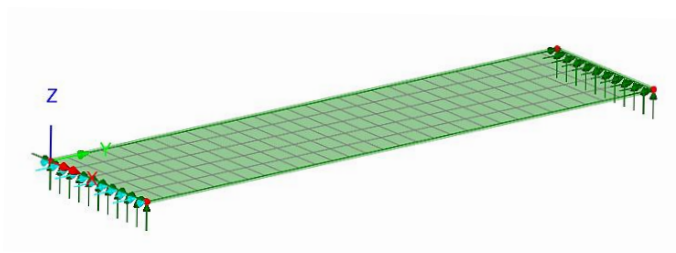


Figure 5-8: 2D flat model having length $L_b = 2 \text{ m}$ (case C).

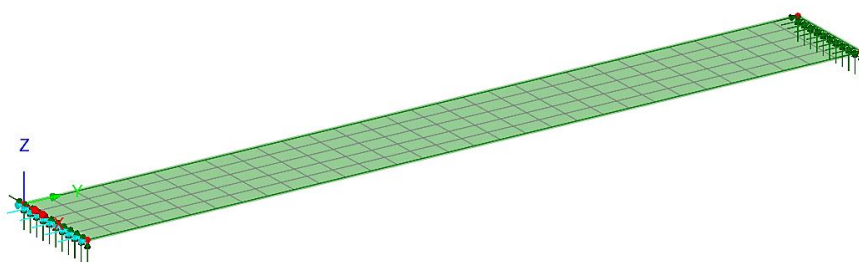


Figure 5-9: 2D flat model having length $L_b = 4 \text{ m}$ (case C).

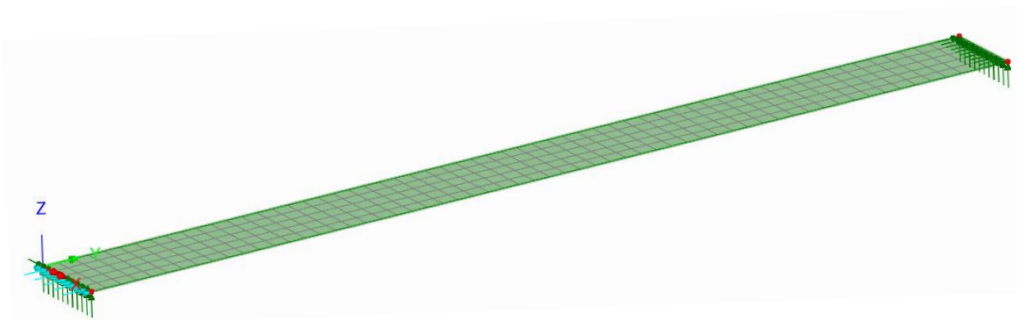


Figure 5-10: 2D flat model having length $L_b = 6m$ (case C).

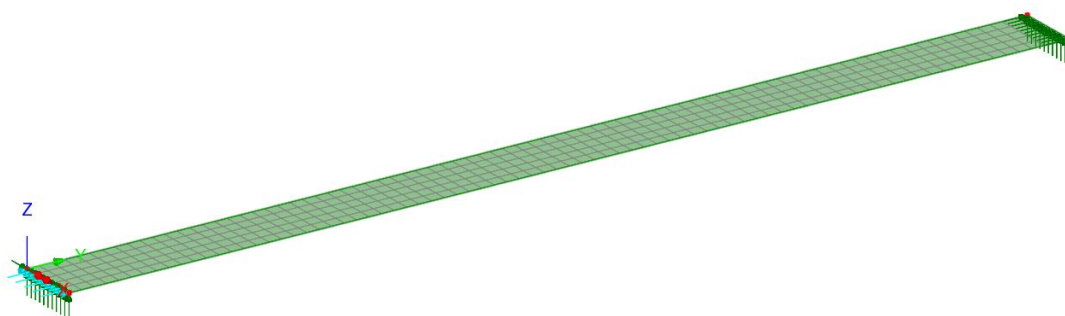


Figure 5-11: 2D flat model having length $L_b = 8m$ (case C).

5.2.8 2D curved models: initial geometric imperfection

In order to carry out geometrically nonlinear buckling analysis (GNA), 2D FE-models with initial geometrical imperfection have been modelled. The initial or basic imperfection e_0 is calculated for each case A, B and C in compliance with the Standard for glass structures CEN/TS 19100-3:2021 [36] (see Paragraph 4.1).

Table 5-6: Basic imperfection e_0 for case A.

2D curved model – Case	Width model b	Length model L_b	$e_{0,length}$	$e_{0,installation}$	e_0
(-)	(mm)	(mm)	(mm)	(mm)	(mm)
2D_A	500	2000	6,01	10,76	12,32
	500	4000	12,01	10,76	16,13
	500	6000	18,02	10,76	20,99
	500	8000	24,02	10,76	26,32

Table 5-7: Basic imperfection e_0 for case B.

2D curved model – Case	Width model b	Length model L_b	$e_{0,length}$	$e_{0,installation}$	e_0
(-)	(mm)	(mm)	(mm)	(mm)	(mm)
2D_B	500	2000	6,01	12,76	14,10
	500	4000	12,01	12,76	17,52
	500	6000	18,02	12,76	22,08
	500	8000	24,02	12,76	27,20

Table 5-8: Basic imperfection e_0 for case C.

2D curved model – Case	Width model b	Length model L_b	$e_{0,length}$	$e_{0,installation}$	e_0
(-)	(mm)	(mm)	(mm)	(mm)	(mm)
2D_C	500	2000	6,01	14,76	15,94
	500	4000	12,01	14,76	19,03
	500	6000	18,02	14,76	23,29
	500	8000	24,02	14,76	28,20

All the other model characteristics – effective thickness, material parameters, mesh density, boundary conditions and applied compressive load – are the same as for 2D-FE flat models.

5.2.9 Overview of 2D curved models

A general overview of 2D curved models (case B), modelled in the FE software LUSAS, is presented from Figure 5-12 to Figure 5-15.

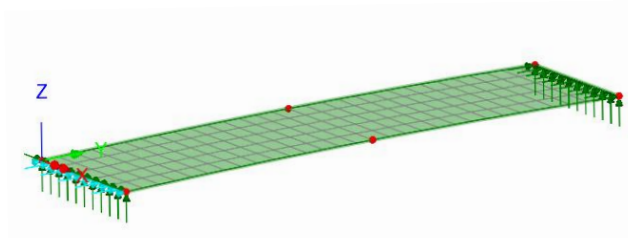


Figure 5-12: 2D curved model having length $L_b=2m$ (case B $e_0=14,10$ mm).

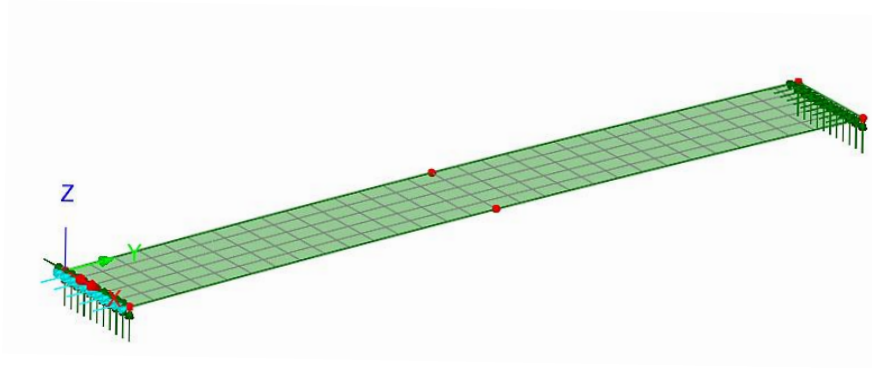


Figure 5-13: 2D curved model having length $L_b = 4m$ (case B $e_0 = 17,52$ mm).

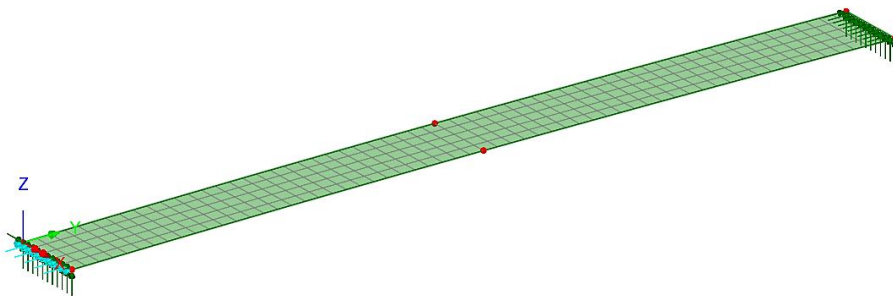


Figure 5-14: 2D curved model having length $L_b = 6m$ (case B $e_0 = 22,08$ mm).

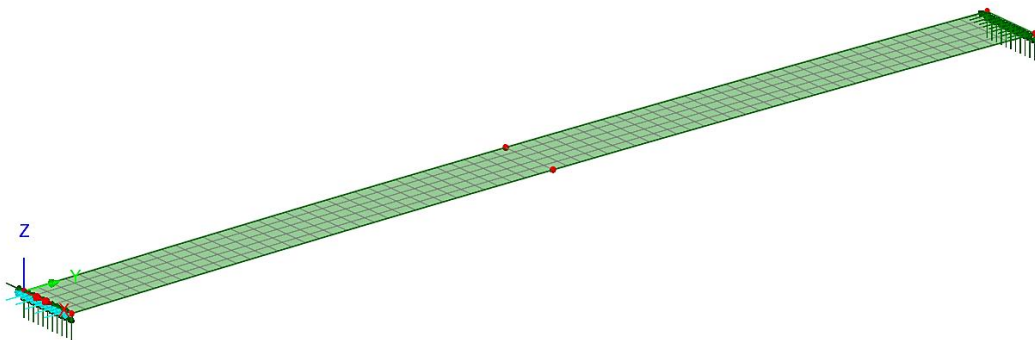


Figure 5-15: 2D curved model having length $L_b = 8m$ (case B $e_0 = 27,20$ mm).

5.3 3D+shell Finite Element models

In order to understand if there could be any considerable discrepancy in buckling behaviour compared to 2D models, also 3D+shell Finite Element models were set up in the Finite Element software *LUSAS*, considering since the beginning an initial geometrical imperfection (e_0).

Each 3D model consists of a PVB interlayer that is modelled by means of three-dimensional (3D) elements and a top and bottom glass ply, which can be described through bidimensional (2D) shell elements. In fact, shell elements are capable to properly simulate bending behaviour of glass panels, instead, PVB interlayer is only able to transfer shear stresses thus 3D elements are more suited.

Since laminated glass panels to be modelled are characterized by the same boundary conditions at both the shorter edges, to simplify the modelling process and to reduce computational time, it is possible to model only a half of the panel by exploiting the symmetry of the problem.

5.3.1 3D+shell model: element types

To describe PVB film, three-dimensional elements with eight nodes (*HXM8*) as well as linear interpolation are chosen in *LUSAS*. *HXM8* elements are characterised by three degrees of freedom (*DoF*) at each node: displacement along X-axis, along Y-axis and, finally, along Z-axis (see Figure 5-16). This kind of element type is also compatible for geometrically nonlinear formulations in order to perform geometrically nonlinear buckling analysis (*GNA*).

The *HXM8* element is chosen since it does not suffer from locking due to parasitic shear or when the material approaches the incompressible limit.

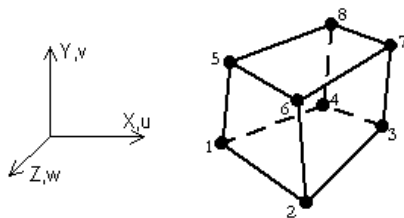


Figure 5-16: 3D Solid Continuum Element with Enhanced Strains (*HXM8*).

Glass plies are modelled by means of semiloof curved thin shell elements (*QSL8*), which have been already discussed in Section 5.2.1 of this document.

5.3.2 Geometric characteristics of 3D+shell models

3D FE-models are built up, as formerly done, for different lengths in a range: $L_b = 2000$ mm, 4000 mm, 6000 mm, 8000 mm. In addition, three different thicknesses of glass plies ($h_1=h_2 = 10$ mm, 12mm, 14mm) are considered during the modelling process of 3D+shells models, as shown in Table 5-9:

Table 5-9: Different thicknesses of glass plies to be considered in modelling process.

Case	Thickness top glass ply h_1	Thickness PVB interlayer h_{int}	Thickness bottom glass ply h_2	Acronym
(-)	(mm)	(mm)	(mm)	(-)
A	10	1,52	10	10/1,52/10
B	12	1,52	12	12/1,52/12
C	14	1,52	14	14/1,52/14

Then, for each case study, the shear modulus G of PVB interlayer is varied within the range: $G = 0,01$ MPa, $0,1$ MPa, 1 MPa, 10 MPa.

The creation of the $3D+shell$ model starts with the realization in the plane X-Y of a volume (PVB) having thickness (h_{int}), and then, the thickness of top and bottom glass ply is assigned to the top and bottom surfaces of the volume, respectively (see Figure 5-17).

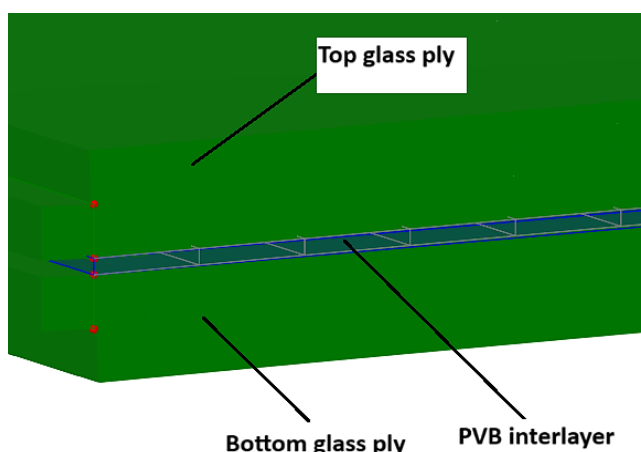


Figure 5-17: Cross-section of 3D+shell models.

The assignment of the thickness for top and bottom glass plies is performed by setting in the FE software $LUSAS$ an eccentricity along the Z-axis, e_z , that is equal to half the thickness of the glass ply itself, as shown in Figure 5-18.

		Value
Thickness	t	0,01
Eccentricity	e_z	$5,0E-3$
Name: top_ply		

		Value
Thickness	t	0,01
Eccentricity	e_z	$-5,0E-3$
Name: bottom_ply		

Figure 5-18: Assignment of the eccentricity to the top glass ply on the left and to the bottom ply on the right, for case A. (Units of measurement are in meters in this figure).

Additionally, in order to properly apply the compressive load $P_0 = 5 \text{ kN/m}$ on the midplane of top and bottom glass plies and also the boundary conditions, owing to modelling reasons, there was the need for “vertical” plate elements in the plane Y-Z, located at both the shorter edges of PVB volume, as illustrated in Figure 5-19.

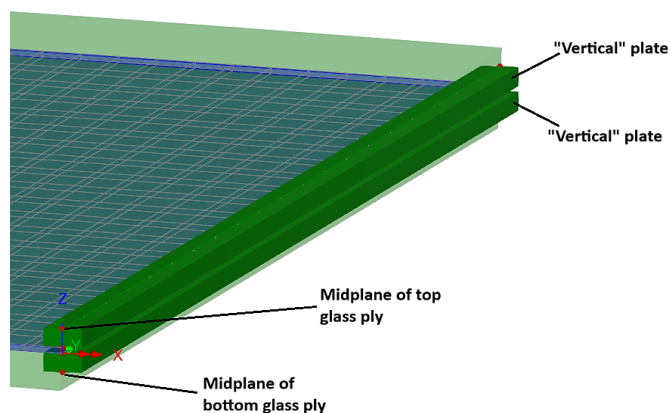


Figure 5-19: "Vertical" plates located at the shorter edges of the model.

The “vertical” plates have been conceived to be significantly stiff, so that, they are made of glass and have the same thickness of the top and bottom glass plies, as illustrated in Figure 5-20.

		Value
Thickness	t	0,01
Eccentricity	ez	0,0
Name vertical plates		

Figure 5-20: Thickness of vertical plates for case A. (Units of measurement are in meters in this figure).

5.3.3 Meshing process

As regards mesh size, it is crucial to have a sufficiently adequate mesh density, especially in 3D models, in order to provide convergence during linear and nonlinear buckling analyses and to capture as best as possible the behaviour of the element that is modelled.

The mesh size, for 3D+shell models, is varied according to the buckling length L_b of the model.

All data concerning the mesh density for each element of 3D models are reported in Table 5-10.

Table 5-10: Mesh size for each element constituting 3D+shell models.

3D Model - Case	Width model b	Length model L_b (half due to symmetry)	Mesh size	Mesh size	Mesh size	Mesh size
			Top glass ply	Bottom glass ply	“Vertical” plates	PVB
			(along b-along L_b)	(along b-along L_b)	(along b-along L_b)	(along b-along L_b -through h_{int})
(-)	(m)	(m)	(m x m)	(m x m)	(m x m)	(m x m x m)
3D_A	0,5	1	0,016 x 0,01	0,016 x 0,01	0,005 x 0,01	$0,016 \times 0,01 \times 1,52e^{-3}$
	0,5	2	0,016 x 0,02	0,016 x 0,02	0,005 x 0,01	$0,016 \times 0,02 \times 1,52e^{-3}$
	0,5	3	0,025 x 0,03	0,025 x 0,03	0,005 x 0,025	$0,025 \times 0,03 \times 1,52e^{-3}$
	0,5	4	0,025 x 0,026	0,025 x 0,026	0,005 x 0,025	$0,025 \times 0,026 \times 1,52e^{-3}$
3D_B	0,5	1	0,016 x 0,01	0,016 x 0,01	0,005 x 0,01	$0,016 \times 0,01 \times 1,52e^{-3}$
	0,5	2	0,016 x 0,02	0,016 x 0,02	0,005 x 0,01	$0,016 \times 0,02 \times 1,52e^{-3}$
	0,5	3	0,025 x 0,03	0,025 x 0,03	0,005 x 0,025	$0,025 \times 0,03 \times 1,52e^{-3}$
	0,5	4	0,025 x 0,026	0,025 x 0,026	0,005 x 0,025	$0,025 \times 0,026 \times 1,52e^{-3}$
3D_C	0,5	1	0,016 x 0,01	0,016 x 0,01	0,005 x 0,01	$0,016 \times 0,01 \times 1,52e^{-3}$
	0,5	2	0,016 x 0,02	0,016 x 0,02	0,005 x 0,01	$0,016 \times 0,02 \times 1,52e^{-3}$
	0,5	3	0,025 x 0,03	0,025 x 0,03	0,005 x 0,025	$0,025 \times 0,03 \times 1,52e^{-3}$
	0,5	4	0,025 x 0,026	0,025 x 0,026	0,005 x 0,025	$0,025 \times 0,026 \times 1,52e^{-3}$

5.3.4 3D+shell models: initial geometric imperfections

In order to carry out geometrically nonlinear buckling analysis (GNA), 3D+shell models have been modelled taking into account the initial imperfection of the panel. The initial or basic imperfection (e_0) is calculated for each case A, B and C in compliance with the Standard for glass structures CEN/TS 19100-3:2021 [36] (see Paragraph 4.1).

 Table 5-11: Basic imperfection e_0 for case A.

3D model – Case	Width model b	Length model L_b	$e_{0,length}$	$e_{0,installation}$	e_0
(-)	(mm)	(mm)	(mm)	(mm)	(mm)
3D_A	500	2000	6,01	10,76	12,32
	500	4000	12,01	10,76	16,13
	500	6000	18,02	10,76	20,99
	500	8000	24,02	10,76	26,32

Table 5-12: Basic imperfection e_0 for case B.

3D model – Case	Width model b	Length model L_b	$e_{0,length}$	$e_{0,installation}$	e_0
(-)	(mm)	(mm)	(mm)	(mm)	(mm)
3D_B	500	2000	6,01	12,76	14,10
	500	4000	12,01	12,76	17,52
	500	6000	18,02	12,76	22,08
	500	8000	24,02	12,76	27,20

Table 5-13: Basic imperfection e_0 for case C.

3D model – Case	Width model b	Length model L_b	$e_{0,length}$	$e_{0,installation}$	e_0
-	(mm)	(mm)	(mm)	(mm)	(mm)
3D_C	500	2000	6,01	14,76	15,94
	500	4000	12,01	14,76	19,03
	500	6000	18,02	14,76	23,29
	500	8000	24,02	14,76	28,20

5.3.5 3D+shell models: boundary conditions and loading

3D laminated glass models are developed in the plane X-Y, on which shorter edges are set along Y-axis while longer edges along X-axis. The thickness of the model is defined along Z-axis. As already mentioned, taking advantage of the symmetry of the problem, only one half of the 3D models has been built up in the Finite Element software LUSAS. Boundary conditions are applied along each longer side of the “vertical” plates, since it represents the midplane of top and bottom glass plies, and then, it is as if boundary conditions are directly applied to the midplane of the plies.

So, the shorter edge of the 3D model, on which the compressive load is applied, is simply supported (see Figure 5-21). On the opposite edge of the model, symmetry boundary conditions are defined, i.e. a slider is introduced, which only allows vertical displacements along Z-axis (see Figure 5-22).

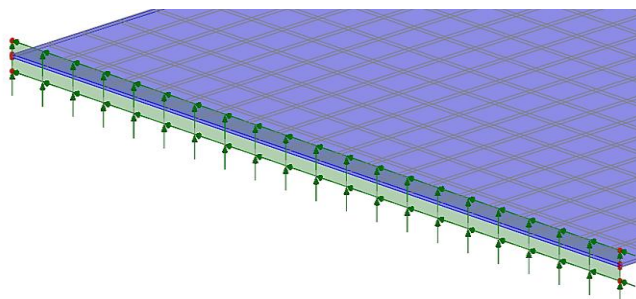


Figure 5-21: Simply supported boundary conditions along the shorter edge, on which the compressive load is applied.

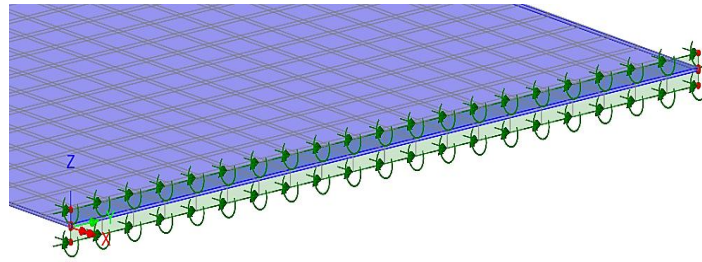


Figure 5-22: Symmetry boundary conditions (slider) along the opposite shorter edge.

A brief resume of the applied boundary conditions is available in Table 5-14:

Table 5-14: Boundary conditions for 3D models.

Edge	Boundary conditions (BCs)
Shorter (on which the load is applied)	Fix u_y , fix u_z
Shorter (symmetry BCs)	Fix u_x , fix u_y , fix ϕ_y
Longer	Free
Longer	Free

As regards loading conditions, two compressive linear loads $P_{0,1} = P_{0,2} = 2,5 \text{ kN/m} = 2,5 \text{ N/mm}$ are applied along the longer sides of the “vertical” plates, which accounting for the midplane of two glass layers, as shown in Figure 5-23.

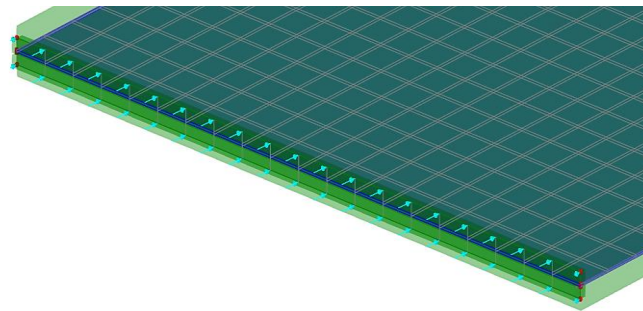


Figure 5-23: Applied compressive loads $P_{0,1} = P_{0,2} = 2,5 \text{ kN/m}$ on 3D models.

5.3.6 3D models: material parameters

In each 3D model, glass has been considered as an isotropic material which behaves linearly elastic. So, it is characterized by a modulus of elasticity $E_g = 70000 \text{ MPa}$ and Poisson’s ratio $\nu = 0,23$. *Poly Vinyl Butyral* (PVB) is a viscoelastic material, i.e. its shear modulus G strongly depends on many factors, such as load duration time and temperature.

Nevertheless, also PVB has been described as a linear elastic material, characterized by “equivalent” mechanical properties able to take into account for the degradation of its shear stiffness G . In each simulation, Poisson’s ratio for PVB was fixed as $\nu = 0,498$ [40].

Glass and PVB properties used for 3D models are summarized in Table 5-15 and Table 5-16.

Table 5-15: Glass parameters used in 3D models.

Parameter	Unit of measurement	Annealed Glass
Young's modulus E_g	MPa	70000
Poisson's ratio ν	-	0,23
Characteristic strength $f_{g,k}$	MPa	45

Table 5-16: PVB parameters used in 3D models.

Parameter	Unit of measurement	PVB
Shear modulus G	MPa	$0,01 \leq G \leq 10$
Poisson's ratio ν	-	0,498

5.3.7 Overview of 3D models

A general overview of 3D+shell models (case A), modelled in the FE software LUSAS, is presented from Figure 5-24 to Figure 5-27.

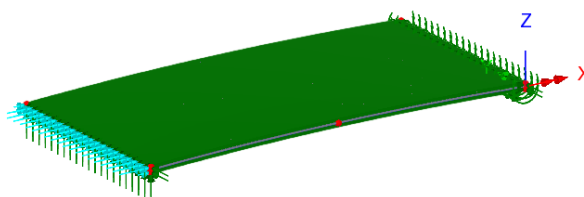


Figure 5-24: 3D model having length $L_b= 2m$ (case A $e_0= 12,32$ mm).

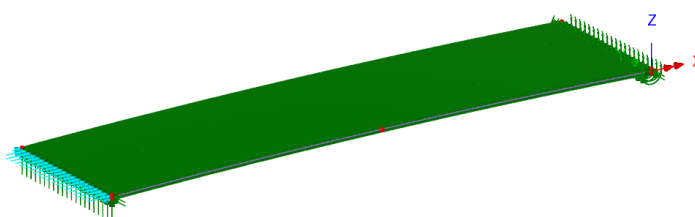


Figure 5-25: 3D model having length $L_b= 4m$ (case A $e_0= 16,13$ mm).

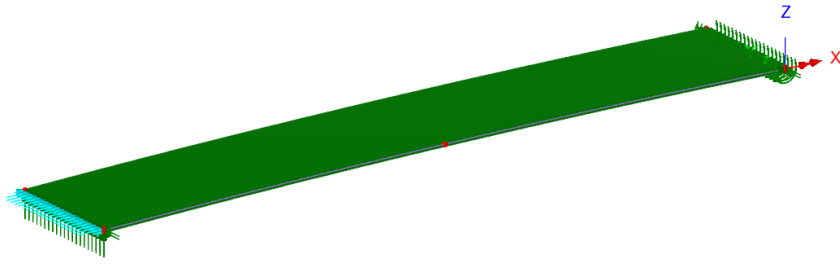


Figure 5-26: 3D model having length $L_b = 6\text{m}$ (case A $e_0 = 20,99\text{ mm}$).

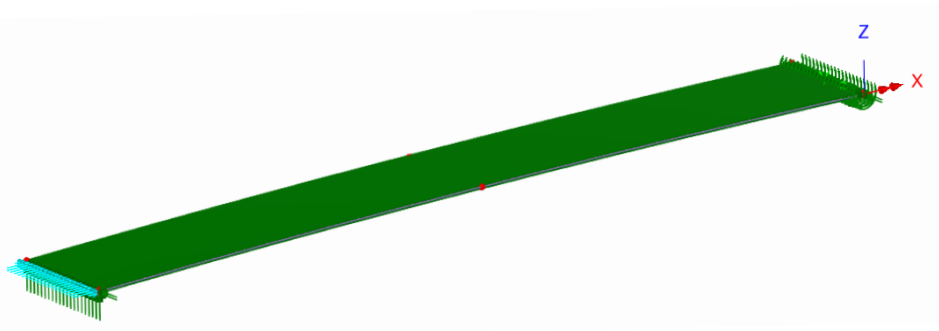


Figure 5-27: 3D model having length $L_b = 8\text{m}$ (case A $e_0 = 26,32\text{ mm}$).

6 RESULTS AND DISCUSSION

This chapter introduces the results derived from numerical simulations on *2D* and *3D* Finite Element models, using the Finite Element software *LUSAS*.

6.1 Overview of numerical analysis

6.1.1 Solution strategies

Three laminated glass units, having different thickness of glass plies, are chosen to be analysed (see Table 5-1) through linear and nonlinear buckling analysis. In order to investigate buckling behaviour, a parametric study involving different values of interlayer shear modulus and lengths of glass panels is conducted. The interlayer shear modulus G is varied within a pre-established range: $G = 0,01$ MPa, $0,1$ MPa, 1 MPa, 10 MPa while the length of glass panel (L_b) ranges between 2m and 8m by multiples of two.

From each buckling analysis, the buckling load factor (*BLF*) is obtained, then critical buckling loads ($N_{cr,FEA}$) and critical buckling stresses ($\sigma_{cr,FEA}$) must be computed.

Eigenvalue analysis (*LBA*), providing the theoretical elastic buckling load, is performed on *FE-2D* flat models. To validate models, numerical buckling loads are compared with those obtained by means of analytical approach, based on the calculation of buckling load according to Annex A of glass Standard *CEN/TS 19100-3* [37].

Geometrically nonlinear buckling analysis (*GNA*) later is carried out on *FE-2D* curved (i.e. with an initial geometric imperfection) and on *3D* models. In this type of analysis, a constant load level incrementation is chosen with the aim of seeking nonlinear solution: starting load factor, maximum total load factor and maximum change in load factor must be introduced in nonlinear and transient *LUSAS* controls. The analysis procedure is iterative and requires reaching convergence at each load incrementation.

As regards *2D-FE* curved models, two approaches are engaged in nonlinear analysis. To derive critical buckling loads, the first solution strategy requires stopping the analysis at a specific load factor, when the characteristic bending strength of annealed glass ($f_{g,k}$) is reached in one of the most stressed points of the panel. In the first approach, *2D* models are characterized by the effective thickness for out-of-plane bending deflection ($h_{ef,w}$).

The second solution strategy is based on limitation of transversal displacement on *2D* models, having thickness equal to $h_{ef,w}$. To derive buckling loads, nonlinear analysis is stopped when a specific value of maximum displacement is reached and then buckling stresses can be calculated, considering the effective thickness for out-of-plane bending stresses ($h_{ef,\sigma,i}$). This second strategy solution is explained in Chapter 6.4 in detail.

Following this, several buckling curves are plotted and compared for the abovementioned three different laminated glass units, as a function of interlayer shear modulus and slenderness ratio of the panel. And, in conclusion, design buckling curves are proposed with a view to assisting the pre-design stage of laminated glass columns.

6.1.2 2D and 3D models: detailing on analysis results

This subsection is devoted to explain some specifics about critical buckling loads ($N_{cr,FEA}$) and critical buckling stresses ($\sigma_{cr,FEA}$), obtained from linear and nonlinear buckling analyses conducted in the Finite Element software *LUSAS*, for each case study. All the findings are tabulated and presented in the Annex D of this document.

Critical buckling loads are calculated according to Eq. (4.3) of Section 4.3. In the case of eigenvalue analysis (*LBA*), they are also compared against analytical buckling loads ($N_{cr,LG}$), calculated by means of analytical Euler's formula (Eq. (3.4) Section 3.3).

Then, critical buckling stresses $\sigma_{cr,FEA}$ are calculated according to Eq. (2.2) of Section 2.10.1, where $N_{cr,FEA}$ is used instead of $N_{cr,EU}$ and the entire cross-sectional area A_{full} is introduced, accounting for the presence of top and bottom glass plies, as well as *PVB* interlayer.

From tables shown in Annex D, it is noteworthy that numerical buckling loads $N_{cr,FEA}$, obtained through linear buckling analysis on *2D* models, are completely aligned with those calculated by means of Euler's formula adapted for laminated glass elements ($N_{cr,LG}$). In addition, for each buckling length of the panels (L_b), as the interlayer shear modulus G increases from 0,01 MPa to 10 MPa, the buckling load $N_{cr,FEA}$ increases. And it was expected, since the structural behaviour of laminated glass panel tend to the monolithic limit when the interlayer shear modulus assumes large values.

6.1.3 Introduction to buckling curves

Numerical results are also compared in the form of graphs, where the so-called buckling curves $\sigma_{cr,FEA}$ vs λ_{panel} have been plotted: $\sigma_{cr,FEA}$ denotes critical buckling stress obtained from *FEA* and λ_{panel} the slenderness ratio of the laminated glass panel.

The aforementioned slenderness ratio is conveniently defined as follows:

$$\lambda_{panel} = \frac{L_b}{\rho_{full}} \quad (5.1)$$

Where:

L_b is the buckling length.

ρ_{full} is the radius of gyration, considering the entire *LG* cross-section.

The radius of gyration ρ_{full} can be calculated according to this formula:

$$\rho_{full} = \sqrt{\frac{J_{full}}{A_{full}}} \quad (5.2)$$

Where:

J_{full} is the moment of inertia of the entire cross-section (also including *PVB* interlayer).

A_{full} is the cross-sectional area of the laminated glass pane (also including *PVB* interlayer).

Both λ_{panel} and ρ_{full} are solely function of the geometric characteristics of the laminated glass pane cross-section, they are thus shown for each typology of cross-section (i.e. case study A, B and C) from Table 6-1 to Table 6-3.

Table 6-1: Calculation of the slenderness ratio of each laminated glass panel (case A).

Model types & case study	Length model L_b	Moment of inertia J_{full}	Radius of gyration ρ_{full}	Slenderness ratio λ_{panel}
(-)	(mm)	(mm ⁴)	(mm)	(-)
2D_A and 3D_A	2000	415255,66	6,21	321,94
	4000	415255,66	6,21	643,89
	6000	415255,66	6,21	965,83
	8000	415255,66	6,21	1287,77

Table 6-2: Calculation of the slenderness ratio of each laminated glass panel (case B).

Model type & case study	Length model L_b	Moment of inertia J_{full}	Radius of gyration ρ_{full}	Slenderness ratio λ_{panel}
(-)	(mm)	(mm ⁴)	(mm)	(-)
2D_B and 3D_B	2000	692517,52	7,37	271,48
	4000	692517,52	7,37	542,96
	6000	692517,52	7,37	814,44
	8000	692517,52	7,37	1085,93

Table 6-3: Calculation of the slenderness ratio of each laminated glass panel (case C).

Model type & case study	Length model L_b	Moment of inertia J_{full}	Radius of gyration ρ_{full}	Slenderness ratio λ_{panel}
(-)	(mm)	(mm ⁴)	(mm)	(-)
2D_C and 3D_C	2000	1071819,39	8,52	234,70
	4000	1071819,39	8,52	469,39
	6000	1071819,39	8,52	704,09
	8000	1071819,39	8,52	938,78

6.2 Effect of slenderness ratio on critical buckling stress (1st solution strategy)

The thermoplastic interlayer plays a significant role in the determination of the structural behaviour of laminated glass, as its shear modulus G varies, so does the shear coupling degree between the glass plies, thus affecting its ability to transmit stresses and also the resistance against fracture.

In this parametric study, the shear modulus of the polymeric film is changed within the following range: $G = 0,01$ MPa, $0,1$ MPa, 1 MPa and 10 MPa. The smallest G -value identifies an extremely soft interlayer, conversely, the largest one accounts for a particularly stiff interlayer.

The following first set of buckling curves, illustrated from Figure 6-1 to Figure 6-3, expose the effect of increment in the slenderness ratio of the panels on critical buckling stress, for several LG panels with different thickness of glass layers (cases A, B and C) and for each interlayer shear modulus G .

Case A :

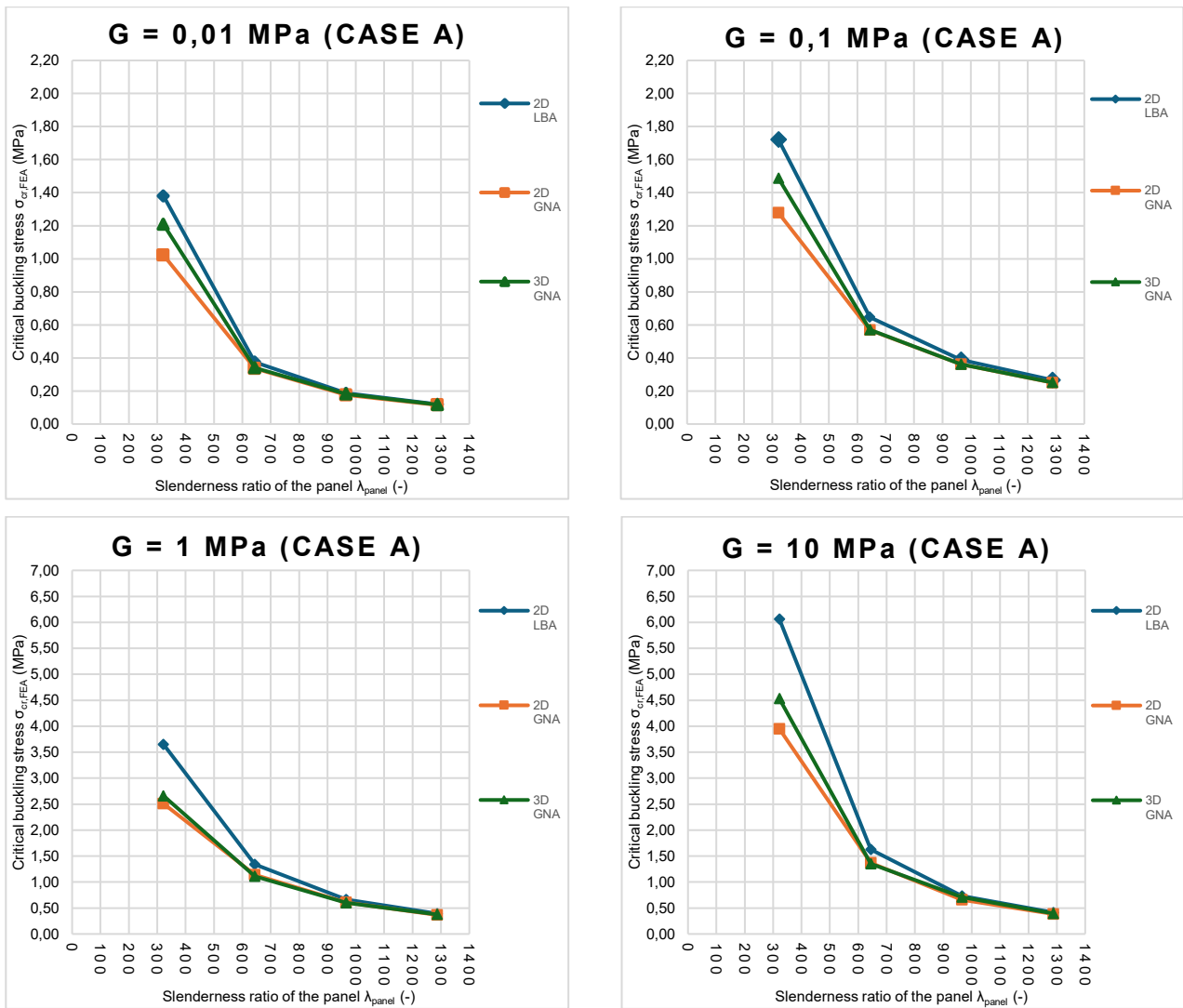


Figure 6-1: Buckling curves for case study A (1st solution strategy).

Case B :

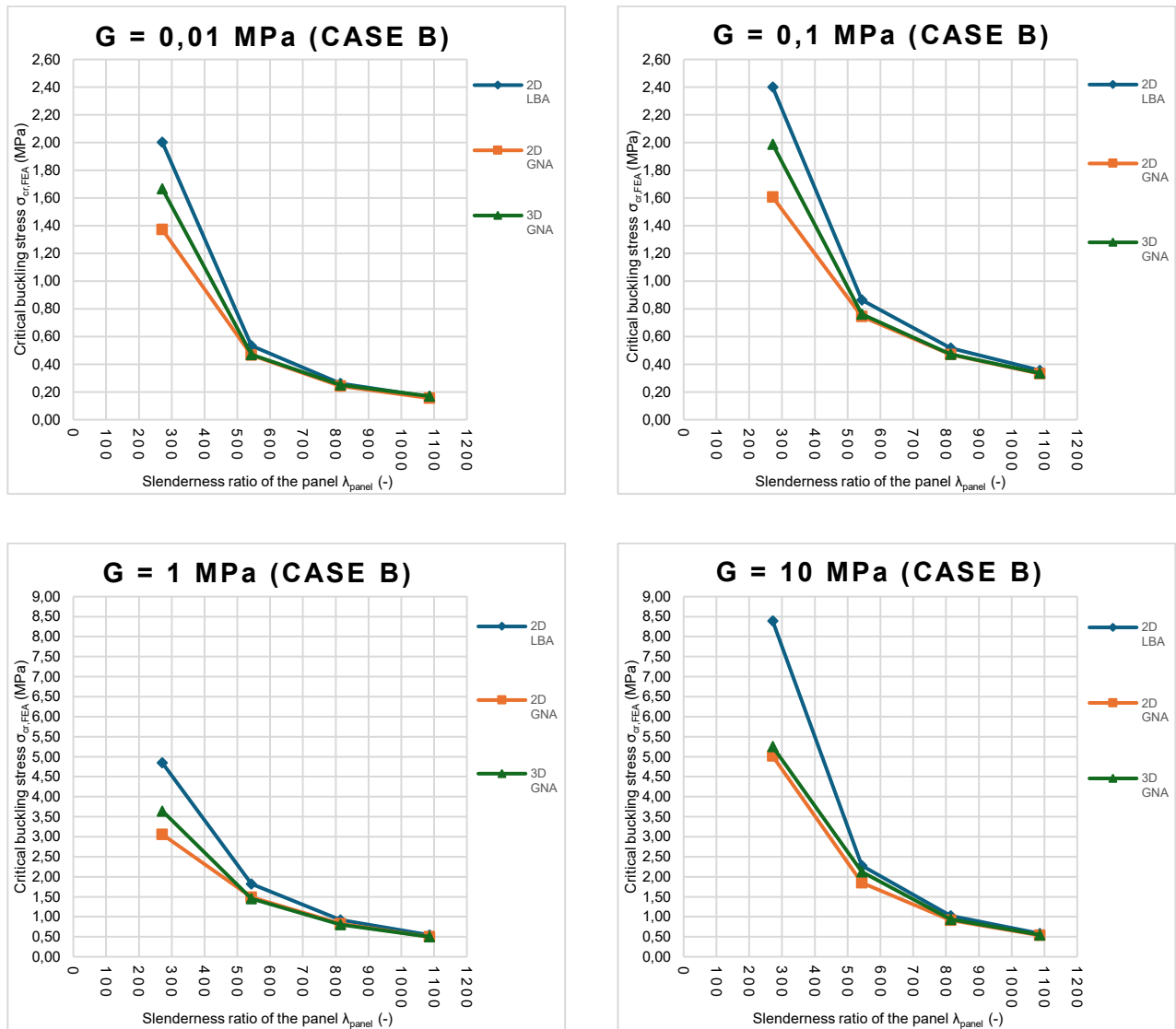


Figure 6-2: Buckling curves for case study B (1st solution strategy).

Case C :

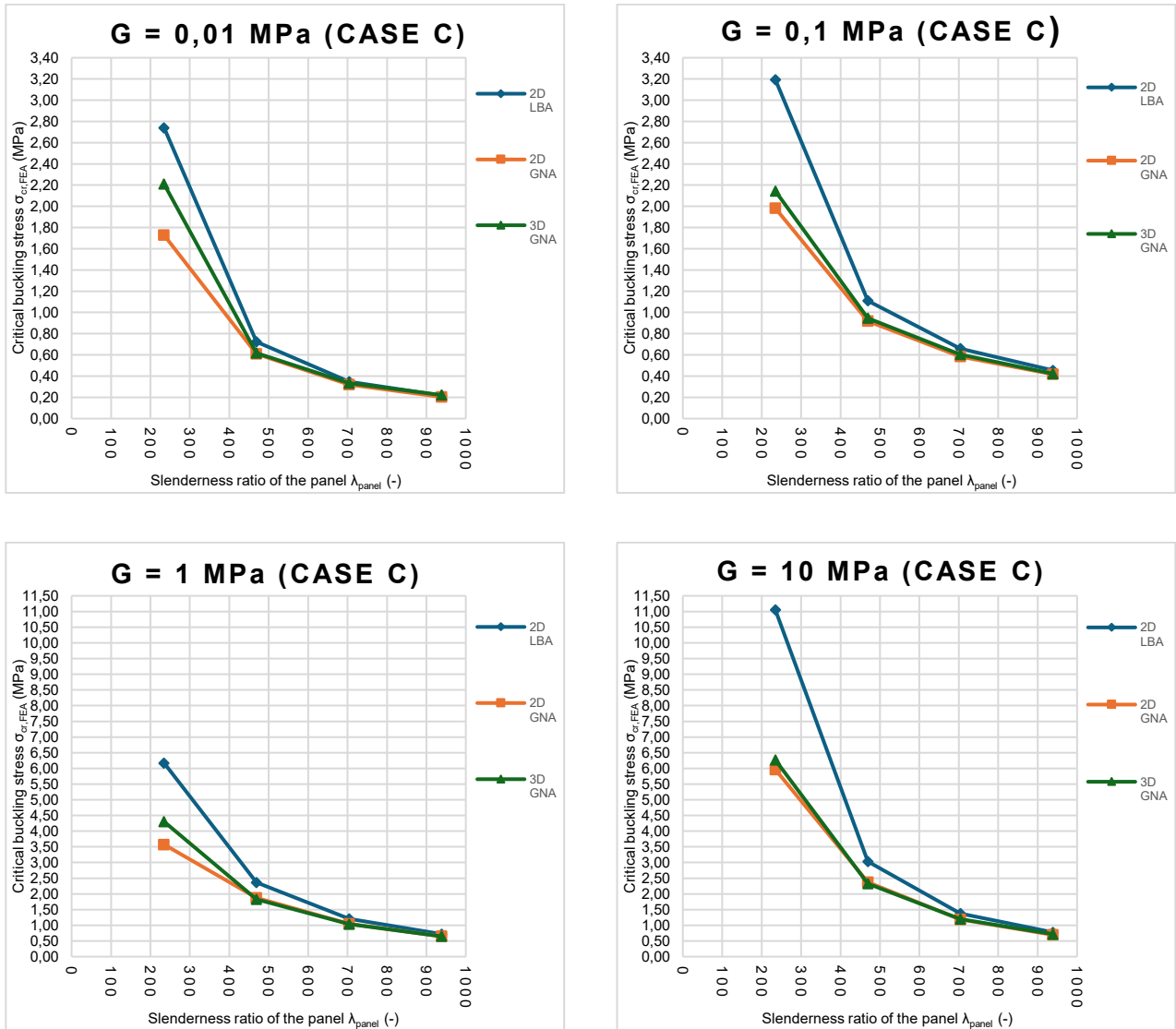


Figure 6-3: Buckling curves for case study C (1st solution strategy).

From the previous graphs, it is possible to highlight the decreasing relationship between critical buckling stress and slenderness ratio of the panel. By increasing the slenderness ratio of the member, which represents the sensitivity to buckle, it is indeed easier to reach the critical load and then failure for buckling.

The blue curve is obtained through eigenvalue analysis on 2D-FE models, therefore it is the theoretical buckling curve to which the other two tend for high values of slenderness, since it assumes a perfectly straight element which behaves linearly elastic, and it is not able to capture any nonlinear behaviour. Buckling curves related to geometrically nonlinear analysis on 2D and 3D curved models are always located below the theoretical one, since geometric nonlinearity affects buckling behaviour by reducing the buckling load. It is worth pointing out that the rate of decrement in critical buckling stress is larger, moving between panels having length equal to 2 meters and 4 meters, and then it greatly reduces between 4 meters and 8 meters.

In addition, buckling curves derived from nonlinear buckling analysis, are almost entirely overlapped ranging from a 4-meters length to an 8-meters length panel.

It entails that the two different typologies of Finite Element models, two-dimensional and three-dimensional, behaves in like manner for large values of slenderness. But an exception is present for the first branch of the orange (2D GNA) and green (3D GNA) curves, since critical buckling stress assumes different values, when analysing the 2D and 3D model having length of 2 meters, by means of nonlinear buckling analysis. In particular, in this specific case, nonlinear analysis performed on three-dimensional model always provide a higher critical buckling stress as compared with that coming from nonlinear analysis on the two-dimensional one. Nevertheless, this trend tends to vanish by increasing the value of the interlayer shear modulus G , in fact, it is quite evident that critical stresses derived from nonlinear analysis, and carried out on 2D and 3D models, are very close when the shear modulus equals 10 MPa.

6.3 Effect of shear modulus on critical buckling load

The effect of shear modulus decay on the critical buckling load $N_{cr,FEA}$ is evaluated for different thicknesses of glass plies, while taking as fixed variable the length of each laminated glass pane ($L_b = 2\text{m}, 4\text{m}, 6\text{m}, 8\text{m}$), as shown from Figure 6-4 to Figure 6-6.

Case A :

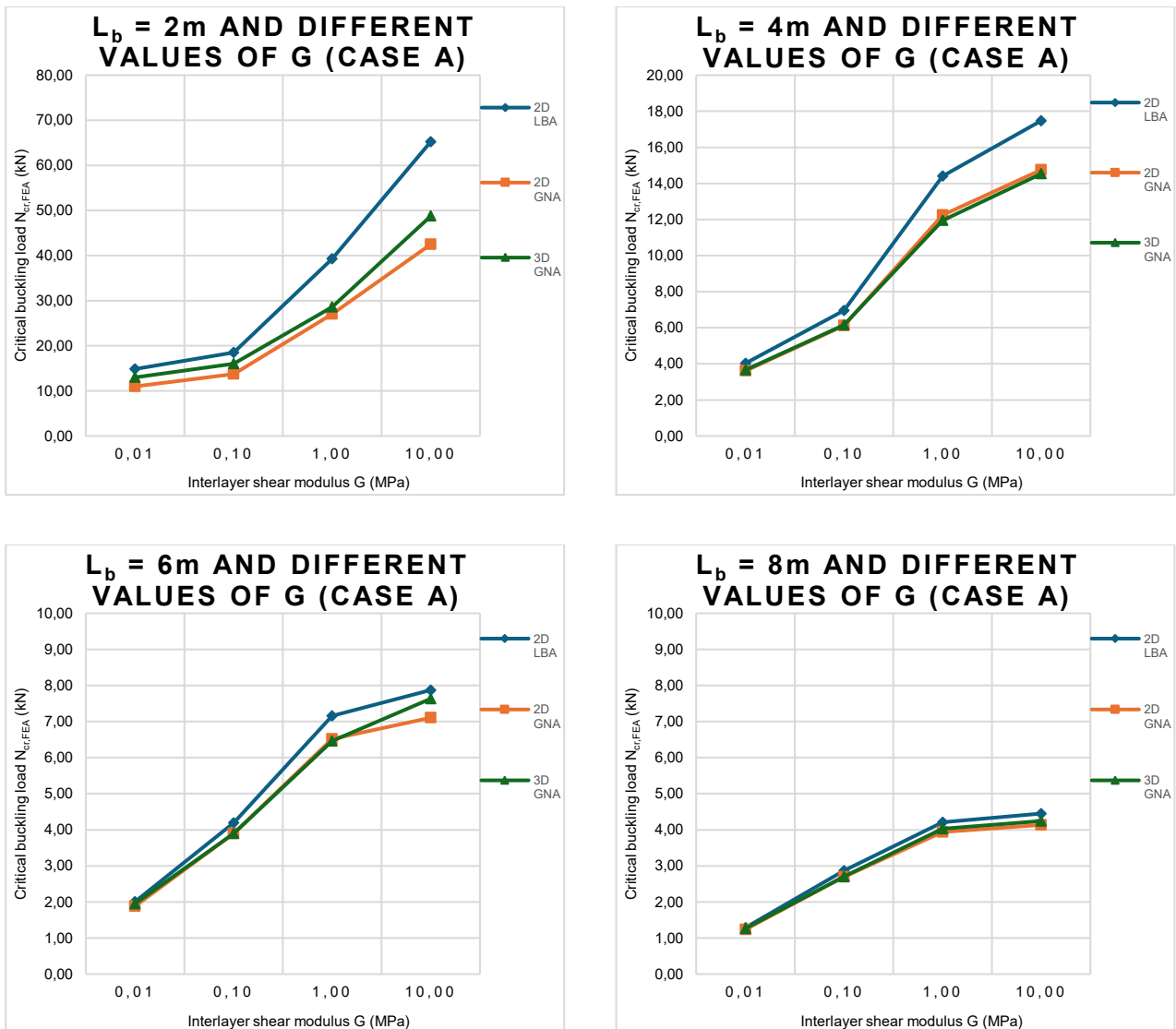


Figure 6-4: Effect of shear modulus G on the critical buckling load $N_{cr,FEA}$ (case A).

Case B :

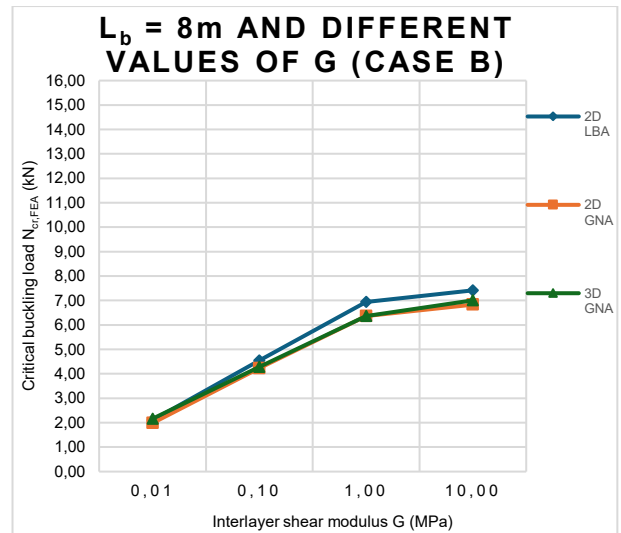
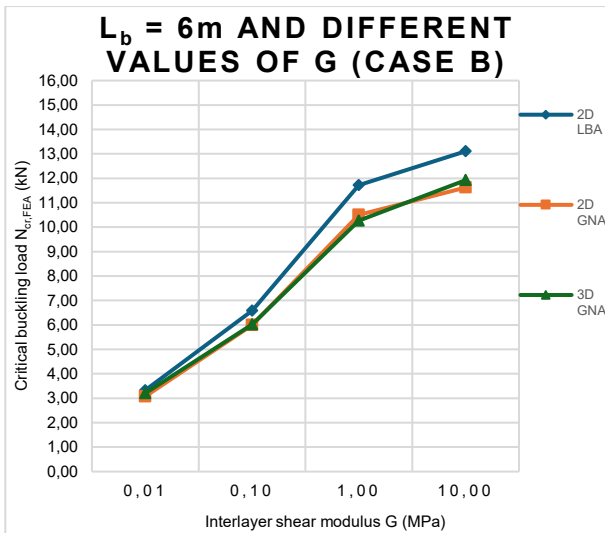
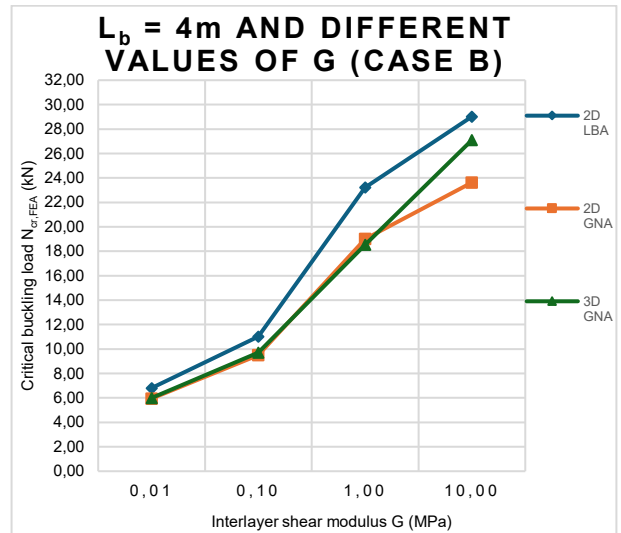
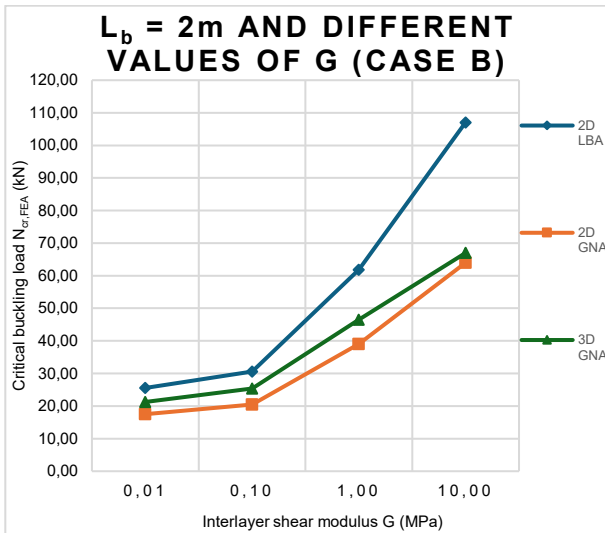


Figure 6-5: Effect of shear modulus G on the critical buckling load $N_{cr,FEA}$ (case B).

Case C :

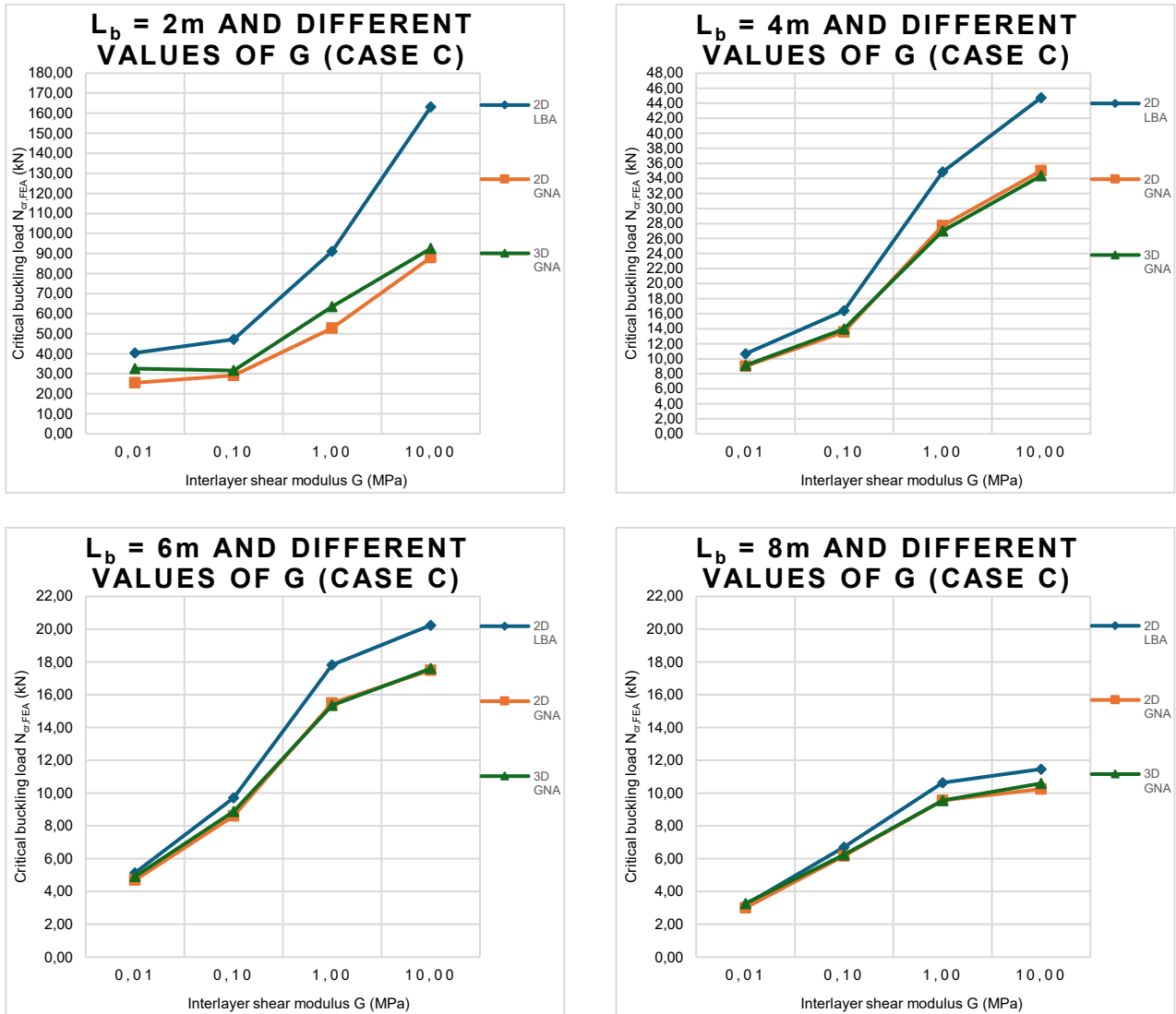


Figure 6-6: Effect of shear modulus G on the critical buckling load $N_{cr,FEA}$ (case C).

From the presented graphs, it can be noticed that geometrically nonlinear analysis (GNA) on 2D models only provides the lowest critical buckling loads for a buckling length $L_b = 2m$, and occasionally for $L_b = 4m$. Buckling loads, corresponding to nonlinear analysis on 3D models, as a whole are larger than 2D, even though are sometimes lower (e.g. $L_b = 4m$ for cases A, B and C). Nevertheless, by increasing the value of shear modulus, nonlinear analysis on both 2D and 3D models provide similar buckling loads within the range $4 m < L_b < 8 m$. Also, geometrically nonlinear analysis provides lower critical loads with respect to those of eigenvalue analysis (2D LBA, i.e. blue curve), as expected.

The interlayer shear modulus has a direct impact on the buckling load, since in case of adequate shear coupling effect and by increasing G , the flexural stiffness of the laminated glass pane increases; thus, it will be subjected to lower stresses and, as a consequence, it is possible to apply larger compressive loads (critical buckling load increases) prior to buckling occurring. Additionally, for $L_b = 6m$ and $8m$, once the value $G = 1$ MPa is overcome and up to 10 MPa, the increment in shear modulus no longer provides a significant benefit in terms of critical load increase, reaching a sort of plateau.

This behaviour may be associated to the shear coupling degree. Full shear coupling requires a certain span to be thoroughly exerted and once reached, it cannot increase more, resulting in a buckling load stand-off.

6.4 2D curved models: geometrically nonlinear buckling analysis results (2nd solution strategy)

2D Finite Element models, in the first solution strategy of this work, were set up using shell elements (*QSL8*) and the thickness to be assigned was the effective thickness for calculating out-of-plane bending deflection ($h_{ef,w}$) (Eq. 3.2 Section 3.2), since it is defined as the thickness of a fictitious monolithic glass element, characterized by equivalent bending properties in terms of deflection compared to the original multi-layered glass element [47]. It was required, since in nonlinear analysis it is crucial to accurately compute deflections rather than stresses. After that, geometrically nonlinear buckling analyses were conducted on 2D curved models: the first solution strategy required stopping the analysis at a specific load factor, when the characteristic bending strength of annealed glass ($f_{g,k}$) is reached in one of the most stressed points of the model.

The first approach implies that stresses are checked on 2D-FE models having thickness equal to $h_{ef,w}$, instead, in the second solution strategy that is going to be illustrated, stresses are checked on 2D models using a more appropriate thickness, that is the effective thickness for calculating out-of-plane bending stresses ($h_{ef,\sigma,i}$).

To be more accurate, it is necessary to derive buckling load factors (*BLF*) by means of nonlinear analysis on 2D curved models, having thickness defined by $h_{ef,w}$.

Subsequently, true stresses, denoted as $\bar{\sigma}$, can be computed using Navier's formula (see Eq. (6.1)), in which the contribution of $h_{ef,\sigma,i}$ is considered through the section modulus $W(h_{ef,\sigma,i})$.

$$\bar{\sigma} = \frac{P_0 \cdot BLF}{A_{full}} + \frac{P_0 \cdot BLF \cdot (\delta_{max} + e_0)}{W(h_{ef,\sigma,i})} \quad (6.1)$$

Where:

δ_{max} is the maximum transversal displacement read on 2D curved models, having thickness equal to $h_{ef,w}$.

$W(h_{ef,\sigma,i})$ is the section modulus of laminated glass with stress-equivalent effective thickness.

All the other parameters have already been defined.

The abovementioned section modulus, for a rectangular cross-section, can be determined as:

$$W(h_{ef,\sigma,i}) = \frac{b \cdot h_{ef,\sigma,i}^2}{6} \quad (6.2)$$

Where all the other parameters have already been specified.

Once obtained $\bar{\sigma}$, it is possible to evaluate the limit transversal displacement (δ_{lim}), which must be used as threshold in order to stop nonlinear buckling analysis on 2D curved models, and reads:

$$\delta_{lim} = \frac{f_{g,k}}{\bar{\sigma}} \cdot (\delta_{max} + e_0) \tag{6.3}$$

By knowing δ_{lim} , additional geometrically nonlinear buckling analyses were performed on 2D curved models for each case study. But currently, to determine critical buckling loads, the second solution strategy requires stopping the analysis at a specific load factor, when the limit transversal displacement δ_{lim} is reached in the midspan of the panel. The calculation of the variables necessary to obtain critical buckling loads and stresses and themselves are tabulated and presented in Annex E.

6.4.1 Effect of slenderness ratio on critical buckling stress (2nd solution strategy)

As shown from Figure 6-7 to Figure 6-9, in this second set of buckling curves, the effect of increment in the slenderness ratio of the panels on critical buckling stress is assessed, for several LG panels' with different thickness of glass layers (cases A, B and C) and for each interlayer shear modulus G .

Case A :

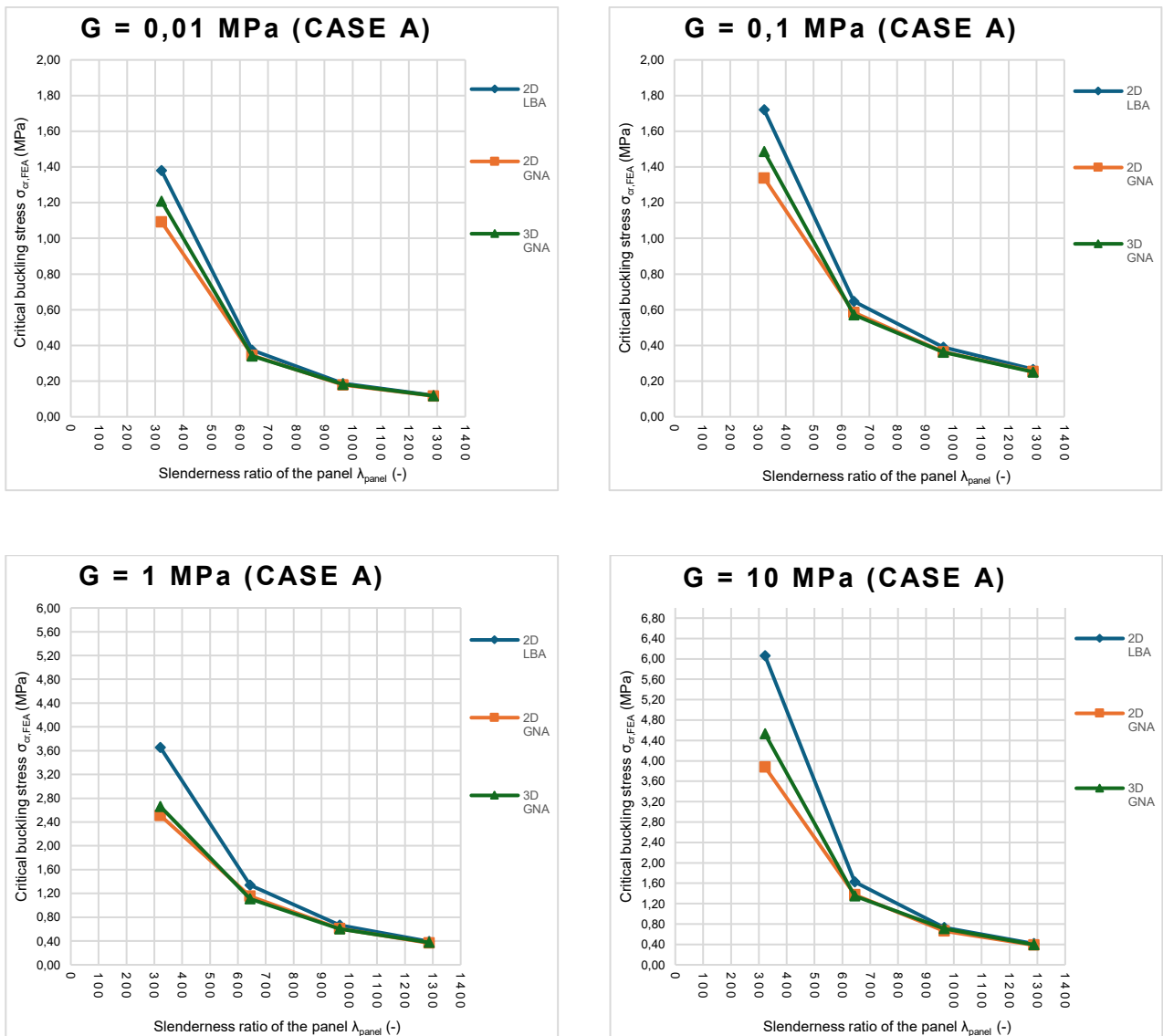


Figure 6-7: Buckling curves for case study A (2nd solution strategy).

Case B :

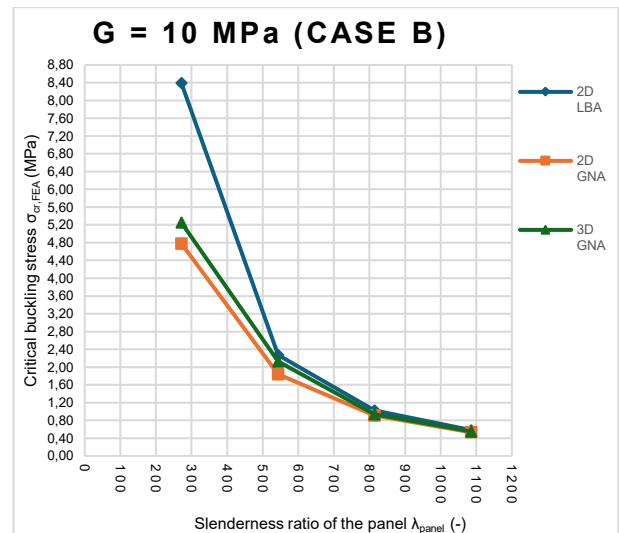
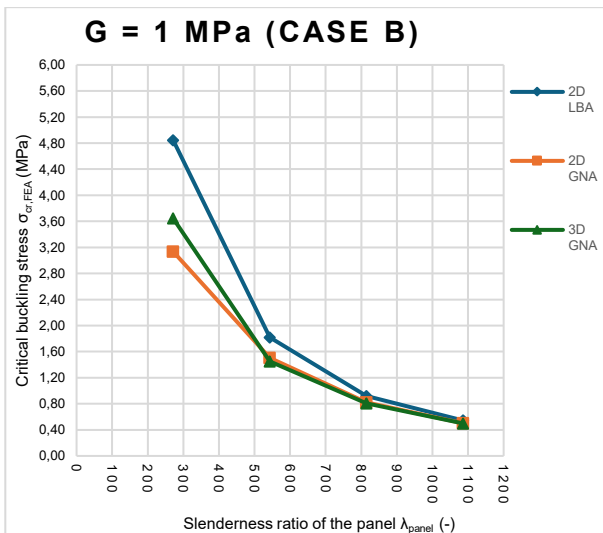
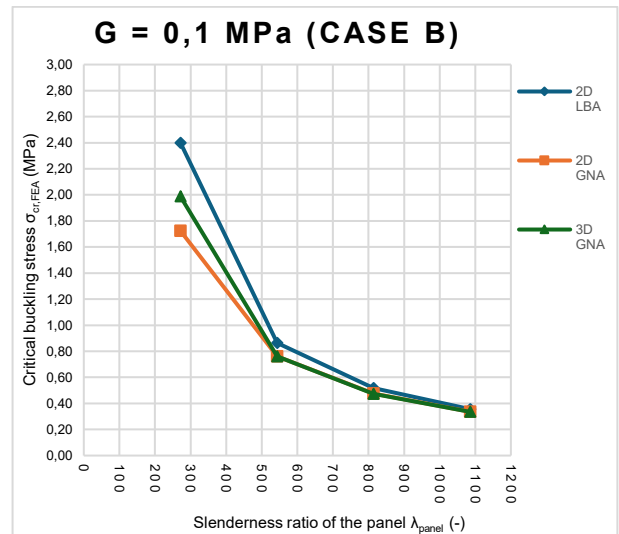
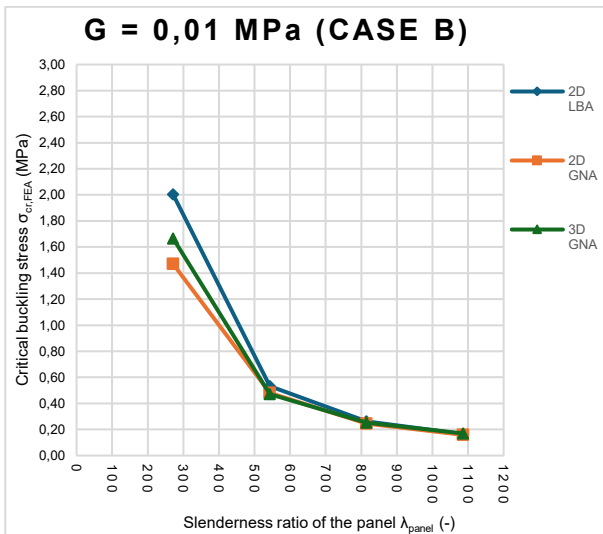


Figure 6-8: Buckling curves for case study B (2nd solution strategy).

Case C :

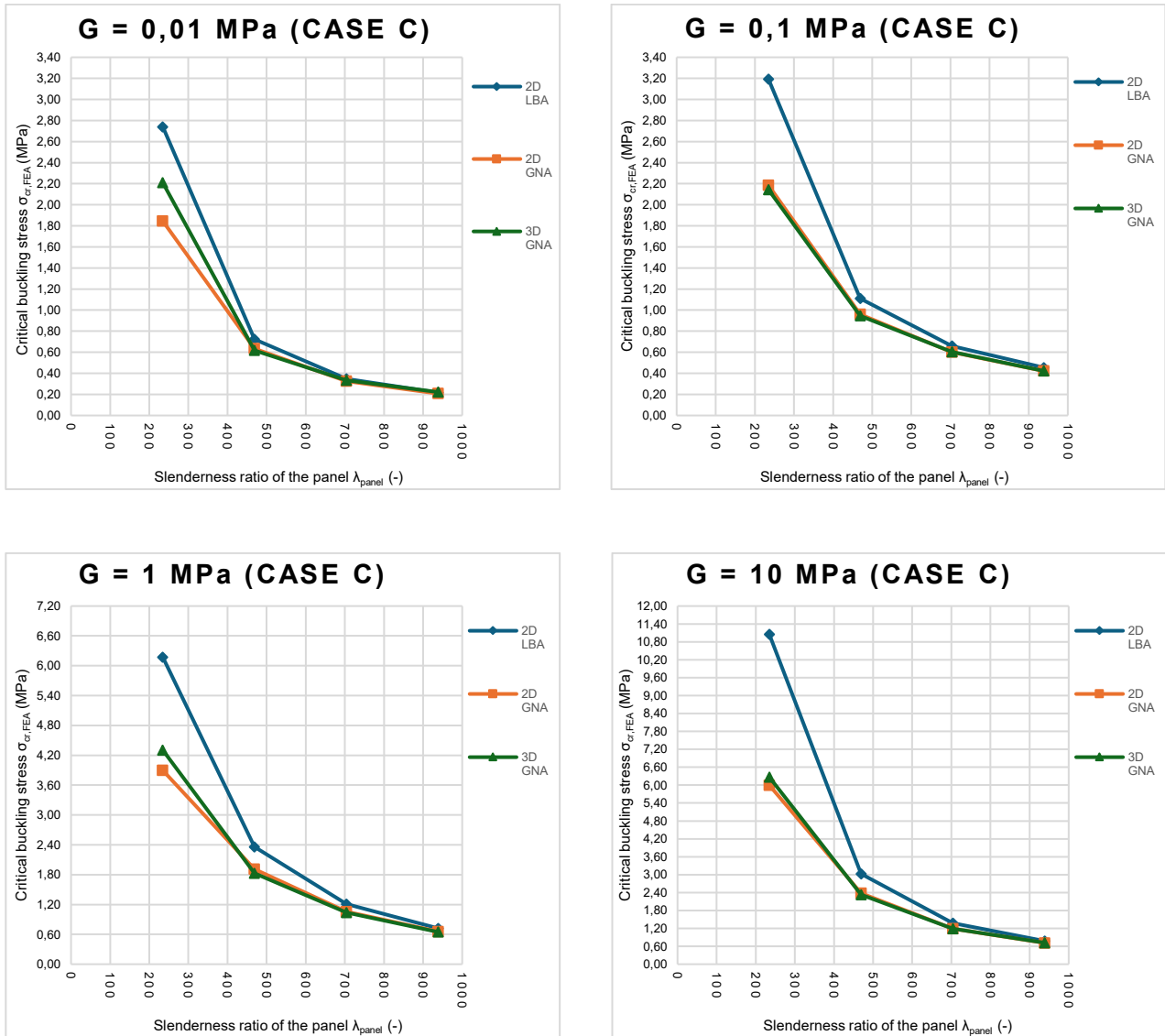


Figure 6-9: Buckling curves for case study C (2nd solution strategy).

Using this second approach, that is more rigorous, the latest buckling load factors (BLF) obtained by means of geometrically nonlinear analysis on 2D curved models, are always lower than the previous one (see Annex D), resulting in lower buckling stresses $\sigma_{cr,FEA}$. It is beneficial, since it allows to be on the safe side during design process and also to face the possibility to build up 2D-FE models, which require less computational costs compared to 3D-FE models.

In this solution strategy, buckling stresses obtained by means of 2D GNA are lower than those coming from 3D GNA, and it becomes mostly visible for lower slenderness ratios, i.e. within the range $2 < L_b < 4$ meters. It must be also observed that, in the same range, 3D-FE models tend to overestimate the critical buckling load. Finally, critical buckling stresses, provided by geometrically nonlinear analyses on 2D curved and 3D models, are similar thus the corresponding curves tend to be aligned for large slenderness ratios (i.e. $4 < L_b < 8$ meters).

6.5 Buckling load-displacement curves

This paragraph is dedicated to illustrate the critical load vs displacement curves for in-plane loaded *LG* panels, which involve only *3D-FE* models (case A), since it is reasonable to assume that they can be regarded as the most accurate and reliable. Also, the effect of interlayer shear modulus *G* is taken into account (*G* = 0,01 MPa, 0,1 MPa, 1 MPa and 10 MPa) in the development of the curves.

The graphs, shown in Figure 6-10, are built up for each models' length (*L_b*) by collecting the critical buckling load (*N_{cr,FEA}*) and corresponding maximum transversal displacement (*δ_{max}*) of each *3D* model, for different glass bending strengths: annealed glass as-is (*f_{g,k}* = 45 MPa), annealed glass considering long-term loads (*f_{g,d}* = 20 MPa) and fully tempered glass considering long-term loads (*f_{g,d}* = 80 MPa).

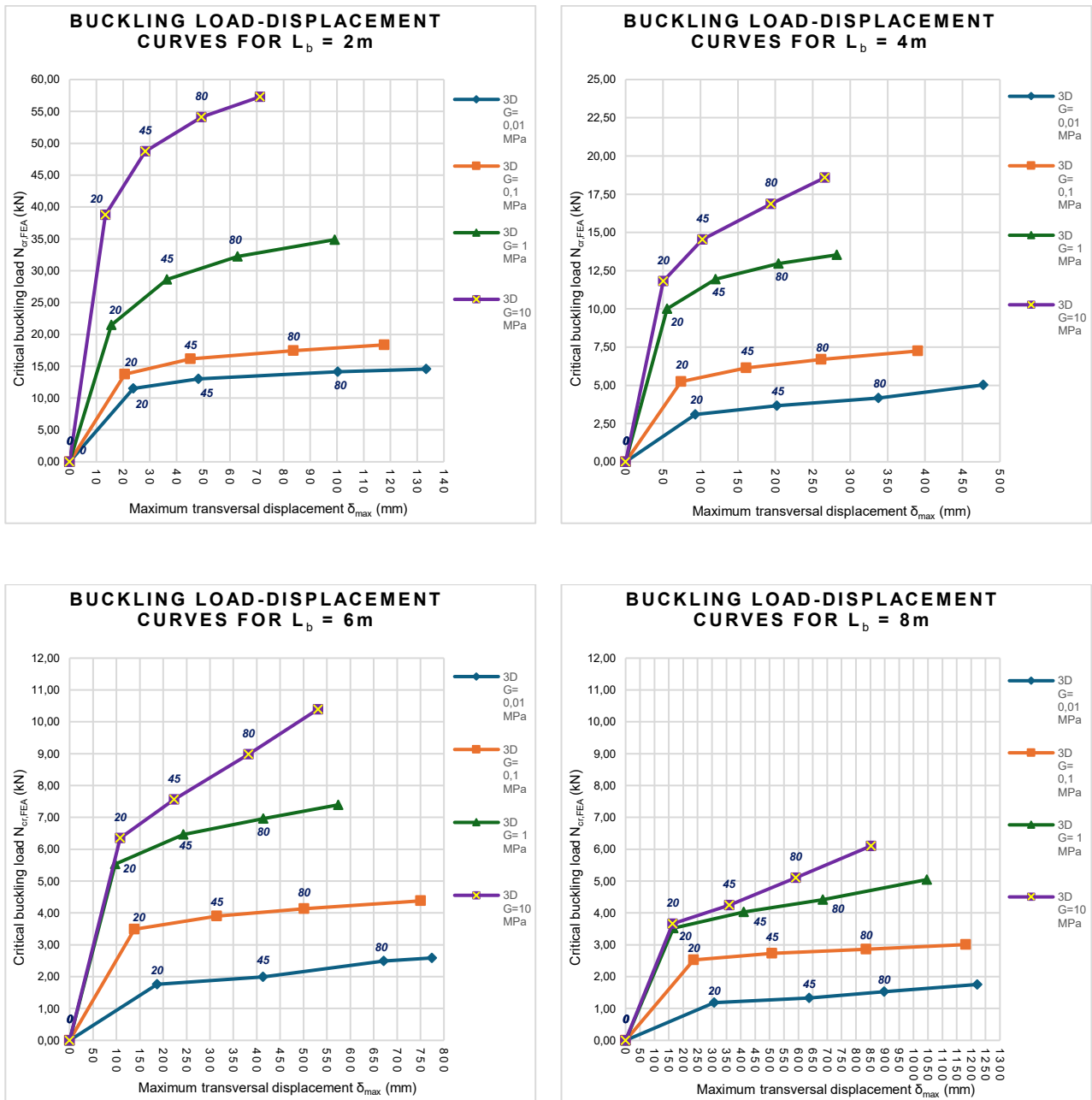


Figure 6-10: Buckling load vs displacement curves for different lengths L_b (case A).

It is possible to notice that, for the same shear modulus G and different buckling lengths L_b , the decreasing trend of buckling load $N_{cr,FEA}$ is not linear. It tends to decrease less rapidly while the maximum transversal displacement increases consistently. For instance, in the case $G=0,01$ MPa and considering the two different glass typologies (*ANG* and *FTG*) with long-term loading conditions, along each curve there is not a noticeable increment in the buckling load for different buckling lengths. In this respect, it is visible that, when the design bending strength of annealed glass considering long-term loads ($f_{g,d}=20$ MPa) is reached, the curves for $G=0,01$ MPa and $G=0,1$ MPa attain a sort of plateau in terms of buckling load. The other curves, related to $G=1$ MPa and $G=10$ MPa, are keeping increasing in buckling load, albeit with different rates.

So, different glass typologies, for extremely low values of interlayer shear modulus, do not play a prominent role in the determination of buckling load, even though their use could be favourable in order to withstand larger transversal displacements until failure. In fact, moving from *ANG* with long-term loading to *FTG* under the same loading conditions, each glass panel may experience greater transversal displacements within a range of 3-4 times. Rationally, with reference to buckling performance, the choice of a specific glass type for *LG* units and the definition of loading term conditions, must be made jointly to the expected interlayer shear modulus. The critical buckling load assumes ever-increasing values as the shear modulus increases, regardless of the length of the glass pane.

Additionally, increasing the span of the model, the curves related to $G=1$ MPa and $G=10$ MPa tend to move closer. In particular, as regards the case $L_b=8$ m, the branches of the two different curves are even almost overlapped up to $f_{g,d}=20$ MPa and then they branch out. As a conclusion, with the approaching of the curves, the buckling load “reserve” for the aforementioned curves is steadily decreasing, indicating that full shear coupling behaviour is rapidly achieved for large values of both interlayer shear modulus and buckling length.

6.6 Design buckling curves for in-plane compressed LG panels

In this section, some design buckling curves for laminated glass elements subjected to in-plane compressive loads are proposed, as illustrated in Figure 6-11. This plot is realised by collecting, for each interlayer shear modulus G , the critical buckling stress ($\sigma_{cr,FEA}$) obtained from geometrically nonlinear analysis and the corresponding slenderness ratio of the panel (λ_{panel}) for each *3D-FE* model. A curve fitting process is then required to find an analytical relationship between the series of data points. To get the best approximate fit, which is able to minimise the error on data, different types of regression functions (polynomial, logarithmic, exponential, power) have been tested. Power law turned out to be the best function in fitting the outcomes, supported by the coefficient of determination R^2 which is always closer to the unit.

The obtained design buckling curves provide a practical tool during the pre-design phase of in-plane loaded glass elements, against buckling phenomena. By knowing the geometric characteristics of the element to be designed (i.e. slenderness ratio of the panel) and the interlayer shear modulus, it is possible to get into the plot and read the critical buckling stress.

The same buckling curves can be also visualized in bi-logarithmic scale, as shown in Figure 6-12. Since regression curves are described by means of power functions, they turn into regression lines using bi-logarithmic scale. In the present diagram, it is possible to note that design buckling curves, related to $G=0,01$ MPa and $G=10$ MPa, are characterised by the same slope (see the exponent of power laws). Starting from $G=0,01$ MPa and increasing the shear modulus, the slope of the lines increases up to $G=1$ MPa whereas, from this point on, slope begins to decrease approaching $G=10$ MPa. It entails that full shear coupling is progressively reached within $1 < G < 10$ MPa. Also, the points of intersection between the different lines evidence that, for different G -values but same slenderness ratio, the behaviour of *3D* models is the same (critical buckling stresses are equal).

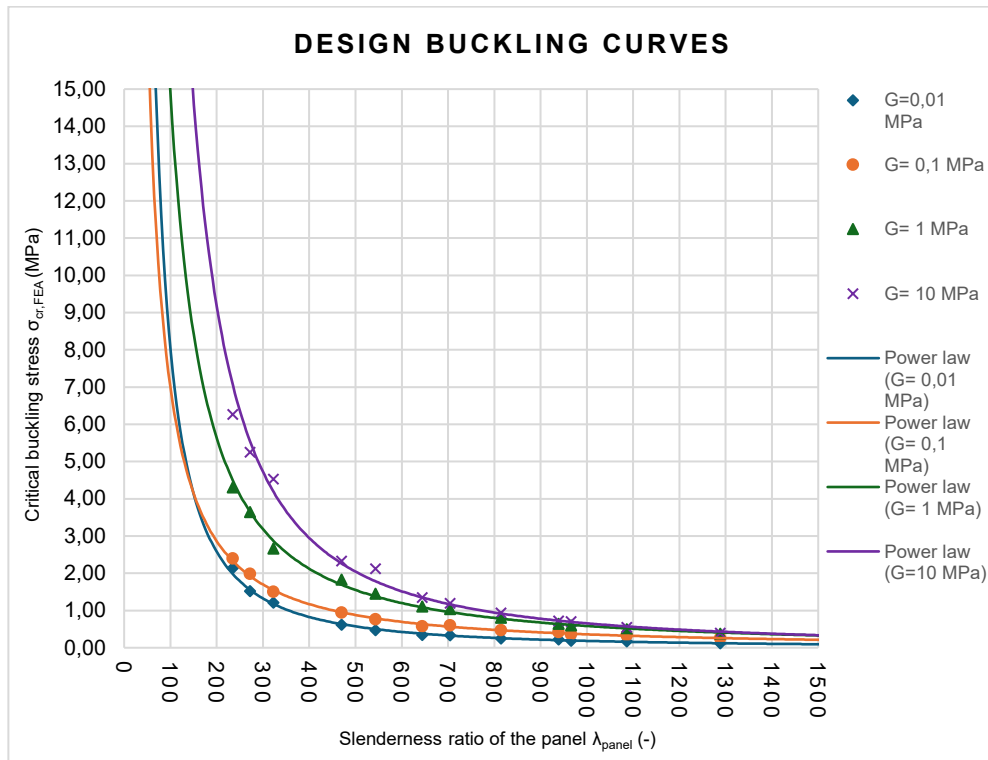


Figure 6-11: Design buckling curves for in-plane loaded LG elements

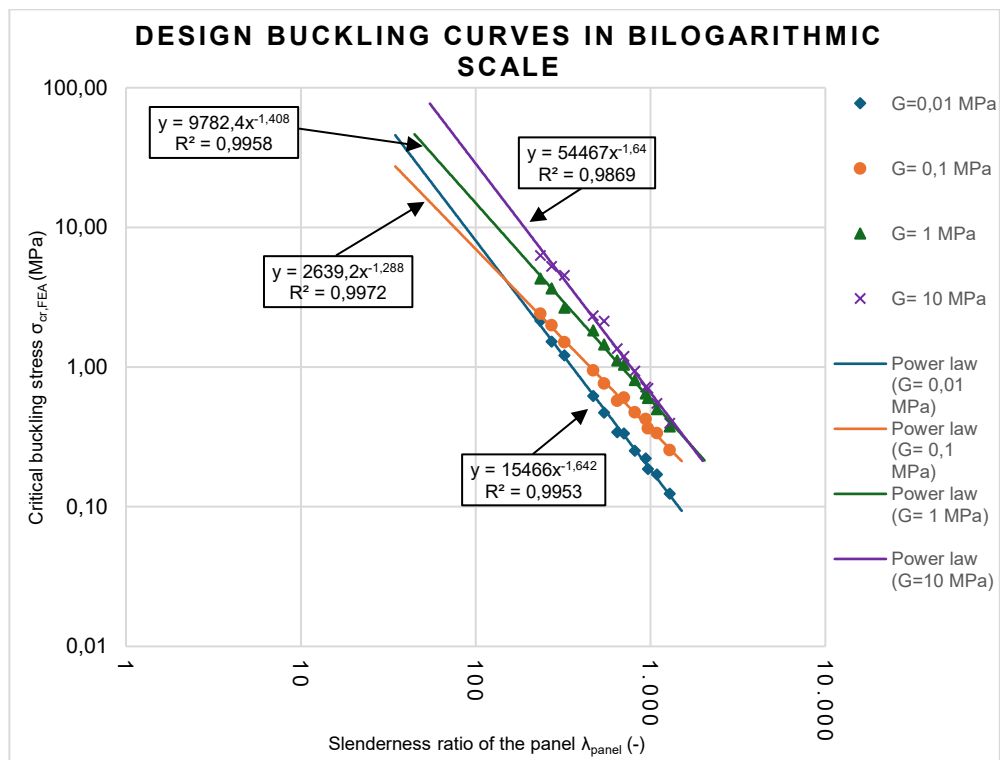


Figure 6-12: Design buckling curves for in-plane loaded LG elements in bi-logarithmic scale

6.7 Design buckling curves for in-plane compressed LG panels based on Eurocode approach

This paragraph is conceived to introduce design buckling curves for laminated glass members subjected to in-plane compressive loading, in compliance with the framework provided by Eurocode 3 [48].

EC3-1-1 for design of steel buildings [48] proposes five design buckling curves (named a_0 , a , b , c , d) for in-plane compressed steel members. Each buckling curve is associated to a specific imperfection factor and consequently, the selection of the appropriate buckling curve must be made taking into consideration the typology of cross-section, the steel grade and the axis about which buckling could occur. Rationally, the approach for steel cannot be applied to *LG* members in its entirety.

The aforementioned Eurocode, to plot the buckling design curves, introduces two nondimensional parameters: nondimensional slenderness ($\bar{\lambda}$) and buckling reduction factor (χ). These last ones can also be used for laminated glass and should be defined as follows:

$$\bar{\lambda} = \sqrt[2]{\frac{A_{full} \cdot f_{g,k}}{N_{cr,LG}}} \quad (6.1)$$

Where $f_{g,k}$ is the characteristic bending strength for float glass. If strengthening processes are involved, in place of $f_{g,k}$, the characteristic bending strength for pre-stressed glass after processes must be used ($f_{b,k}$).

$$\chi = \frac{1}{\Phi + \sqrt{\Phi^2 - \bar{\lambda}^2}} \quad (6.2)$$

Where:

$$\Phi = 0,5 \cdot [1 + \alpha_{imp} \cdot (\bar{\lambda} - \alpha_0) + \bar{\lambda}^2] \quad (6.3)$$

α_{imp} and α_0 are imperfection coefficients, appropriately calibrated, and based on numerical, experimental tests and data available in literature on monolithic and laminated glass beams. More specifically, the coefficient α_0 identifies the values of nondimensional slenderness associated to a buckling reduction factor (χ) equal to 1, while the value of the coefficient α_{imp} individuates the maximum allowable imperfection for the compressed member [40].

Considering that, the imperfection coefficients for glass can be set as: $\alpha_{imp} = 0,71$ and $\alpha_0 = 0,60$ [40].

In addition, for the purpose of plotting numerical results coming from geometrically nonlinear analysis on *3D-FE* models, it is also convenient to define the buckling reduction factor as:

$$\chi_{FEM} = \frac{N_{cr,FEM}}{A_{full} \cdot f_{g,k}} \quad (6.4)$$

Where $f_{g,k}$ is the characteristic bending strength for float glass. If strengthening processes are involved, in place of $f_{g,k}$, the characteristic bending strength for pre-stressed glass after processes must be used ($f_{b,k}$).

All the other parameters have already been defined.

The Eurocode-based design buckling curves can be easily used during pre-design phase of in-plane loaded glass elements, against buckling phenomena. By knowing the geometric characteristics of the member and the type of glass constituting the *LG* pane (i.e. area of laminated glass and glass characteristic bending strength), it is possible to compute the non-dimensional slenderness ($\bar{\lambda}$). Subsequently, by computing the factor Φ , the reduction factor for the relevant buckling mode (χ) can be obtained by graphical approach.

By knowing the buckling reduction factor, the design buckling resistance of compressed laminated glass member should be taken as:

$$N_{b,Rd} = \frac{\chi \cdot A_{full} \cdot f_{g,d}}{\gamma_{M1}} \quad (6.5)$$

Where γ_{M1} is a buckling safety factor ($\gamma_{M1} = 1,40$) [40]. The other terms have already been defined.

Then, buckling verification should be checked:

$$N_{Ed} \leq N_{b,Rd} \quad (6.6)$$

Where:

N_{Ed} is the design compressive load.

$N_{b,Rd}$ is the design buckling resistance of the laminated glass member.

All the calculations regarding buckling parameters are tabulated and presented in Annex F.

As shown from Figure 6-13 to Figure 6-16, several design buckling curves, consistent with EC3 approach [48], are obtained and plotted. They are mapped out for the three main glass types: annealed (*ANG*), heat strengthened (*HSG*) and fully tempered (*FTG*).

Firstly, the graphs are realised using analytical calculations: calculating and collecting the nondimensional slenderness ($\bar{\lambda}$) using Eq. (6.1), and the corresponding buckling reduction factor (χ) using Eq. (6.2), for each model length (case studies A, B and C). To validate analytical buckling curves, the same approach is used to plot design buckling curves by making use of *3D-FEM* numerical results, with the only difference being that the reduction factor (χ_{FEM}) shall be computed with Eq. (6.4).

A curve fitting process is then required to find an analytical relationship between the series of data points. Even then, power law turned out to be the best function in fitting the outcomes, supported by the coefficient of determination R^2 which is always closer to the unit. In addition, to better visualize the results and since regression curves are described by means of power functions, bi-logarithmic scale can be used.

It is possible to note that nondimensional slenderness values for laminated glass are typically larger (within a range 3-25) compared to those of design buckling curves for steel (within a range 0,2-3). Laminated glass panes are commonly characterised by large values of area as compared to critical buckling load, resulting in large nondimensional slenderness values. Furthermore, in glass design buckling curves, the limit regarding the reduction factor ($\chi = 1$) is quite difficult to be attained. This limit would imply having stubby *LG* panes but, normally, glass plies have small thickness, which, compared to the length of the panels, makes them really slender.

The graphs show similar results for both analytical design buckling curves and those obtained by means of numerical simulations on 3D models. In detail, bi-logarithmic graphs, illustrating the comparison between analytical and numerical buckling regression lines, indicate that numerical simulations tend to slightly underestimate buckling reduction factors for low values of nondimensional slenderness, while they marginally overestimate them for large values.

And lastly, Figure 6-16 presents the final EC-based design buckling curve for laminated glass members in compression, obtained by combining all the analytical design buckling curves for different glass types.

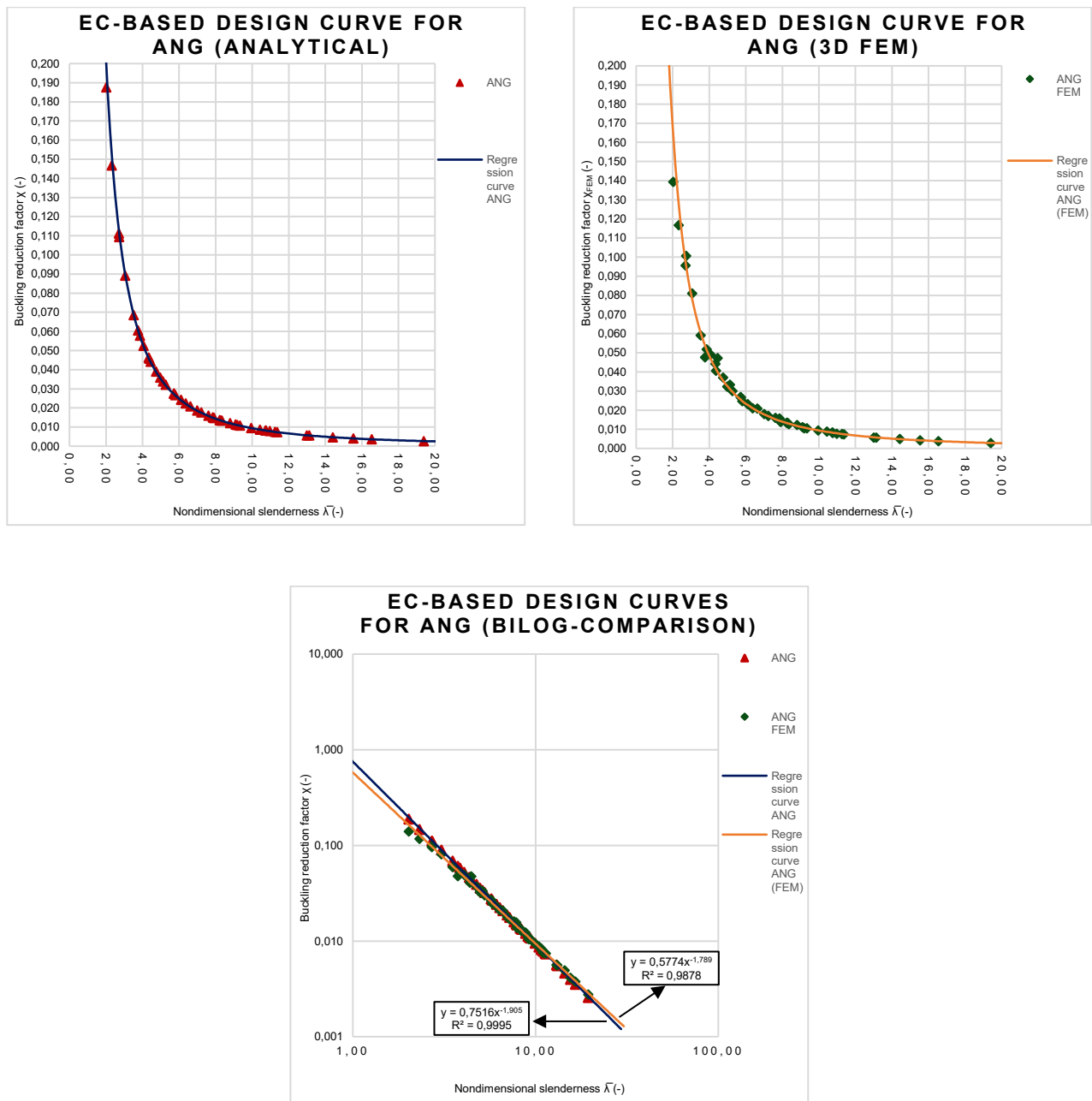


Figure 6-13: Design buckling curves based on Eurocode for annealed glass (ANG).

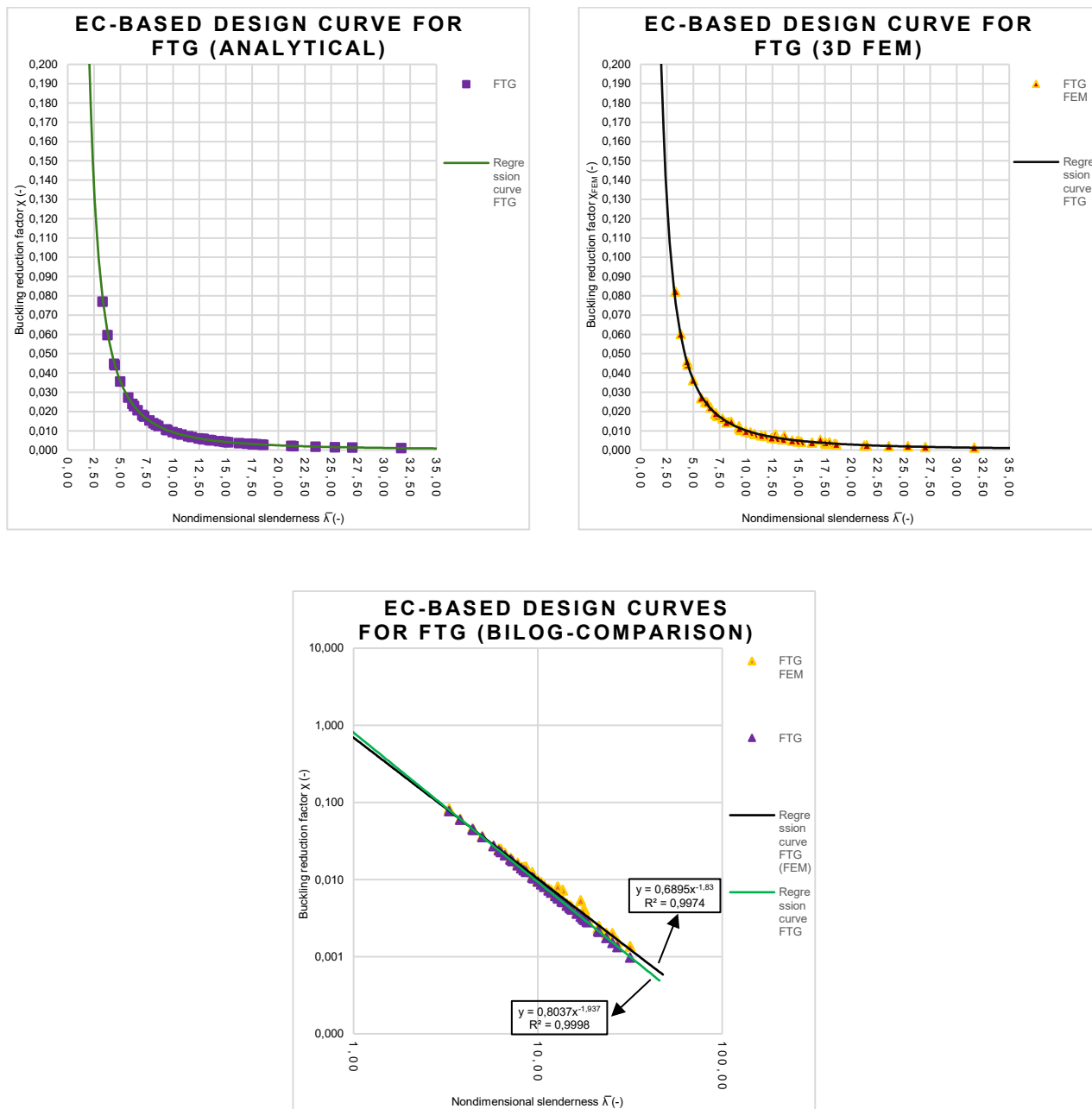


Figure 6-14: Design buckling curves based on Eurocode for fully tempered glass (FTG).

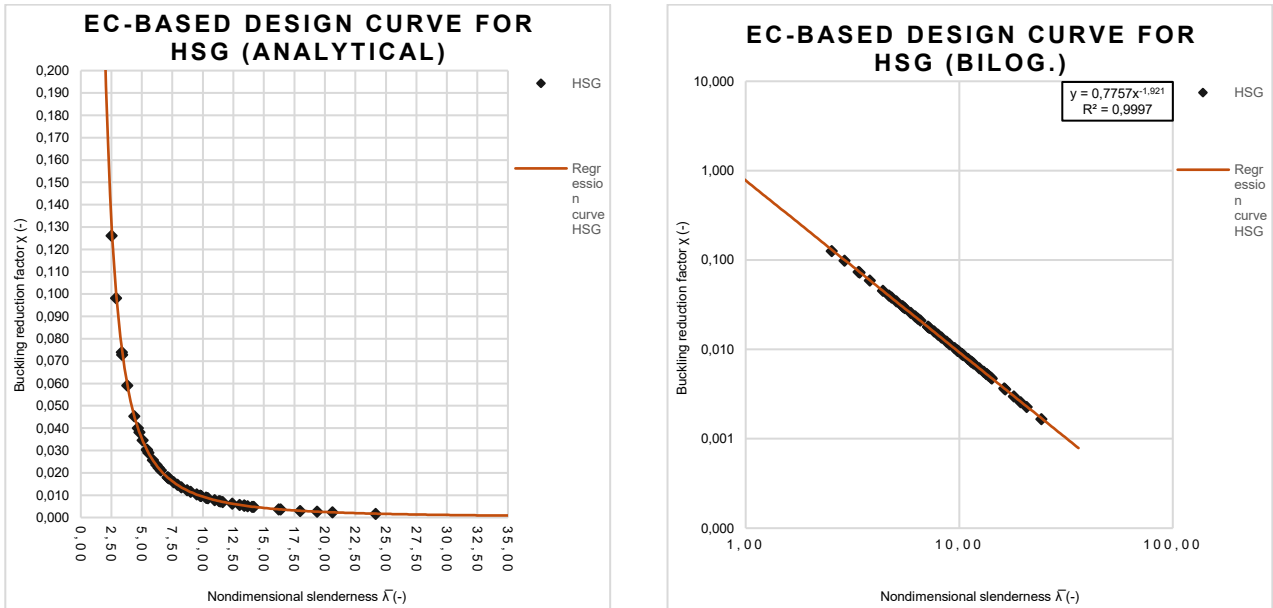


Figure 6-15: Design buckling curves based on Eurocode for heat strengthened glass (HSG).

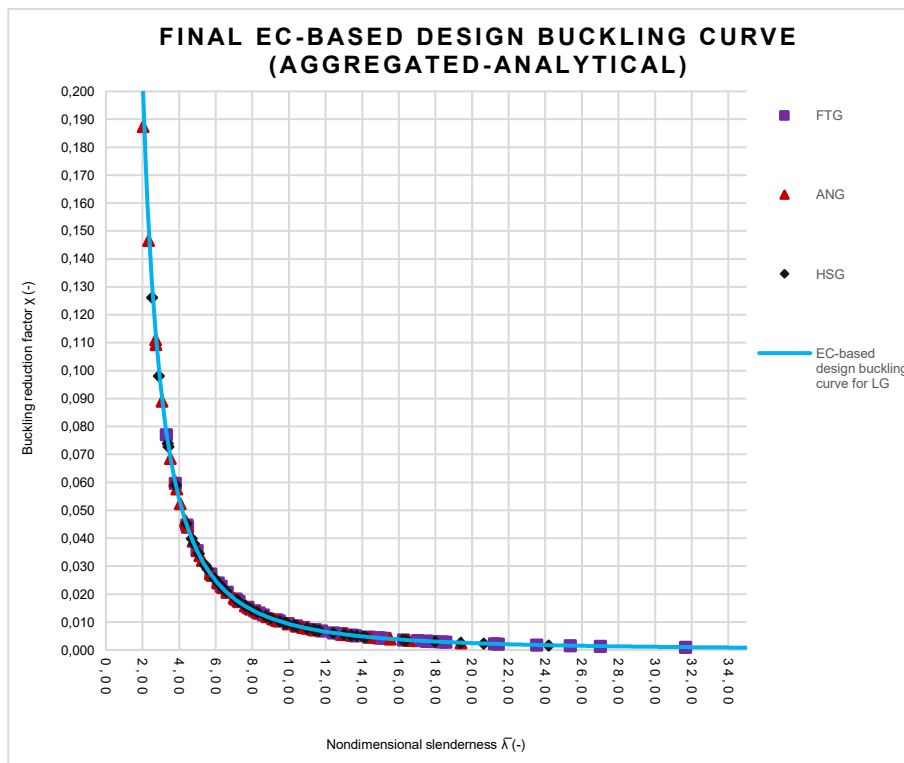


Figure 6-16: Final Eurocode-based design buckling curve for laminated glass members in compression

6.7.1 Practical implementation of EC-based design buckling curve for laminated glass

Let's consider a double laminated glass member which must bear a portion of the roof. The glass column is pinned along short edges and free along longer sides. The panel has width $b = 400$ mm and length $L_b = 3000$ mm and it is subjected to a design compressive load $N_{Ed} = 10$ kN/m. The resultant of the design load is equal to 4000 N. The laminated glass unit consists of two glass plies (fully tempered FTG), having thickness $h_1 = h_2 = 16$ mm, held together by two PVB foils. Each foil has nominal thickness $t = 0,76$ mm (total thickness $h_{int} = 1,52$ mm). Let's consider an unfavourable case, in which the interlayer shear modulus (G) is characterised by a low value: $G = 0,1$ MPa. It is required to evaluate the design buckling resistance of the laminated glass member, using the EC-based design buckling curve.

Firstly, it is necessary to calculate the elastic critical buckling load ($N_{cr,LG}$) according to Eq. (3.4):

$$N_{cr,LG} = \frac{\pi^2 E_g I_{z,eff}}{L_b^2} = 28235,63 \text{ N}$$

Then, it is necessary to compute the nondimensional slenderness ($\bar{\lambda}$), using Eq. (6.2):

$$\bar{\lambda} = \sqrt{\frac{A_{full} \cdot f_{b,k}}{N_{cr,LG}}} = 7,549 \cong 7,5$$

Where:

$$A_{full} = 2(400 \cdot 16) \text{ mm} + (400 \cdot 1,52) \text{ mm} = 13408 \text{ mm}^2$$

$$f_{b,k} = 120 \text{ MPa}$$

Subsequently, the buckling reduction factor (χ) can be calculated analytically, by means of Eq. (6.2) or derived by getting into the EC-based design buckling curve. Let's apply both the analytical and graphic approach.

Analytical approach:

$$\Phi = 0,5 \cdot [1 + \alpha_{imp} \cdot (\bar{\lambda} - \alpha_0) + \bar{\lambda}^2] = 31,460$$

Where the imperfection coefficients can be set as: $\alpha_{imp} = 0,71$ and $\alpha_0 = 0,60$ for glass members [40].

$$\chi = \frac{1}{\Phi + \sqrt{\Phi^2 - \bar{\lambda}^2}} = 0,0161$$

Graphical approach:

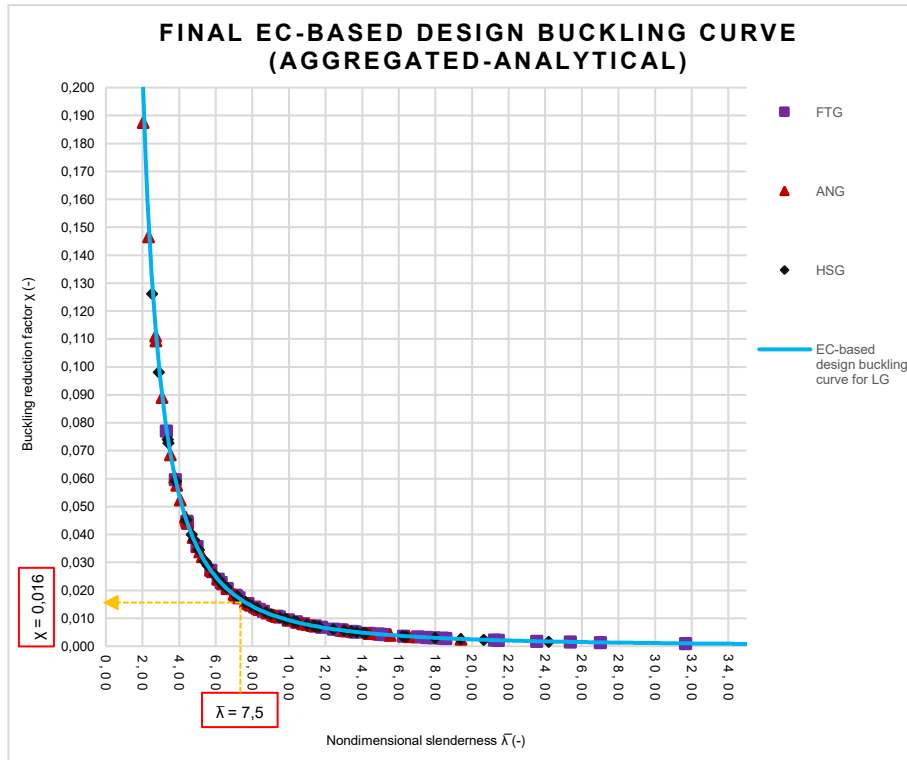


Figure 6-17: Practical implementation of EC-based design buckling curve for glass.

It can be noted that the buckling reduction factor, obtained by means of the two approaches, is very similar. Once the buckling reduction factor is known, the design buckling resistance of compressed laminated glass member should be computed with Eq. (6.5):

$$N_{b,Rd} = \frac{\chi \cdot A_{full} \cdot f_{g,d}}{\gamma_{M1}} = 8827,49 \text{ N}$$

Where γ_{M1} is a buckling safety factor ($\gamma_{M1} = 1,40$) [40].

The design bending strength of glass ($f_{g,d}$) has been calculated using Eq. (3.1):

$$f_{g,d} = k_e \cdot k_{sp} \cdot \lambda_A \cdot \lambda_1 \cdot k_{mod} \cdot \frac{f_{g,k}}{\gamma_M} + k_p \cdot k_{e,p} \cdot \frac{f_{b,k} - f_{g,k}}{\gamma_p} = 57,25 \text{ MPa}$$

Where:

- $k_e = 1,0$ (polished edges)
- $k_{sp} = 1,0$ (surface not sandblasted)
- $\lambda_A = 1,0$ (area of the pane does not exceed 18 m²)
- $\lambda_1 = 1,0$ (area of the pane does not exceed 18 m²)
- $k_{mod} = 0,29$ (for permanent loads)
- $f_{g,k} = 45 \text{ MPa}$ (characteristic bending strength of annealed glass)
- $\gamma_M = 1,8$ (material partial safety factor)
- $k_p = 1,0$ (heat treatment with horizontal process)
- $k_{e,p} = 0,8$ (since edges are polished and the load is in-plane)

$f_{b,k}$ = 120 MPa (characteristic bending strength of fully tempered glass after thermal process)
 γ_p = 1,2 (Class of consequence 2 – CC2)

Then, buckling verification should be checked:

$$N_{Ed} \leq N_{b,Rd} = 4000 N \leq 8827,49 N \quad \mathbf{VERIFIED} \quad (6.6)$$

7 FINAL CONCLUSIONS

This section presents a brief recap of the entire work and the main findings obtained from analyses, also including some study limitations and recommendations for future works.

7.1 General conclusions

The leading objective of this study regards the structural behaviour of laminated glass, in more detail, the problem of buckling instability, for the purpose of highlighting the dependency and variation of the critical buckling load/stress on slenderness ratio and interlayer shear modulus of the glass pane.

Chapter 3 represents the starting point of the whole work, since illustrates the Enhanced Effective Thickness Theory and some analytical formulas, suggested by glass Technical Specifications, for glass design as regards design bending strength and buckling load calculation. Then, Chapter 4 provides a theoretical background concerning the two different typologies of numerical simulations: linear buckling and geometrically nonlinear buckling analyses, performed in a commercial Finite Element program, *LUSAS*.

Chapter 5 is devoted to describe the set of models - *2D* flat, *2D* and *3D FE*-models characterized by initial geometric imperfection - realized in *LUSAS*, in all their relevant parts: element types, mesh density, geometric and materials characteristics, boundary and loading conditions.

Thereafter, Chapter 6 illustrates a series of significant findings obtained from numerical simulations (linear and nonlinear analyses), in the form of graphs. The first solution strategy for nonlinear analysis requires to stop it when the characteristic bending strength of annealed glass $f_{g,k}$ is reached, and then, buckling loads are obtained and buckling stresses can be computed.

Firstly, through a parametric analysis, the effect of slenderness ratio on critical buckling stress is assessed and compared between the three sets of models, emphasizing the decreasing relationship between critical buckling stress and slenderness ratio of the panel. From a graphical point of view, some numerical buckling curves, are plotted, providing buckling stresses which are always lower than those provided by theoretical one, since geometric nonlinearity affects buckling behaviour by reducing the buckling load. Also, the two different typologies of Finite Element models, two-dimensional and three-dimensional, behaves in a similar way for relatively high values of slenderness ratio, entailing the option to model laminated glass by means of *3D* models, which require high computational costs owing to the large number of degrees of freedom and the complexity of the model itself.

Secondly, the effect of interlayer shear modulus degradation on critical buckling stress is analysed and compared between the three sets of models, by carrying out a parametric analysis. It was found that geometrically nonlinear analysis on *2D* models provides, in principle, the lowest critical buckling loads only for a buckling length L_b equal to 2 meters. Then, increasing the length of the pane and also the shear modulus, provide similar buckling loads on both *2D* and *3D* models, which are always lower than those obtained from eigenvalue analysis.

After that, to be really consistent, a second solution strategy for nonlinear analysis is used and requires to stop it when a threshold in terms of displacement is reached, and then, buckling loads are obtained and buckling stresses can be computed. By doing this, it can be concluded that geometrically nonlinear analysis on *2D* models provides the lowest critical buckling loads with respect to *3D* models. Moreover, this result is favourable, since it is for safety's sake during design process of a possible *2D* model. Finally, several buckling curves and also design buckling curves are obtained and discussed.

7.2 Limitations of the work

Finite Element Method is considered as a reliable technique to reproduce and predict the behaviour of a physical object for a certain phenomenon. For this reason, some basic assumptions must be taken into account, since the reality is too complex to be analysed as it is.

The first assumption is related to materials, in particular to *PVB* interlayer, since it is defined and categorized as a viscoelastic material, implying that its physical properties are not constant over the time, but they could strongly vary, depending on load duration and temperature. However, in this study, *PVB* is assumed as a linear elastic material, characterized by “equivalent” mechanical properties, able to account for the degradation of its shear stiffness G . The second assumption regards the form of the initial geometric imperfection of the curved *2D* and *3D* models. It can be assumed that sinusoidal shape is able to well-describe the initial geometric imperfection in laminated glass, but in view of simplifying the realization of curved models, the initial imperfection was described as a simple arch.

Some challenges were encountered during modelling stage of *3D* models, in particular, as regards the selection of the mesh size and also the application of the eccentric load to the midplane of glass plies. It is known that the more refined is the mesh size, the more the solution will be accurate; conversely, it will result in longer computational time. In the case of *3D* models simulations, due to their complexity and large number of degrees of freedom, is more than necessary to find an optimal balance between accuracy and efficiency. This consideration led to use a coarse mesh in order to ensure reasonable computational time. Also, as concerns the compressive in-plane load, it was applied to the midplane of glass layers making use of extremely stiff “vertical plates”, there being no other way to apply an eccentric load in the Finite Element software.

The last assumption relates to boundary coefficient ψ_b , which is contained in the coupling parameter formula. It is used to compute the two effective thicknesses of glass: firstly, since laminated glass elements under analysis are very slender, the coupling parameter for beams $\eta_{b,2}$ was chosen, and secondly, the boundary coefficient for a simply supported static scheme with an out-of-plane distributed loading was selected (the glass Standard UNI CEN/TS 19100 does not provide any boundary coefficient for in-plane loaded glass components).

7.3 Future developments

This study is focused on the analysis of flexural buckling on double layered slender glass members by means of parametric analysis, which involves relevant factors such as the slenderness ratio of the panel and the shear modulus of the interlayer.

Future developments should focus on the buckling analysis of triple laminated glass panes, also considering the effect of load eccentricities and initial imperfections. Extensive investigations should be carried out as regards different types of restraints, as well as different boundary conditions. Lastly, other buckling forms such as torsional, lateral-torsional and dynamic buckling should be studied in depth.

REFERENCES

- [1] Leslie Forehand, "Glass in Architecture – Building Construction and Materials: An Open Educational Resource Textbook." Accessed: Jan. 10, 2025. [Online]. Available: <https://lbcc.pressbooks.pub/buildingconstruction/chapter/glass-in-architecture/>
- [2] "Energy saving: EU action to reduce energy consumption | Topics | European Parliament." Accessed: Jan. 11, 2025. [Online]. Available: <https://www.europarl.europa.eu/topics/en/article/20221128STO58002/energy-saving-eu-action-to-reduce-energy-consumption>
- [3] J. Savic, D. Djuric-Mijovic, and V. Bogdanovic, "Architectural glass: Types, performance and legislation," *Facta universitatis - series: Architecture and Civil Engineering*, vol. 11, no. 1, pp. 35–45, 2013, doi: 10.2298/FUACE1301035S.
- [4] "Building glass into the circular economy How to guide," 2018.
- [5] R. Green, A. Crosby, and T. McDonnell, "Structural Glass Design Manual," *Challenging Glass Conference Proceedings*, vol. 9, Jun. 2024, doi: 10.47982/cgc.9.598.
- [6] S. C. Rasmussen, "A Brief History of Early Silica Glass: Impact on Science and Society," *Substantia*, vol. 3, no. 2, pp. 125–138, 2019, doi: 10.13128/SUBSTANTIA-267.
- [7] ش. سلامه, "The study of the historical development of glass in ancient times," *مجلة العمارة والفنون والعلوم الإنسانية*, vol. 4, no. 17, pp. 12–20, Sep. 2019, doi: 10.21608/MJAF.2019.12434.1145.
- [8] "Glassblowing | Artisanal, Handcrafted, Sculpting | Britannica." Accessed: Jan. 10, 2025. [Online]. Available: <https://www.britannica.com/technology/glassblowing>
- [9] "History of Glassmaking - Lamberts Glass." Accessed: Jan. 10, 2025. [Online]. Available: <https://lamberts.de/history-of-glassmaking>
- [10] "Stained Glass in Medieval Europe | Essay | The Metropolitan Museum of Art | Heilbrunn Timeline of Art History." Accessed: Jan. 10, 2025. [Online]. Available: https://www.metmuseum.org/toah/hd/glas/hd_glas.htm
- [11] "History of Chartres cathedral | C'Chartres Tourisme." Accessed: Jan. 10, 2025. [Online]. Available: <https://www.chartres-tourisme.com/en/do-not-miss/the-chartres-cathedral/history-of-chartres-cathedral>
- [12] "Cylinder process." Accessed: Jan. 10, 2025. [Online]. Available: <https://www.pilkington.com/en-gb/uk/about/heritage/cylinder-process#>
- [13] "The Evolution of Glass in Building Design: A Historical Perspective- Singapore Safety Glass." Accessed: Jan. 10, 2025. [Online]. Available: <https://ssg.com.sg/the-evolution-of-glass-in-building-design-a-historical-perspective/>
- [14] B. Addis, "The crystal palace and its place in structural history," *International Journal of Space Structures*, vol. 21, no. 1, pp. 3–19, 2006, doi: 10.1260/026635106777641199.
- [15] "AD Classics: The Crystal Palace / Joseph Paxton | ArchDaily." Accessed: Jan. 10, 2025. [Online]. Available: <https://www.archdaily.com/397949/ad-classic-the-crystal-palace-joseph-paxton>
- [16] B. Addis, "The crystal palace and its place in structural history," *International Journal of Space Structures*, vol. 21, no. 1, pp. 3–19, 2006, doi: 10.1260/026635106777641199.
- [17] C O' Regan, "Structural use of glass in buildings (Second edition)," Oct. 2015.

- [18] “Story1 | People & Technology | NSG Group 100th Anniversary Website.” Accessed: Jan. 10, 2025. [Online]. Available: <https://100th.nsg.com/story/01/>
- [19] “The Best Uses of Glass in Modern Architecture | Osborn Glass.” Accessed: Jan. 10, 2025. [Online]. Available: <https://www.southlondonglass.co.uk/news/the-best-uses-of-glass-in-modern-architecture/>
- [20] “Material Masters: Glass is More with Mies van der Rohe | ArchDaily.” Accessed: Jan. 10, 2025. [Online]. Available: <https://www.archdaily.com/574575/material-masters-glass-is-more-with-mies-van-der-rohe>
- [21] “Apple Westlake, Hangzhou | Retail.” Accessed: Jan. 13, 2025. [Online]. Available: <https://www.fosterandpartners.com/projects/apple-westlake-hangzhou>
- [22] M. Haldimann, A. Luble, M. Overend, *Structural Use of Glass*. IABSE-AIPC-IVBH, ETH Zurich, 2008.
- [23] UNI Ente Italiano di Normazione, “EN 1748-1-1:2004 BSG properties.” Accessed: Jan. 17, 2025. [Online]. Available: <https://store.uni.com/en-1748-1-1-2004>
- [24] UNI Ente Italiano di Normazione, “UNI EN 572-1:2004- SLSG properties.” Accessed: Jan. 17, 2025. [Online]. Available: <https://store.uni.com/uni-en-572-1-2004>
- [25] “Physical properties of glass.” Accessed: Jan. 15, 2025. [Online]. Available: <https://www.eag.com/app-note/physical-properties-of-glass/>
- [26] “Sir Alastair Pilkington.” Accessed: Jan. 15, 2025. [Online]. Available: <https://www.pilkington.com/en/global/knowledge-base/glass-technology/sir-alastair-pilkington>
- [27] “A Brief Explanation of Chemically Strengthened Glass | glassonweb.com.” Accessed: Jan. 16, 2025. [Online]. Available: <https://www.glassonweb.com/article/brief-explanation-chemically-strengthened-glass>
- [28] M. Kozłowski, A. Malewski, V. Akmadžić, and A. Vrdoljak, “GLASS IN STRUCTURAL APPLICATIONS PRIMJENA STAKLA KAO NOSIVOG ELEMENTA,” 2019. [Online]. Available: <https://www.researchgate.net/publication/338608864>
- [29] “Autoclaving | Luc Moeyersons | glassonweb.com.” Accessed: Jan. 16, 2025. [Online]. Available: <https://www.glassonweb.com/article/autoclaving-luc-moeyersons>
- [30] M. C. Tanzi, S. Farè, and G. Candiani, “Mechanical Properties of Materials,” *Foundations of Biomaterials Engineering*, pp. 105–136, 2019, doi: 10.1016/B978-0-08-101034-1.00002-5.
- [31] *UNI CEN/TS 19100-1: 2021*. 2021.
- [32] M. Feldmann *et al.*, “The new CEN/TS 19100: Design of glass structures,” *Glass Structures and Engineering*, vol. 8, no. 3, Springer Science and Business Media Deutschland GmbH, pp. 317–337, Oct. 01, 2023. doi: 10.1007/s40940-023-00219-y.
- [33] Alberto Carpinteri, *Advanced Structural Mechanics*. CRC Press Taylor & Francis Group, 2016.
- [34] N. S. Trahair, *Flexural-Torsional Buckling of Structures - N. S. Trahair - Google Libri*. CRC Press Inc., 1993. Accessed: Jan. 17, 2025. [Online]. Available: https://books.google.it/books?id=gal8mSMK_RoC&printsec=frontcover&hl=it#v=onepage&q&f=false
- [35] L. Galuppi and G. Royer-Carfagni, “Enhanced Effective Thickness of multi-layered laminated glass,” *Compos B Eng*, vol. 64, pp. 202–213, Aug. 2014, doi: 10.1016/J.COMPOSITESB.2014.04.018.
- [36] *UNI CEN/TS 19100-2: 2021*. 2021.
- [37] *UNI CEN/TS 19100-3: 2021*. 2021.

- [38] O. Pesek, J. Melcher, M. Horacek, and I. Balazs, "On the Problem of the Imperfections of the Structural Glass Members Made of Flat Glass," *IOP Conf Ser Mater Sci Eng*, vol. 471, no. 5, Feb. 2019, doi: 10.1088/1757-899X/471/5/052042.
- [39] J. Belis, D. Mocibob, A. Luible, and M. Vandebroek, "On the size and shape of initial out-of-plane curvatures in structural glass components," *Constr Build Mater*, vol. 25, no. 5, pp. 2700–2712, May 2011, doi: 10.1016/J.CONBUILDMAT.2010.12.021.
- [40] C. Bedon, "Buckling Verification of Laminated Glass Elements in Compression," 2012. [Online]. Available: <https://www.researchgate.net/publication/225303054>
- [41] "Understanding Geometric Nonlinearity in Engineering- Structural Guide." Accessed: Jan. 21, 2025. [Online]. Available: <https://www.structuralguide.com/geometric-nonlinearity/>
- [42] LUSAS, *Theory Manual Volume 1*, vol. 1.
- [43] "STRAUS Technical Articles Page 2." Accessed: Jan. 22, 2025. [Online]. Available: <https://www.hsh.info/articl2.htm>
- [44] "Nonlinear Iterative Solution Procedures." Accessed: Jan. 23, 2025. [Online]. Available: https://www.lusas.com/user_area/theory/Nonlinear_Iterative_Procedures.html
- [45] J. N. Reddy, *An Introduction to the Finite Element Method*, Second edition. McGraw-Hill, 1993.
- [46] I. D. Erhunmwun and U. B. Ikponmwosa, "Review on finite element method," *Journal of Applied Sciences and Environmental Management*, vol. 21, no. 5, p. 999, Nov. 2017, doi: 10.4314/JASEM.V21I5.30.
- [47] L. Galuppi and G. Royer-Carfagni, "Enhanced Effective Thickness of Multi-Layered Laminated Glass".
- [48] *UNI EN 1993-1-1:2022*. <https://store.uni.com/uni-en-1993-1-1-2022>, 2022.

ANNEXES

A. DESIGN BENDING STRENGTH OF GLASS: FACTORS

This annex presents the evaluation of the factors necessary to calculate the design bending strength of glass, according to CEN/TS 19100-1 [31].

The first factors present in the formula of glass design bending strength are the edge or hole finishing factor (k_e) and the surface profile factor (k_{sp}). They are always lower or equal to one and are used to include in the design the effect of defects along the edges and on the glass surfaces. The values of the aforementioned factors are tabulated in Table A-1 and Table A-2.

Table A-1: Values for edge or hole finishing factor for verifications near edges and holes under tension.

Edge or hole finishing factor k_e			
Glass material	As-cut, arressed or ground edges	Seamed edges	Polished edges
(-)	(-)	(-)	(-)
Float	0,8	0,9	1,0
Patterned	0,8	0,8	0,8
Polished wired	0,8	0,8	0,8
Wired patterned	0,8	0,8	0,8

Table A-2: Values for surface profile factor for various surface conditions.

Surface profile factor k_{sp}		
Glass material	As produced	Sandblasted
(-)	(-)	(-)
Float	1,0	0,6
Drawn sheet	1,0	0,6
Enamelled float or drawn sheet	1,0	0,6
Patterned	0,75	0,45
Enamelled patterned	0,75	0,45
Polished wired	0,75	0,45
Patterned wired	0,6	0,36

The values of size effect factors, λ_A and λ_I , are provided by Technical Specifications for glass buildings[31] in a note, that reads: “The size effect λ_A and λ_I can be set to a value of 1 unless the area of the pane exceeds 18 m² or the length of a side exceeds 6 m. In cases where these limits are exceeded additional investigation on the areal or size effect is needed”.

Another significant factor is the modification factor (k_{mod}), and its values are shown in Table A-3. The modification factor depends on the type and time duration of the action and takes into account the variability of glass bending strength during its lifetime.

Table A-3: Values for modification factor for annealed glass.

Modification factor k_{mod}			
Type of action	Load duration	Action	k_{mod}
(-)	(-)	(-)	(-)
Permanent	Permanent	Self-weight, difference in altitude, permanent cold bending	0,29
Variable	Intermediate	Snow (3 to 4 weeks)	0,43
Variable	Intermediate	Imposed vertical action (1 week)	0,45
Variable	Intermediate	Temperature change and change in the meteorological barometric pressure (8 h)	0,58
Variable	Short	Maintenance load (30 min)	0,69
Variable	Short	Wind (10 min)	0,74
Variable	Short	Barrier personnel loads – crowds (5 min)	0,77
Variable	Short	Barrier personnel loads – normal duty (30 s)	0,89
Variable	Very short	Wind (3 s)	1,00
Variable	Dynamic	Impact (100 ms)	1,20

The pre-stressing process factor (k_p) depends on the type of industrial process used to pre-stress the glass element. The edge or hole pre-stressing factor ($k_{e,p}$) is able to take into consideration the effect of pre-stress on the edge of the element. The values of both factors are shown in Table A-4 and in Table A-5.

Table A-4: Values for pre-stressing process factor.

Pre-stressing process factor k_p	
Pre-stressing treatment	k_p
(-)	(-)
None	0,0
Heat treatment with horizontal process	1,0
Heat treatment with vertical process	0,60
Chemical strengthening	See Note 1

Note 1 regards chemical strengthening process and it requires that: “In case of chemically strengthened glass, the k_p values can be taken from a transparent and reproducible assessment that complies with all the requirements of EN 1990”.

Table A-5: Values for the edge pre-stressing factor for verifications near edges and holes under tension.

Edge or hole pre-stressing factor $k_{e,p}$					
Type of glass	Type of loading	As cut	Arrissed	Ground/smooth ground	Polished
(-)	(-)	(-)	(-)	(-)	(-)
Heat strengthened	Out-of-plane loading	To be avoided	1,0	1,0	1,0
Heat strengthened	In-plane loading (including pure tension)	To be avoided	0,8	0,8	0,8
Thermally toughened	Out-of-plane loading	To be avoided	1,0	1,0	1,0
Thermally toughened	In-plane loading (including pure tension)	To be avoided	0,8	0,8	0,8
Chemically strengthened	Out-of-plane loading	To be avoided	To be avoided	See Note 2	See Note 2
Chemically strengthened	In-plane loading (including pure tension)	To be avoided	To be avoided	See Note 2	See Note 2

Note 2 regards chemical strengthening process and it requires that: “In case of chemically strengthened glass, the $k_{e,p}$ values can be taken from a transparent and reproducible assessment that complies with all the requirements of EN 1990”.

The material partial factor (γ_M) and the partial factor for pre-stress on the surface (γ_p) depend on the consequence class (CC), that must be predicted by the designer. Table A-6 illustrates the three different classes of consequence and each of them is associated to a specific level of damage and impact on human, economic and social life.

Table A-6: Class of consequences: description and examples

Class of consequences (CC)		
Class of consequence	Description	Example of building
(-)	(-)	(-)
CC3	High consequence for loss of human life, or economic, social or environmental consequences very great	Grandstands, public buildings
CC2	Medium consequence for loss of human life, or economic, social or environmental consequences considerable	Residential and office buildings
CC1	Low consequence for loss of human life, or economic, social or environmental consequences small or negligible	Agricultural buildings

Lastly, the aforementioned partial safety factors γ_M and γ_p are defined according to the class of consequence, as shown in Table A-7.

Table A-7: Partial safety factors γ_M and γ_p for glass.

Partial safety factors γ_M and γ_p				
Design situations	Type of partial factor	CC1	CC2	CC3
(-)	(-)	(-)	(-)	(-)
Persistent & transient (fundamental combination)	Basic material γ_M	1,6	1,8	2,0
Persistent & transient (fundamental combination)	Surface pre-stress γ_p	1,1	1,2	1,3
Accidental	Basic material γ_M	1,0	1,1	1,2
Accidental	Surface pre-stress γ_p	1,0	1,0	1,0

B. COUPLING PARAMETER FOR BEAMS

The present annex is dedicated to explain the computation of the coupling parameter which is used to compute the two effective thicknesses for laminated glass elements. Glass Standard *CEN/TS 19100-2:2021* [36] in its Annex A proposes two different formulas for coupling parameter depending on the thickness of glass plies, whether it is the same for each glass ply or not.

The following formula is valid for a laminated glass pane, composed of n -plies having the same thickness. In the specific case of this document, since different laminated glass composed of only two plies with same thickness are studied, the formula of coupling parameter for beams $\eta_{b,2}$ reads:

$$\eta_{b,2} = \frac{1}{1 + \frac{h_{int} \cdot E_g \cdot n \cdot h_1^3 \cdot (n + 1) \cdot \Psi_b}{12G \cdot [h_1^2 + (h_1 + h_{int})^2 \cdot (n^2 - 1)]}} \quad (\text{A.1})$$

Where:

- h_{int} is the thickness of the interlayer.
- E_g is the Young's modulus of glass.
- n is the number of glass plies.
- h_1 is the thickness of the top glass ply.
- Ψ_b is the boundary coefficient for beams.
- G is the interlayer shear modulus.

The boundary coefficient for beams (Ψ_b) depends on the boundary and loading conditions of the member. The aforementioned Technical Specifications for glass in buildings, in its Annex A, provide a table with all the cases of practical significance; in this document, the boundary coefficient for a simply supported scheme subjected to out-of-plane distributed load is chosen, as shown in the following Figure B-1.

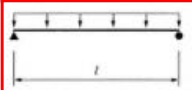
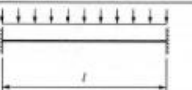
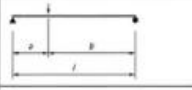
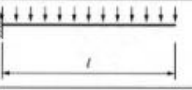
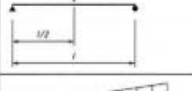
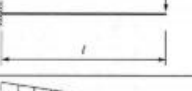
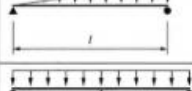
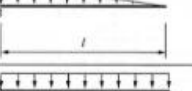

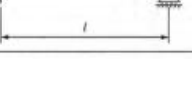
Loadings and boundary conditions	Boundary coefficient Ψ_b	Loadings and boundary conditions	Boundary coefficient Ψ_b
	$\Psi_b = \frac{168}{17 \times l^2}$		$\Psi_b = \frac{42}{l^2}$
	$\Psi_b = \frac{15}{l^2 + 2 \times a \times b}$		$\Psi_b = \frac{14}{5 \times l^2}$
	$\Psi_b = \frac{10}{l^2}$		$\Psi_b = \frac{5}{2 \times l^2}$
	$\Psi_b = \frac{135}{13 \times l^2}$		$\Psi_b = \frac{45}{14 \times l^2}$
	$\Psi_b = \frac{21}{l^2}$		$\Psi_b = \frac{21}{l^2}$

Figure B-1: Coupling parameter for beams Ψ_b for different loading and boundary conditions.

C. 2D FLAT AND CURVED MODELS: EFFECTIVE THICKNESS FOR OUT-OF-PLANE BENDING DEFLECTION

This annex presents the effective thickness for calculating out-of-plane bending deflection assigned to flat and curved (i.e. with initial geometric imperfection) 2D-FE models, for each case study.

Case A :

Table C-1: Effective thickness for bending deflection for $G = 0,01$ MPa (case A).

2D Model - Case A	Thicknesses $h_1/h_{int}/h_2$	Length model L_b	Width model b	Shear modulus G	Effective thickness $h_{ef,w}$
(-)	(mm)	(mm)	(mm)	(MPa)	(mm)
2D_A1	10/1,52/10	2000	500	0,01	12,72
2D_A2	10/1,52/10	4000	500	0,01	13,08
2D_A3	10/1,52/10	6000	500	0,01	13,59
2D_A4	10/1,52/10	8000	500	0,01	14,20

Table C-2: Effective thickness for bending deflection for $G = 0,1$ MPa (case A).

2D Model - Case A	Thicknesses $h_1/h_{int}/h_2$	Length model L_b	Width model b	Shear modulus G	Effective thickness $h_{ef,w}$
(-)	(mm)	(mm)	(mm)	(MPa)	(mm)
2D_A5	10/1,52/10	2000	500	0,1	13,69
2D_A6	10/1,52/10	4000	500	0,1	15,69
2D_A7	10/1,52/10	6000	500	0,1	17,37
2D_A8	10/1,52/10	8000	500	0,1	18,54

Table C-3: Effective thickness for bending deflection for $G = 1$ MPa (case A).

2D Model - Case A	Thicknesses $h_1/h_{int}/h_2$	Length model L_b	Width model b	Shear modulus G	Effective thickness $h_{ef,w}$
(-)	(mm)	(mm)	(mm)	(MPa)	(mm)
2D_A9	10/1,52/10	2000	500	1,0	17,59
2D_A10	10/1,52/10	4000	500	1,0	20,00
2D_A11	10/1,52/10	6000	500	1,0	20,76
2D_A12	10/1,52/10	8000	500	1,0	21,07

Table C-4: Effective thickness for bending deflection for $G = 10 \text{ MPa}$ (case A).

2D Model - Case A	Thicknesses $h_1/h_{int}/h_2$	Length model L_b	Width model b	Shear modulus G	Effective thickness $h_{ef,w}$
(-)	(mm)	(mm)	(mm)	(MPa)	(mm)
2D_A13	10/1,52/10	2000	500	10,0	20,83
2D_A14	10/1,52/10	4000	500	10,0	21,33
2D_A15	10/1,52/10	6000	500	10,0	21,43
2D_A16	10/1,52/10	8000	500	10,0	21,47

Case B :

Table C-5: Effective thickness for bending deflection for $G = 0,01 \text{ MPa}$ (case B).

2D Model - Case B	Thicknesses $h_1/h_{int}/h_2$	Length model L_b	Width model b	Shear modulus G	Effective thickness $h_{ef,w}$
(-)	(mm)	(mm)	(mm)	(MPa)	(mm)
2D_B1	12/1,52/12	2000	500	0,01	15,24
2D_B2	12/1,52/12	4000	500	0,01	15,58
2D_B3	12/1,52/12	6000	500	0,01	16,09
2D_B4	12/1,52/12	8000	500	0,01	16,72

Table C-6: Effective thickness for bending deflection for $G = 0,1 \text{ MPa}$ (case B).

2D Model - Case B	Thicknesses $h_1/h_{int}/h_2$	Length model L_b	Width model b	Shear modulus G	Effective thickness $h_{ef,w}$
(-)	(mm)	(mm)	(mm)	(MPa)	(mm)
2D_B5	12/1,52/12	2000	500	0,1	16,19
2D_B6	12/1,52/12	4000	500	0,1	18,29
2D_B7	12/1,52/12	6000	500	0,1	20,20
2D_B8	12/1,52/12	8000	500	0,1	21,61

Table C-7: Effective thickness for bending deflection for $G = 1 \text{ MPa}$ (case B).

2D Model - Case B	Thicknesses $h_1/h_{int}/h_2$	Length model L_b	Width model b	Shear modulus G	Effective thickness $h_{ef,w}$
(-)	(mm)	(mm)	(mm)	(MPa)	(mm)
2D_B9	12/1,52/12	2000	500	1,0	20,46
2D_B10	12/1,52/12	4000	500	1,0	23,45
2D_B11	12/1,52/12	6000	500	1,0	24,47
2D_B12	12/1,52/12	8000	500	1,0	24,90

Table C-8: Effective thickness for bending deflection for $G = 10 \text{ MPa}$ (case B).

2D Model - Case B	Thicknesses $h_1/h_{int}/h_2$	Length model L_b	Width model b	Shear modulus G	Effective thickness $h_{ef,w}$
(-)	(mm)	(mm)	(mm)	(MPa)	(mm)
2D_B13	12/1,52/12	2000	500	10,0	24,57
2D_B14	12/1,52/12	4000	500	10,0	25,26
2D_B15	12/1,52/12	6000	500	10,0	25,40
2D_B16	12/1,52/12	8000	500	10,0	25,45

Case C :

Table C-9: Effective thickness for bending deflection for $G = 0,01 \text{ MPa}$ (case C).

2D Model - Case C	Thicknesses $h_1/h_{int}/h_2$	Length model L_b	Width model b	Shear modulus G	Effective thickness $h_{ef,w}$
(-)	(mm)	(mm)	(mm)	(MPa)	(mm)
2D_C1	14/1,52/14	2000	500	0,01	17,76
2D_C2	14/1,52/14	4000	500	0,01	18,09
2D_C3	14/1,52/14	6000	500	0,01	18,60
2D_C4	14/1,52/14	8000	500	0,01	19,23

Table C-10: Effective thickness for bending deflection for $G = 0,1$ MPa (case C).

2D Model - Case C	Thicknesses $h_1/h_{int}/h_2$	Length model L	Width model b	Shear modulus G	Effective thickness $h_{ef,w}$
(-)	(mm)	(mm)	(mm)	(MPa)	(mm)
2D_C5	14/1,52/14	2000	500	0,1	18,69
2D_C6	14/1,52/14	4000	500	0,1	20,88
2D_C7	14/1,52/14	6000	500	0,1	22,99
2D_C8	14/1,52/14	8000	500	0,1	24,61

Table C-11: Effective thickness for bending deflection for $G = 1$ MPa (case C).

2D Model - Case C	Thicknesses $h_1/h_{int}/h_2$	Length model L_b	Width model b	Shear modulus G	Effective thickness $h_{ef,w}$
(-)	(mm)	(mm)	(mm)	(MPa)	(mm)
2D_C9	14/1,52/14	2000	500	1,0	23,28
2D_C10	14/1,52/14	4000	500	1,0	26,85
2D_C11	14/1,52/14	6000	500	1,0	28,14
2D_C12	14/1,52/14	8000	500	1,0	28,70

Table C-12: Effective thickness for bending deflection for $G = 10$ MPa (case C).

2D Model - Case C	Thicknesses $h_1/h_{int}/h_2$	Length model L_b	Width model b	Shear modulus G	Effective thickness $h_{ef,w}$
(-)	(mm)	(mm)	(mm)	(MPa)	(mm)
2D_C13	14/1,52/14	2000	500	10,0	28,27
2D_C14	14/1,52/14	4000	500	10,0	29,18
2D_C15	14/1,52/14	6000	500	10,0	29,36
2D_C16	14/1,52/14	8000	500	10,0	29,43

D.2D (1ST SOLUTION STRATEGY) AND 3D MODELS: NUMERICAL RESULTS

This annex is dedicated to present in tabular format critical buckling loads $N_{cr,FEA}$ and stresses $\sigma_{cr,FEA}$, obtained by eigenvalue analysis (LBA) and geometrically nonlinear analysis (GNA), for each case study and interlayer shear modulus.

Case A :

Table D-1: Critical buckling loads and stresses for 2D flat models with $G = 0,01$ MPa (case A – 1st solution strategy).

2D flat models - Case A - $G = 0,01$ MPa								
Length model	Effective thickness	Type of buckling analysis	Buckling load factor	Applied linear load	Critical buckling load	Critical buckling load	Area of laminated glass	Critical buckling stress
L_b	$h_{ef,w}$		BLF	P_0	$N_{cr,FEA}$	$N_{cr,LG}$	A_{full}	$\sigma_{cr,FEA}$
(mm)	(mm)	(-)	(-)	(N/mm)	(kN)	(kN)	(mm ²)	(MPa)
2000	12,72	Linear	5,942	5,00	14,86	14,81	10760	1,38
4000	13,08	Linear	1,611	5,00	4,03	4,02	10760	0,37
6000	13,59	Linear	0,803	5,00	2,01	2,01	10760	0,19
8000	14,20	Linear	0,515	5,00	1,29	1,29	10760	0,12

Table D-2: Critical buckling loads and stresses for 2D flat models with $G = 0,1$ MPa (case A – 1st solution strategy).

2D flat models - Case A - $G = 0,1$ MPa								
Length model	Effective thickness	Type of buckling analysis	Buckling load factor	Applied linear load	Critical buckling load	Critical buckling load	Area of laminated glass	Critical buckling stress
L_b	$h_{ef,w}$		BLF	P_0	$N_{cr,FEA}$	$N_{cr,LG}$	A_{full}	$\sigma_{cr,FEA}$
(mm)	(mm)	(-)	(-)	(N/mm)	(kN)	(kN)	(mm ²)	(MPa)
2000	13,69	Linear	7,408	5,00	18,43	18,43	10760	1,72
4000	15,69	Linear	2,782	5,00	6,94	6,94	10760	0,65
6000	17,37	Linear	1,676	5,00	4,19	4,19	10760	0,39
8000	18,54	Linear	1,146	5,00	2,87	2,86	10760	0,27

Table D-3: Critical buckling loads and stresses for 2D flat models with $G = 1$ MPa (case A – 1st solution strategy).

2D flat models - Case A - $G = 1$ MPa								
Length model	Effective thickness	Type of buckling analysis	Buckling load factor BLF	Applied linear load P_0	Critical buckling load $N_{cr,FEA}$	Critical buckling load $N_{cr,LG}$	Area of laminated glass A_{full}	Critical buckling stress $\sigma_{cr,FEA}$
L_b	$h_{ef,w}$	(-)	(-)	(N/mm)	(kN)	(kN)	(mm ²)	(MPa)
(mm)	(mm)	(-)	(-)	(N/mm)	(kN)	(kN)	(mm ²)	(MPa)
2000	17,59	Linear	15,715	5,00	39,29	39,15	10760	3,65
4000	20,00	Linear	5,762	5,00	14,41	14,37	10760	1,34
6000	20,76	Linear	2,862	5,00	7,16	7,15	10760	0,66
8000	21,07	Linear	1,683	5,00	4,21	4,21	10760	0,39

Table D-4: Critical buckling loads and stresses for 2D flat models with $G = 10$ MPa (case A – 1st solution strategy).

2D flat models - Case A - $G = 10$ MPa								
Length model	Effective thickness	Type of buckling analysis	Buckling load factor BLF	Applied linear load P_0	Critical buckling load $N_{cr,FEA}$	Critical buckling load $N_{cr,LG}$	Area of laminated glass A_{full}	Critical buckling stress $\sigma_{cr,FEA}$
L_b	$h_{ef,w}$	(-)	(-)	(N/mm)	(kN)	(kN)	(mm ²)	(MPa)
(mm)	(mm)	(-)	(-)	(N/mm)	(kN)	(kN)	(mm ²)	(MPa)
2000	20,83	Linear	26,097	5,00	65,24	64,99	10760	6,06
4000	21,33	Linear	6,989	5,00	17,47	17,45	10760	1,62
6000	21,43	Linear	3,149	5,00	7,87	7,87	10760	0,73
8000	21,47	Linear	1,780	5,00	4,45	4,45	10760	0,41

Case B :

Table D-5: Critical buckling loads and stresses for 2D flat models with $G = 0,01$ MPa (case B – 1st solution strategy).

2D flat models - Case B - $G = 0,01$ MPa								
Length model	Effective thickness	Type of buckling analysis	Buckling load factor BLF	Applied linear load P_0	Critical buckling load $N_{cr,FEA}$	Critical buckling load $N_{cr,LG}$	Area of laminated glass A_{full}	Critical buckling stress $\sigma_{cr,FEA}$
L_b	$h_{ef,w}$	(-)	(-)	(N/mm)	(kN)	(kN)	(mm ²)	(MPa)
(mm)	(mm)	(-)	(-)	(N/mm)	(kN)	(kN)	(mm ²)	(MPa)
2000	15,24	Linear	10,220	5,00	25,55	25,44	12760	2,00
4000	15,58	Linear	2,723	5,00	6,81	6,80	12760	0,53
6000	16,09	Linear	1,332	5,00	3,33	3,33	12760	0,26
8000	16,72	Linear	0,841	5,00	2,10	2,10	12760	0,16

Table D-6: Critical buckling loads and stresses for 2D flat models with $G = 0,1$ MPa (case B – 1st solution strategy).

2D flat models - Case B - $G = 0,1$ MPa								
Length model	Effective thickness	Type of buckling analysis	Buckling load factor BLF	Applied linear load P_0	Critical buckling load $N_{cr,FEA}$	Critical buckling load $N_{cr,LG}$	Area of laminated glass A_{full}	Critical buckling stress $\sigma_{cr,FEA}$
L_b	$h_{ef,w}$	(-)	(-)	(N/mm)	(kN)	(kN)	(mm ²)	(MPa)
(mm)	(mm)	(-)	(-)	(N/mm)	(kN)	(kN)	(mm ²)	(MPa)
2000	16,19	Linear	12,250	5,00	30,63	30,50	12760	2,40
4000	18,29	Linear	4,406	5,00	11,02	11,01	12760	0,86
6000	20,20	Linear	2,637	5,00	6,59	6,59	12760	0,52
8000	21,61	Linear	1,816	5,00	4,54	4,53	12760	0,36

Table D-7: Critical buckling loads and stresses for 2D flat models with $G = 1$ MPa (case B – 1st solution strategy).

2D flat models - Case B - $G = 1$ MPa								
Length model	Effective thickness	Type of buckling analysis	Buckling load factor BLF	Applied linear load P_0	Critical buckling load $N_{cr,FEA}$	Critical buckling load $N_{cr,LG}$	Area of laminated glass A_{full}	Critical buckling stress $\sigma_{cr,FEA}$
L_b	$h_{ef,w}$	(-)	(-)	(N/mm)	(kN)	(kN)	(mm ²)	(MPa)
(mm)	(mm)	(-)	(-)	(N/mm)	(kN)	(kN)	(mm ²)	(MPa)
2000	20,46	Linear	24,731	5,00	61,83	61,61	12760	4,85
4000	23,45	Linear	9,287	5,00	23,22	23,19	12760	1,82
6000	24,47	Linear	4,688	5,00	11,72	11,71	12760	0,92
8000	24,90	Linear	2,778	5,00	6,95	6,94	12760	0,54

Table D-8: Critical buckling loads and stresses for 2D flat models with $G = 10$ MPa (case B – 1st solution).

2D flat models - Case B - $G = 10$ MPa								
Length model	Effective thickness	Type of buckling analysis	Buckling load factor BLF	Applied linear load P_0	Critical buckling load $N_{cr,FEA}$	Critical buckling load $N_{cr,LG}$	Area of laminated glass A_{full}	Critical buckling stress $\sigma_{cr,FEA}$
L_b	$h_{ef,w}$	(-)	(-)	(N/mm)	(kN)	(kN)	(mm ²)	(MPa)
(mm)	(mm)	(-)	(-)	(N/mm)	(kN)	(kN)	(mm ²)	(MPa)
2000	24,57	Linear	42,830	5,00	107,80	106,60	12760	8,39
4000	25,26	Linear	11,608	5,00	29,02	28,97	12760	2,27
6000	25,40	Linear	5,243	5,00	13,11	13,09	12760	1,03
8000	25,45	Linear	2,966	5,00	7,42	7,41	12760	0,58

Case C :

Table D-9: Critical buckling loads and stresses for 2D flat models with $G = 0,01$ MPa (case C – 1st solution strategy).

2D flat models - Case C - $G = 0,01$ MPa								
Length model	Effective thickness	Type of buckling analysis	Buckling load factor	Applied linear load	Critical buckling load	Critical buckling load	Area of laminated glass	Critical buckling stress
L_b	$h_{ef,w}$		BLF	P_0	$N_{cr,FEA}$	$N_{cr,LG}$	A_{full}	$\sigma_{cr,FEA}$
(mm)	(mm)	(-)	(-)	(N/mm)	(kN)	(kN)	(mm ²)	(MPa)
2000	17,76	Linear	16,175	5,00	40,44	40,24	14760	2,74
4000	18,09	Linear	4,263	5,00	10,66	10,64	14760	0,72
6000	18,60	Linear	2,058	5,00	5,15	5,14	14760	0,35
8000	19,23	Linear	1,279	5,00	3,20	3,19	14760	0,22

Table D-10: Critical buckling loads and stresses for 2D flat models with $G = 0,1$ MPa (case C – 1st solution strategy).

2D flat models - Case C - $G = 0,1$ MPa								
Length model	Effective thickness	Type of buckling analysis	Buckling load factor	Applied linear load	Critical buckling load	Critical buckling load	Area of laminated glass	Critical buckling stress
L_b	$h_{ef,w}$		BLF	P_0	$N_{cr,FEA}$	$N_{cr,LG}$	A_{full}	$\sigma_{cr,FEA}$
(mm)	(mm)	(-)	(-)	(N/mm)	(kN)	(kN)	(mm ²)	(MPa)
2000	18,69	Linear	18,852	5,00	47,13	46,79	14760	3,19
4000	20,88	Linear	6,556	5,00	16,39	16,37	14760	1,11
6000	22,99	Linear	3,887	5,00	9,72	9,70	14760	0,66
8000	24,61	Linear	2,682	5,00	6,71	6,70	14760	0,45

Table D-11: Critical buckling loads and stresses for 2D flat models with $G = 1$ MPa (case C – 1st solution strategy).

2D flat models - Case C - $G = 1$ MPa								
Length model	Effective thickness	Type of buckling analysis	Buckling load factor	Applied linear load	Critical buckling load	Critical buckling load	Area of laminated glass	Critical buckling stress
L_b	$h_{ef,w}$		BLF	P_0	$N_{cr,FEA}$	$N_{cr,LG}$	A_{full}	$\sigma_{cr,FEA}$
(mm)	(mm)	(-)	(-)	(N/mm)	(kN)	(kN)	(mm ²)	(MPa)
2000	23,28	Linear	36,432	5,00	91,08	90,75	14760	6,17
4000	26,85	Linear	13,941	5,00	34,85	34,79	14760	2,36
6000	28,14	Linear	7,129	5,00	17,82	17,81	14760	1,21
8000	28,70	Linear	4,254	5,00	10,64	10,62	14760	0,72

Table D-12: Critical buckling loads and stresses for 2D flat models with $G = 10$ MPa (case C – 1st solution strategy).

2D flat models - Case C - $G = 10$ MPa								
Length model L_b	Effective thickness $h_{ef,w}$	Type of buckling analysis	Buckling load factor BLF	Applied linear load P_0	Critical buckling load $N_{cr,FEA}$	Critical buckling load $N_{cr,LG}$	Area of laminated glass A_{full}	Critical buckling stress $\sigma_{cr,FEA}$
(mm)	(mm)	(-)	(-)	(N/mm)	(kN)	(kN)	(mm ²)	(MPa)
2000	28,27	Linear	65,239	5,00	163,10	162,35	14760	11,05
4000	29,18	Linear	17,895	5,00	44,74	44,63	14760	3,03
6000	29,36	Linear	8,097	5,00	20,24	20,22	14760	1,37
8000	29,43	Linear	4,587	5,00	11,47	11,45	14760	0,78

Case A :

 Table D-13: Critical buckling loads and stresses for 2D curved models with $G = 0,01$ MPa (case A – 1st solution strategy).

2D curved models - Case A - $G = 0,01$ MPa								
Length model L_b	Effective thickness $h_{ef,w}$	Basic imperfection e_0	Type of buckling analysis	Buckling load factor BLF	Applied linear load P_0	Critical buckling load $N_{cr,FEA}$	Area of laminated glass A_{full}	Critical buckling stress $\sigma_{cr,FEA}$
(mm)	(mm)	(mm)	(-)	(-)	(N/mm)	(kN)	(mm ²)	(MPa)
2000	12,72	12,32	Nonlinear	4,400	5,00	11,00	10760	1,02
4000	13,08	16,13	Nonlinear	1,444	5,00	3,61	10760	0,34
6000	13,59	20,99	Nonlinear	0,754	5,00	1,89	10760	0,18
8000	14,20	26,32	Nonlinear	0,496	5,00	1,24	10760	0,12

 Table D-14: Critical buckling loads and stresses for 2D curved models with $G = 0,1$ MPa (case A – 1st solution strategy).

2D curved models - Case A - $G = 0,1$ MPa								
Length model L_b	Effective thickness $h_{ef,w}$	Basic imperfection e_0	Type of buckling analysis	Buckling load factor BLF	Applied linear load P_0	Critical buckling load $N_{cr,FEA}$	Area of laminated glass A_{full}	Critical buckling stress $\sigma_{cr,FEA}$
(mm)	(mm)	(mm)	(-)	(-)	(N/mm)	(kN)	(mm ²)	(MPa)
2000	13,69	12,32	Nonlinear	5,500	5,00	13,75	10760	1,28
4000	15,69	16,13	Nonlinear	2,450	5,00	6,13	10760	0,57
6000	17,37	20,99	Nonlinear	1,542	5,00	3,86	10760	0,36
8000	18,54	26,32	Nonlinear	1,077	5,00	2,69	10760	0,25

Table D-15: Critical buckling loads and stresses for 2D curved models with $G = 1 \text{ MPa}$ (case A – 1st solution strategy).

2D curved models - Case A - $G = 1 \text{ MPa}$								
Length model L_b	Effective thickness $h_{ef,w}$	Basic imperfection e_0	Type of buckling analysis	Buckling load factor BLF	Applied linear load P_0	Critical buckling load $N_{cr,FEA}$	Area of laminated glass A_{full}	Critical buckling stress $\sigma_{cr,FEA}$
(mm)	(mm)	(mm)	(-)	(-)	(N/mm)	(kN)	(mm ²)	(MPa)
2000	17,59	12,32	Nonlinear	10,800	5,00	27,00	10760	2,51
4000	20,00	16,13	Nonlinear	4,900	5,00	12,25	10760	1,14
6000	20,76	20,99	Nonlinear	2,606	5,00	6,52	10760	0,61
8000	21,07	26,32	Nonlinear	1,574	5,00	3,94	10760	0,37

Table D-16: Critical buckling loads and stresses for 2D curved models with $G = 10 \text{ MPa}$ (case A – 1st solution strategy).

2D curved models - Case A - $G = 10 \text{ MPa}$								
Length model L_b	Effective thickness $h_{ef,w}$	Basic imperfection e_0	Type of buckling analysis	Buckling load factor BLF	Applied linear load P_0	Critical buckling load $N_{cr,FEA}$	Area of laminated glass A_{full}	Critical buckling stress $\sigma_{cr,FEA}$
(mm)	(mm)	(mm)	(-)	(-)	(N/mm)	(kN)	(mm ²)	(MPa)
2000	20,83	12,32	Nonlinear	17,000	5,00	42,50	10760	3,95
4000	21,33	16,13	Nonlinear	5,900	5,00	14,75	10760	1,37
6000	21,43	20,99	Nonlinear	2,842	5,00	7,11	10760	0,66
8000	21,47	26,32	Nonlinear	1,654	5,00	4,14	10760	0,38

Case B :

Table D-17: Critical buckling loads and stresses for 2D curved models with $G = 0,01 \text{ MPa}$ (case B – 1st solution strategy).

2D curved models - Case B - $G = 0,01 \text{ MPa}$								
Length model L_b	Effective thickness $h_{ef,w}$	Basic imperfection e_0	Type of buckling analysis	Buckling load factor BLF	Applied linear load P_0	Critical buckling load $N_{cr,FEA}$	Area of laminated glass A_{full}	Critical buckling stress $\sigma_{cr,FEA}$
(mm)	(mm)	(mm)	(-)	(-)	(N/mm)	(kN)	(mm ²)	(MPa)
2000	15,24	14,10	Nonlinear	7,000	5,00	17,50	12760	1,37
4000	15,58	17,52	Nonlinear	2,377	5,00	5,94	12760	0,47
6000	16,09	22,08	Nonlinear	1,232	5,00	3,08	12760	0,24
8000	16,72	27,20	Nonlinear	0,793	5,00	1,98	12760	0,16

Table D-18: Critical buckling loads and stresses for 2D curved models with $G = 0,1$ MPa (case B – 1st solution strategy).

2D curved models - Case B - $G = 0,1$ MPa								
Length model L_b	Effective thickness $h_{ef,w}$	Basic imperfection e_0	Type of buckling analysis	Buckling load factor BLF	Applied linear load P_0	Critical buckling load $N_{cr,FEA}$	Area of laminated glass A_{full}	Critical buckling stress $\sigma_{cr,FEA}$
(mm)	(mm)	(mm)	(-)	(-)	(N/mm)	(kN)	(mm ²)	(MPa)
2000	16,19	14,10	Nonlinear	8,200	5,00	20,50	12760	1,61
4000	18,29	17,52	Nonlinear	3,800	5,00	9,50	12760	0,74
6000	20,20	22,08	Nonlinear	2,400	5,00	6,00	12760	0,47
8000	21,61	27,20	Nonlinear	1,693	5,00	4,23	12760	0,33

 Table D-19: Critical buckling loads and stresses for 2D curved models with $G = 1$ MPa (case B – 1st solution strategy).

2D curved models - Case B - $G = 1$ MPa								
Length model L_b	Effective thickness $h_{ef,w}$	Basic imperfection e_0	Type of buckling analysis	Buckling load factor BLF	Applied linear load P_0	Critical buckling load $N_{cr,FEA}$	Area of laminated glass A_{full}	Critical buckling stress $\sigma_{cr,FEA}$
(mm)	(mm)	(mm)	(-)	(-)	(N/mm)	(kN)	(mm ²)	(MPa)
2000	20,46	14,10	Nonlinear	15,600	5,00	39,00	12760	3,06
4000	23,45	17,52	Nonlinear	7,600	5,00	19,00	12760	1,49
6000	24,47	22,08	Nonlinear	4,200	5,00	10,50	12760	0,82
8000	24,90	27,20	Nonlinear	2,545	5,00	6,36	12760	0,50

 Table D-20: Critical buckling loads and stresses for 2D curved models with $G = 10$ MPa (case B – 1st solution strategy).

2D curved models - Case B - $G = 10$ MPa								
Length model L_b	Effective thickness $h_{ef,w}$	Basic imperfection e_0	Type of buckling analysis	Buckling load factor BLF	Applied linear load P_0	Critical buckling load $N_{cr,FEA}$	Area of laminated glass A_{full}	Critical buckling stress $\sigma_{cr,FEA}$
(mm)	(mm)	(mm)	(-)	(-)	(N/mm)	(kN)	(mm ²)	(MPa)
2000	24,57	14,10	Nonlinear	25,600	5,00	64,00	12760	5,02
4000	25,26	17,52	Nonlinear	9,450	5,00	23,63	12760	1,85
6000	25,40	22,08	Nonlinear	4,650	5,00	11,63	12760	0,91
8000	25,45	27,20	Nonlinear	2,732	5,00	6,83	12760	0,54

Case C :

Table D-21: Critical buckling loads and stresses for 2D curved models with $G = 0,01$ MPa (case C – 1st solution strategy).

2D curved models - Case C - $G = 0,01$ MPa								
Length model L_b	Effective thickness $h_{ef,w}$	Basic imperfection e_0	Type of buckling analysis	Buckling load factor BLF	Applied linear load P_0	Critical buckling load $N_{cr,FEA}$	Area of laminated glass A_{full}	Critical buckling stress $\sigma_{cr,FEA}$
(mm)	(mm)	(mm)	(-)	(-)	(N/mm)	(kN)	(mm ²)	(MPa)
2000	17,76	15,94	Nonlinear	10,200	5,00	25,50	14760	1,73
4000	18,09	19,03	Nonlinear	3,600	5,00	9,00	14760	0,61
6000	18,60	23,29	Nonlinear	1,880	5,00	4,70	14760	0,32
8000	19,23	28,20	Nonlinear	1,203	5,00	3,01	14760	0,20

Table D-22: Critical buckling loads and stresses for 2D curved models with $G = 0,1$ MPa (case C – 1st solution strategy).

2D curved models - Case C - $G = 0,1$ MPa								
Length model L_b	Effective thickness $h_{ef,w}$	Basic imperfection e_0	Type of buckling analysis	Buckling load factor BLF	Applied linear load P_0	Critical buckling load $N_{cr,FEA}$	Area of laminated glass A_{full}	Critical buckling stress $\sigma_{cr,FEA}$
(mm)	(mm)	(mm)	(-)	(-)	(N/mm)	(kN)	(mm ²)	(MPa)
2000	18,69	15,94	Nonlinear	11,700	5,00	29,25	14760	1,98
4000	20,88	19,03	Nonlinear	5,420	5,00	13,55	14760	0,92
6000	22,99	23,29	Nonlinear	3,450	5,00	8,63	14760	0,58
8000	24,61	28,20	Nonlinear	2,465	5,00	6,16	14760	0,42

Table D-23: Critical buckling loads and stresses for 2D curved models with $G = 1$ MPa (case C – 1st solution strategy).

2D curved models - Case C - $G = 1$ MPa								
Length model L_b	Effective thickness $h_{ef,w}$	Basic imperfection e_0	Type of buckling analysis	Buckling load factor BLF	Applied linear load P_0	Critical buckling load $N_{cr,FEA}$	Area of laminated glass A_{full}	Critical buckling stress $\sigma_{cr,FEA}$
(mm)	(mm)	(mm)	(-)	(-)	(N/mm)	(kN)	(mm ²)	(MPa)
2000	23,28	15,94	Nonlinear	21,100	5,00	52,75	14760	3,57
4000	26,85	19,03	Nonlinear	11,090	5,00	27,73	14760	1,88
6000	28,14	23,29	Nonlinear	6,200	5,00	15,50	14760	1,05
8000	28,70	28,20	Nonlinear	3,823	5,00	9,56	14760	0,65

Table D-24: Critical buckling loads and stresses for 2D curved models with $G = 10$ MPa (case C – 1st solution strategy).

2D curved models - Case C - $G = 10$ MPa								
Length model L_b	Effective thickness $h_{ef,w}$	Basic imperfection e_0	Type of buckling analysis	Buckling load factor BLF	Applied linear load P_0	Critical buckling load $N_{cr,FEA}$	Area of laminated glass A_{full}	Critical buckling stress $\sigma_{cr,FEA}$
(mm)	(mm)	(mm)	(-)	(-)	(N/mm)	(kN)	(mm ²)	(MPa)
2000	28,27	15,94	Nonlinear	35,200	5,00	88,00	14760	5,96
4000	29,18	19,03	Nonlinear	14,000	5,00	35,00	14760	2,37
6000	29,36	23,29	Nonlinear	7,000	5,00	17,50	14760	1,19
8000	29,43	28,20	Nonlinear	4,100	5,00	10,25	14760	0,69

Case A :

Table D-25: Critical buckling loads and stresses for 3D models with $G = 0,01$ MPa (case A).

3D models - Case A - $G = 0,01$ MPa								
Length model L_b	Thicknes ses $h_1/h_{int}/h_2$	Basic imperfe ction e_0	Type of buckling analysis	Buckling load factor BLF	Applied linear load P_0	Critical buckling load $N_{cr,FEA}$	Area of laminated glass A_{full}	Critical buckling stress $\sigma_{cr,FEA}$
(mm)	(mm)	(mm)	(-)	(-)	(N/mm)	(kN)	(mm ²)	(MPa)
2000	10/1,52/ 10	12,32	Nonlinear	5,200	5,00	13,00	10760	1,21
4000	10/1,52/ 10	16,13	Nonlinear	1,464	5,00	3,66	10760	0,34
6000	10/1,52/ 10	20,99	Nonlinear	0,798	5,00	2,00	10760	0,18
8000	10/1,52/ 10	26,32	Nonlinear	0,532	5,00	1,33	10760	0,12

Table D-26: Critical buckling loads and stresses for 3D models with $G = 0,1$ MPa (case A).

3D models - Case A - $G = 0,1$ MPa								
Length model L_b	Thicknes ses $h_1/h_{int}/h_2$	Basic imperfe ction e_0	Type of buckling analysis	Buckling load factor BLF	Applied linear load P_0	Critical buckling load $N_{cr,FEA}$	Area of laminated glass A_{full}	Critical buckling stress $\sigma_{cr,FEA}$
(mm)	(mm)	(mm)	(-)	(-)	(N/mm)	(kN)	(mm ²)	(MPa)
2000	10/1,52/10	12,32	Nonlinear	6,454	5,00	16,14	10760	1,49
4000	10/1,52/10	16,13	Nonlinear	2,459	5,00	6,15	10760	0,57
6000	10/1,52/10	20,99	Nonlinear	1,560	5,00	2,87	10760	0,36
8000	10/1,52/10	26,32	Nonlinear	1,082	5,00	2,71	10760	0,25

Table D-27: Critical buckling loads and stresses for 3D models with $G = 1$ MPa (case A).

3D models - Case A - $G = 1$ MPa								
Length model L_b	Thicknes ses $h_1/h_{int}/h_2$	Basic imperfe ction e_0	Type of buckling analysis	Buckling load factor BLF	Applied linear load P_0	Critical buckling load $N_{cr,FEA}$	Area of laminated glass A_{full}	Critical buckling stress $\sigma_{cr,FEA}$
(mm)	(mm)	(mm)	(-)	(-)	(N/mm)	(kN)	(mm ²)	(MPa)
2000	10/1,52/10	12,32	Nonlinear	11,450	5,00	28,63	10760	2,66
4000	10/1,52/10	16,13	Nonlinear	4,779	5,00	11,95	10760	1,11
6000	10/1,52/10	20,99	Nonlinear	2,585	5,00	6,46	10760	0,60
8000	10/1,52/10	26,32	Nonlinear	1,612	5,00	4,03	10760	0,37

Table D-28: Critical buckling loads and stresses for 3D models with $G = 10$ MPa (case A).

3D models - Case A - $G = 10$ MPa								
Length model L_b	Thicknes ses $h_1/h_{int}/h_2$	Basic imperfe ction e_0	Type of buckling analysis	Buckling load factor BLF	Applied linear load P_0	Critical buckling load $N_{cr,FEA}$	Area of laminated glass A_{full}	Critical buckling stress $\sigma_{cr,FEA}$
(mm)	(mm)	(mm)	(-)	(-)	(N/mm)	(kN)	(mm ²)	(MPa)
2000	10/1,52/ 10	12,32	Nonlinear	19,500	5,00	48,75	10760	4,53
4000	10/1,52/ 10	16,13	Nonlinear	5,812	5,00	14,53	10760	1,35
6000	10/1,52/ 10	20,99	Nonlinear	3,053	5,00	7,63	10760	0,71
8000	10/1,52/ 10	26,32	Nonlinear	1,697	5,00	4,24	10760	0,39

Case B :

Table D-29: Critical buckling loads and stresses for 3D models with $G = 0,01$ MPa (case B).

3D models - Case B - $G = 0,01$ MPa								
Length model L_b	Thicknes ses $h_1/h_{int}/h_2$	Basic imperfe ction e_0	Type of buckling analysis	Buckling load factor BLF	Applied linear load P_0	Critical buckling load $N_{cr,FEA}$	Area of laminated glass A_{full}	Critical buckling stress $\sigma_{cr,FEA}$
(mm)	(mm)	(mm)	(-)	(-)	(N/mm)	(kN)	(mm ²)	(MPa)
2000	12/1,52/ 12	14,10	Nonlinear	8,500	5,00	21,25	12760	1,67
4000	12/1,52/ 12	17,52	Nonlinear	2,398	5,00	6,00	12760	0,47
6000	12/1,52/ 12	22,08	Nonlinear	1,283	5,00	3,21	12760	0,25
8000	12/1,52/ 12	27,20	Nonlinear	0,865	5,00	2,16	12760	0,17

Table D-30: Critical buckling loads and stresses for 3D models with $G = 0,1$ MPa (case B).

3D models - Case B - $G = 0,1$ MPa								
Length model L_b	Thicknes ses $h_1/h_{int}/h_2$	Basic imperfe ction e_0	Type of buckling analysis	Buckling load factor BLF	Applied linear load P_0	Critical buckling load $N_{cr,FEA}$	Area of laminated glass A_{full}	Critical buckling stress $\sigma_{cr,FEA}$
(mm)	(mm)	(mm)	(-)	(-)	(N/mm)	(kN)	(mm ²)	(MPa)
2000	12/1,52/12	14,10	Nonlinear	10,146	5,00	25,37	12760	1,99
4000	12/1,52/12	17,52	Nonlinear	3,886	5,00	9,72	12760	0,76
6000	12/1,52/12	22,08	Nonlinear	2,412	5,00	6,03	12760	0,47
8000	12/1,52/12	27,20	Nonlinear	1,710	5,00	4,28	12760	0,34

Table D-31: Critical buckling loads and stresses for 3D models with $G = 1$ MPa (case B).

3D models - Case B - $G = 1$ MPa								
Length model L_b	Thicknes ses $h_1/h_{int}/h_2$	Basic imperfe ction e_0	Type of buckling analysis	Buckling load factor BLF	Applied linear load P_0	Critical buckling load $N_{cr,FEA}$	Area of laminated glass A_{full}	Critical buckling stress $\sigma_{cr,FEA}$
(mm)	(mm)	(mm)	(-)	(-)	(N/mm)	(kN)	(mm ²)	(MPa)
2000	12/1,52/12	14,10	Nonlinear	18,600	5,00	46,50	12760	3,64
4000	12/1,52/12	17,52	Nonlinear	7,408	5,00	18,52	12760	1,45
6000	12/1,52/12	22,08	Nonlinear	4,108	5,00	10,27	12760	0,80
8000	12/1,52/12	27,20	Nonlinear	2,548	5,00	6,37	12760	0,50

Table D-32: Critical buckling loads and stresses for 3D models with $G = 10$ MPa (case B).

3D models - Case B - $G = 10$ MPa								
Length model L_b	Thicknes ses $h_1/h_{int}/h_2$	Basic imperfe ction e_0	Type of buckling analysis	Buckling load factor BLF	Applied linear load P_0	Critical buckling load $N_{cr,FEA}$	Area of laminated glass A_{full}	Critical buckling stress $\sigma_{cr,FEA}$
(mm)	(mm)	(mm)	(-)	(-)	(N/mm)	(kN)	(mm ²)	(MPa)
2000	12/1,52/12	14,10	Nonlinear	26,800	5,00	67,00	12760	5,25
4000	12/1,52/12	17,52	Nonlinear	10,839	5,00	27,10	12760	2,12
6000	12/1,52/12	22,08	Nonlinear	4,770	5,00	11,93	12760	0,93
8000	12/1,52/12	27,20	Nonlinear	2,803	5,00	7,01	12760	0,55

Case C :

Table D-33: Critical buckling loads and stresses for 3D models with $G = 0,01$ MPa (case C).

3D models - Case C - $G = 0,01$ MPa								
Length model L_b	Thicknes ses $h_1/h_{int}/h_2$	Basic imperfe ction e_0	Type of buckling analysis	Buckling load factor BLF	Applied linear load P_0	Critical buckling load $N_{cr,FEA}$	Area of laminated glass A_{full}	Critical buckling stress $\sigma_{cr,FEA}$
(mm)	(mm)	(mm)	(-)	(-)	(N/mm)	(kN)	(mm ²)	(MPa)
2000	14/1,52/14	15,94	Nonlinear	13,040	5,00	32,60	14760	2,21
4000	14/1,52/14	19,03	Nonlinear	3,650	5,00	9,13	14760	0,62
6000	14/1,52/14	23,29	Nonlinear	1,967	5,00	4,92	14760	0,33
8000	14/1,52/14	28,20	Nonlinear	1,309	5,00	3,27	14760	0,22

Table D-34: Critical buckling loads and stresses for 3D models with $G = 0,1$ MPa (case C).

3D models - Case C - $G = 0,1$ MPa								
Length model L_b	Thicknes ses $h_1/h_{int}/h_2$	Basic imperfe ction e_0	Type of buckling analysis	Buckling load factor BLF	Applied linear load P_0	Critical buckling load $N_{cr,FEA}$	Area of laminated glass A_{full}	Critical buckling stress $\sigma_{cr,FEA}$
(mm)	(mm)	(mm)	(-)	(-)	(N/mm)	(kN)	(mm ²)	(MPa)
2000	14/1,52/14	15,94	Nonlinear	12,653	5,00	31,63	14760	2,14
4000	14/1,52/14	19,03	Nonlinear	5,580	5,00	13,95	14760	0,95
6000	14/1,52/14	23,29	Nonlinear	3,556	5,00	8,89	14760	0,60
8000	14/1,52/14	28,20	Nonlinear	2,495	5,00	6,24	14760	0,42

Table D-35: Critical buckling loads and stresses for 3D models with $G = 1$ MPa (case C).

3D models - Case C - $G = 1$ MPa								
Length model L_b	Thicknes ses $h_1/h_{int}/h_2$	Basic imperfe ction e_0	Type of buckling analysis	Buckling load factor BLF	Applied linear load P_0	Critical buckling load $N_{cr,FEA}$	Area of laminated glass A_{full}	Critical buckling stress $\sigma_{cr,FEA}$
(mm)	(mm)	(mm)	(-)	(-)	(N/mm)	(kN)	(mm ²)	(MPa)
2000	14/1,52/14	15,94	Nonlinear	25,400	5,00	63,50	14760	4,30
4000	14/1,52/14	19,03	Nonlinear	10,793	5,00	26,98	14760	1,83
6000	14/1,52/14	23,29	Nonlinear	6,139	5,00	15,35	14760	1,04
8000	14/1,52/14	28,20	Nonlinear	3,820	5,00	9,55	14760	0,65

Table D-36: Critical buckling loads and stresses for 3D models with $G = 10$ MPa (case C).

3D models - Case C - $G = 10$ MPa								
Length model L_b	Thicknes ses $h_1/h_{int}/h_2$	Basic imperfe ction e_0	Type of buckling analysis	Buckling load factor BLF	Applied linear load P_0	Critical buckling load $N_{cr,FEA}$	Area of laminated glass A_{full}	Critical buckling stress $\sigma_{cr,FEA}$
(mm)	(mm)	(mm)	(-)	(-)	(N/mm)	(kN)	(mm ²)	(MPa)
2000	14/1,52/ 14	15,94	Nonlinear	37,000	5,00	92,50	14760	6,27
4000	14/1,52/ 14	19,03	Nonlinear	13,741	5,00	34,35	14760	2,33
6000	14/1,52/ 14	23,29	Nonlinear	7,039	5,00	17,60	14760	1,19
8000	14/1,52/ 14	28,20	Nonlinear	4,239	5,00	10,60	14760	0,72

E. 2D-FE CURVED MODELS: PRELIMINARY CALCULATIONS AND NUMERICAL RESULTS (2ND SOLUTION STRATEGY)

This annex is intended for presenting in tabular form preliminary calculations, regarding section modulus $W(h_{ef,\sigma,i})$ and true buckling stress $\bar{\sigma}$. Additionally, there are also present tables, which include critical buckling loads ($N_{cr,FEA}$) and stresses ($\sigma_{cr,FEA}$) for each case study, obtained by means of geometrically nonlinear analysis (GNA) on 2D curved models.

Case A :

Table E-1: Section modulus and effective thickness for bending stress for 2D curved models with $G = 0,01$ MPa (case A).

2D curved models - Case A - $G = 0,01$ MPa					
Model type & case study	Width model b	Length model L_b	Area of laminated glass A_{full}	Effective thickness $h_{ef,\sigma,i}$	Section modulus $W(h_{ef,\sigma,i})$
(-)	(mm)	(mm)	(mm ²)	(mm)	(mm ³)
2D_A	500	2000	10760	14,29	17017,01
	500	4000	10760	14,70	18007,50
	500	6000	10760	15,29	19482,01
	500	8000	10760	15,96	21226,80

Table E-2: Section modulus and effective thickness for bending stress for 2D curved models with $G = 0,1$ MPa (case A).

2D curved models - Case A - $G = 0,1$ MPa					
Model type & case study	Width model b	Length model L_b	Area of laminated glass A_{full}	Effective thickness $h_{ef,\sigma,i}$	Section modulus $W(h_{ef,\sigma,i})$
(-)	(mm)	(mm)	(mm ²)	(mm)	(mm ³)
2D_A	500	2000	10760	15,39	19737,68
	500	4000	10760	17,44	25346,13
	500	6000	10760	18,89	29736,01
	500	8000	10760	19,76	32538,13

Table E-3: Section modulus and effective thickness for bending stress for 2D curved models with $G = 1$ MPa (case A).

2D curved models - Case A - $G = 1$ MPa					
Model type & case study	Width model b	Length model L_b	Area of laminated glass A_{full}	Effective thickness $h_{ef,\sigma,i}$	Section modulus $W(h_{ef,\sigma,i})$
(-)	(mm)	(mm)	(mm ²)	(mm)	(mm ³)
2D_A	500	2000	10760	19,06	30273,63
	500	4000	10760	20,69	35673,01
	500	6000	10760	21,12	37171,20
	500	8000	10760	21,29	37772,01

Table E-4: Section modulus and effective thickness for bending stress for 2D curved models with $G = 10$ MPa (case A).

2D curved models - Case A - $G = 10$ MPa					
Model type & case study	Width model b	Length model L_b	Area of laminated glass A_{full}	Effective thickness $h_{ef,\sigma,i}$	Section modulus $W(h_{ef,\sigma,i})$
(-)	(mm)	(mm)	(mm ²)	(mm)	(mm ³)
2D_A	500	2000	10760	21,16	37312,13
	500	4000	10760	21,42	38234,70
	500	6000	10760	21,47	38413,41
	500	8000	10760	21,49	38485,01

Table E-5: Calculation of true buckling stress for 2D curved models with $G = 0,01$ MPa (case A).

2D curved models - Case A - $G = 0,01$ MPa						
Length of glass pane L_b	Type of buckling analysis	Applied load P_0	Maximum displacement δ_{max}	Basic imperfection e_0	$(\delta_{max} + e_0)$	True buckling stress $\bar{\sigma}$
(mm)	(-)	(N)	(mm)	(mm)	(mm)	(MPa)
2000	Nonlinear	2500	38,66	12,32	50,98	33,98
4000	Nonlinear	2500	144,32	16,13	160,45	32,50
6000	Nonlinear	2500	314,07	20,99	335,06	32,59
8000	Nonlinear	2500	560,042	26,32	586,74	34,39

Table E-6: Calculation of true buckling stress for 2D curved models with $G = 0,1$ MPa (case A).

2D curved models - Case A - $G = 0,1$ MPa						
Length of glass pane L_b	Type of buckling analysis	Applied load P_0	Maximum displacement δ_{max}	Basic imperfection e_0	$(\delta_{max} + e_0)$	True buckling stress $\bar{\sigma}$
(mm)	(-)	(N)	(mm)	(mm)	(mm)	(MPa)
2000	Nonlinear	2500	39,09	12,32	51,41	37,09
4000	Nonlinear	2500	124,35	16,13	140,48	34,52
6000	Nonlinear	2500	246,75	20,99	267,74	35,48
8000	Nonlinear	2500	400,68	26,32	427,00	35,58

Table E-7: Calculation of true buckling stress for 2D curved models with $G = 1$ MPa (case A).

2D curved models - Case A - $G = 1$ MPa						
Length of glass pane L_b	Type of buckling analysis	Applied load P_0	Maximum displacement δ_{max}	Basic imperfection e_0	$(\delta_{max} + e_0)$	True buckling stress $\bar{\sigma}$
(mm)	(-)	(N)	(mm)	(mm)	(mm)	(MPa)
2000	Nonlinear	2500	30,13	12,32	42,45	40,37
4000	Nonlinear	2500	99,19	16,13	115,32	40,74
6000	Nonlinear	2500	222,09	20,99	243,08	43,21
8000	Nonlinear	2500	379,77	26,32	406,09	42,67

Table E-8: Calculation of true buckling stress for 2D curved models with $G = 10$ MPa (case A).

2D curved models - Case A - $G = 10$ MPa						
Length of glass pane L_b	Type of buckling analysis	Applied load P_0	Maximum displacement δ_{max}	Basic imperfection e_0	$(\delta_{max} + e_0)$	True buckling stress $\bar{\sigma}$
(mm)	(-)	(N)	(mm)	(mm)	(mm)	(MPa)
2000	Nonlinear	2500	25,69	12,32	38,01	47,24
4000	Nonlinear	2500	94,63	16,13	110,76	44,10
6000	Nonlinear	2500	204,01	20,99	225,00	42,28
8000	Nonlinear	2500	348,38	26,32	374,70	40,64

 Table E-9: Critical buckling loads and stresses for 2D curved models with $G = 0,01$ MPa (case A – 2nd solution strategy).

2D curved models - Case A - $G = 0,01$ MPa							
Length model L_b	Ratio $f_{g,k}/\bar{\sigma}$	Type of buckling analysis	Applied load P_0	Limit displacement δ_{lim}	New buckling load factor BLF	Critical buckling load $N_{cr,FEA}$	Critical buckling stress $\sigma_{cr,FEA}$
(mm)	(-)	(-)	(N)	(mm)	(-)	(N)	(MPa)
2000	1,32	Nonlinear	2500	51,20	4,700	11750,00	1,09
4000	1,38	Nonlinear	2500	199,82	1,481	3702,50	0,34
6000	1,38	Nonlinear	2500	433,61	0,772	1930,00	0,18
8000	1,31	Nonlinear	2500	733,31	0,503	1257,50	0,12

 Table E-10: Critical buckling loads and stresses for 2D curved models with $G = 0,1$ MPa (case A – 2nd solution strategy).

2D curved models - Case A - $G = 0,1$ MPa							
Length model L_b	Ratio $f_{g,k}/\bar{\sigma}$	Type of buckling analysis	Applied load P_0	Limit displacement δ_{lim}	New buckling load factor BLF	Critical buckling load $N_{cr,FEA}$	Critical buckling stress $\sigma_{cr,FEA}$
(mm)	(-)	(-)	(N)	(mm)	(-)	(N)	(MPa)
2000	1,21	Nonlinear	2500	47,42	5,760	14400,00	1,34
4000	1,30	Nonlinear	2500	162,12	2,520	6300,00	0,59
6000	1,27	Nonlinear	2500	312,98	1,564	3910,00	0,36
8000	1,26	Nonlinear	2500	506,70	1,091	2727,50	0,25

Table E-11: Critical buckling loads and stresses for 2D curved models with $G = 1$ MPa (case A – 2nd solution strategy).

2D curved models - Case A - G = 1 MPa							
Length model L_b	Ratio $f_{g,k}/\bar{\sigma}$	Type of buckling analysis	Applied load P_0	Limit displacement δ_{lim}	New buckling load factor BLF	Critical buckling load $N_{cr,FEA}$	Critical buckling stress $\sigma_{cr,FEA}$
(mm)	(-)	(-)	(N)	(mm)	(-)	(N)	(MPa)
2000	1,11	Nonlinear	2500	33,59	10,800	27000,00	2,51
4000	1,10	Nonlinear	2500	109,56	4,950	12375,00	1,15
6000	1,04	Nonlinear	2500	213,29	2,614	6535,00	0,61
8000	1,05	Nonlinear	2500	400,50	1,571	3927,50	0,37

Table E-12: Critical buckling loads and stresses for 2D curved models with $G = 10$ MPa (case A – 2nd solution strategy).

2D curved models- Case A- G = 10 MPa							
Length model L_b	Ratio $f_{g,k}/\bar{\sigma}$	Type of buckling analysis	Applied load P_0	Limit displacement δ_{lim}	New buckling load factor BLF	Critical buckling load $N_{cr,FEA}$	Critical buckling stress $\sigma_{cr,FEA}$
(mm)	(-)	(-)	(N)	(mm)	(-)	(N)	(MPa)
2000	0,95	Nonlinear	2500	24,47	16,700	41750,00	3,88
4000	1,02	Nonlinear	2500	96,56	5,900	14750,00	1,37
6000	1,06	Nonlinear	2500	217,15	2,860	7150,00	0,66
8000	1,11	Nonlinear	2500	385,72	1,660	4150,00	0,39

Case B :Table E-13: Section modulus and effective thickness for bending stress for 2D curved models with $G = 0,01$ MPa (case B).

2D curved models - Case B - G = 0,01 MPa					
Model type & case study	Width model b	Length model L_b	Area of laminated glass A_{full}	Effective thickness $h_{ef,\sigma,i}$	Section modulus $W(h_{ef,\sigma,i})$
(-)	(mm)	(mm)	(mm ²)	(mm)	(mm ³)
2D_B	500	2000	12760	17,11	24396,01
	500	4000	12760	17,51	25550,01
	500	6000	12760	18,09	27270,68
	500	8000	12760	18,77	29359,41

Table E-14: Section modulus and effective thickness for bending stress for 2D curved models with $G = 0,1$ MPa (case B).

2D curved models - Case B - $G = 0,1$ MPa					
Model type & case study	Width model b	Length model L_b	Area of laminated glass A_{full}	Effective thickness $h_{ef,\sigma,i}$	Section modulus $W(h_{ef,\sigma,i})$
(-)	(mm)	(mm)	(mm ²)	(mm)	(mm ³)
2D_B	500	2000	12760	18,20	27603,33
	500	4000	12760	20,38	34612,03
	500	6000	12760	22,07	40590,41
	500	8000	12760	23,15	44660,21

Table E-15: Section modulus and effective thickness for bending stress for 2D curved models with $G = 1$ MPa (case B).

2D curved models - Case B - $G = 1$ MPa					
Model type & case study	Width model b	Length model L_b	Area of laminated glass A_{full}	Effective thickness $h_{ef,\sigma,i}$	Section modulus $W(h_{ef,\sigma,i})$
(-)	(mm)	(mm)	(mm ²)	(mm)	(mm ³)
2D_B	500	2000	12760	22,28	41366,53
	500	4000	12760	24,38	49532,03
	500	6000	12760	24,97	51958,41
	500	8000	12760	25,20	52920,00

Table E-16: Section modulus and effective thickness for bending stress for 2D curved models with $G = 10$ MPa (case B).

2D curved models - Case B - $G = 10$ MPa					
Model type & case study	Width model b	Length model L_b	Area of laminated glass A_{full}	Effective thickness $h_{ef,\sigma,i}$	Section modulus $W(h_{ef,\sigma,i})$
(-)	(mm)	(mm)	(mm ²)	(mm)	(mm ³)
2D_B	500	2000	12760	25,02	52166,70
	500	4000	12760	25,39	53721,01
	500	6000	12760	25,46	54017,63
	500	8000	12760	25,48	54102,53

Table E-17: Calculation of true buckling stress for 2D curved models with $G = 0,01$ MPa (case B).

2D curved models - Case B - $G = 0,01$ MPa						
Length of glass pane L_b	Type of buckling analysis	Applied load P_0	Maximum displacement δ_{max}	Basic imperfection e_0	$(\delta_{max} + e_0)$	True buckling stress $\bar{\sigma}$
(mm)	(-)	(N)	(mm)	(mm)	(mm)	(MPa)
2000	Nonlinear	2500	33,66	14,10	47,76	35,63
4000	Nonlinear	2500	127,23	17,52	144,75	34,13
6000	Nonlinear	2500	272,24	22,08	294,32	33,48
8000	Nonlinear	2500	434,63	27,20	461,83	31,34

Table E-18: Calculation of true buckling stress for 2D curved models with $G = 0,1$ MPa (case B).

2D curved models - Case B - $G = 0,1$ MPa						
Length of glass pane L_b	Type of buckling analysis	Applied load P_0	Maximum displacement δ_{max}	Basic imperfection e_0	$(\delta_{max} + e_0)$	True buckling stress $\bar{\sigma}$
(mm)	(-)	(N)	(mm)	(mm)	(mm)	(MPa)
2000	Nonlinear	2500	31,42	14,10	45,52	35,41
4000	Nonlinear	2500	114,91	17,52	132,43	37,09
6000	Nonlinear	2500	231,32	22,08	253,40	37,93
8000	Nonlinear	2500	376,58	27,20	403,78	38,60

Table E-19: Calculation of true buckling stress for 2D curved models with $G = 1$ MPa (case B).

2D curved models - Case B - $G = 1$ MPa						
Length of glass pane L_b	Type of buckling analysis	Applied load P_0	Maximum displacement δ_{max}	Basic imperfection e_0	$(\delta_{max} + e_0)$	True buckling stress $\bar{\sigma}$
(mm)	(-)	(N)	(mm)	(mm)	(mm)	(MPa)
2000	Nonlinear	2500	26,64	14,10	40,74	41,47
4000	Nonlinear	2500	85,43	17,52	102,95	40,98
6000	Nonlinear	2500	199,72	22,08	221,80	45,65
8000	Nonlinear	2500	306,93	27,20	334,13	40,67

Table E-20: Calculation of true buckling stress for 2D curved models with $G = 10$ MPa (case B).

2D curved models - Case B - $G = 10$ MPa						
Length of glass pane L_b	Type of buckling analysis	Applied load P_0	Maximum displacement δ_{max}	Basic imperfection e_0	$(\delta_{max} + e_0)$	True buckling stress $\bar{\sigma}$
(mm)	(-)	(N)	(mm)	(mm)	(mm)	(MPa)
2000	Nonlinear	2500	23,20	14,10	37,30	50,78
4000	Nonlinear	2500	83,12	17,52	100,64	46,11
6000	Nonlinear	2500	182,18	22,08	204,26	44,87
8000	Nonlinear	2500	325,56	27,20	352,76	45,07

 Table E-21: Critical buckling loads and stresses for 2D curved models with $G = 0,01$ MPa (case B – 2nd solution strategy).

2D curved models- Case B - $G = 0,01$ MPa							
Length model L_b	Ratio $f_{g,k}/\bar{\sigma}$	Type of buckling analysis	Applied load P_0	Limit displacement δ_{lim}	New buckling load factor BLF	Critical buckling load $N_{cr,FEA}$	Critical buckling stress $\sigma_{cr,FEA}$
(mm)	(-)	(-)	(N)	(mm)	(-)	(N)	(MPa)
2000	1,26	Nonlinear	2500	42,51	7,500	18750,00	1,47
4000	1,32	Nonlinear	2500	167,74	2,450	6125,00	0,48
6000	1,34	Nonlinear	2500	365,89	1,255	3137,50	0,25
8000	1,44	Nonlinear	2500	624,06	0,811	2027,50	0,16

 Table E-22: Critical buckling loads and stresses for 2D curved models with $G = 0,1$ MPa (case B – 2nd solution strategy).

2D curved models- Case B - $G = 0,1$ MPa							
Length model L_b	Ratio $f_{g,k}/\bar{\sigma}$	Type of buckling analysis	Applied load P_0	Limit displacement δ_{lim}	New buckling load factor BLF	Critical buckling load $N_{cr,FEA}$	Critical buckling stress $\sigma_{cr,FEA}$
(mm)	(-)	(-)	(N)	(mm)	(-)	(N)	(MPa)
2000	1,27	Nonlinear	2500	39,93	8,800	22000,00	1,72
4000	1,21	Nonlinear	2500	139,41	3,880	9700,00	0,76
6000	1,19	Nonlinear	2500	274,46	2,430	6075,00	0,48
8000	1,17	Nonlinear	2500	439,04	1,713	4282,50	0,34

Table E-23: Critical buckling loads and stresses for 2D curved models with $G = 1$ MPa (case B – 2nd solution strategy).

2D curved models- Case B - G = 1 MPa							
Length model L_b	Ratio $f_{g,k}/\bar{\sigma}$	Type of buckling analysis	Applied load P_0	Limit displacement δ_{lim}	New buckling load factor BLF	Critical buckling load $N_{cr,FEA}$	Critical buckling stress $\sigma_{cr,FEA}$
(mm)	(-)	(-)	(N)	(mm)	(-)	(N)	(MPa)
2000	1,09	Nonlinear	2500	28,91	16,000	40000,00	3,13
4000	1,10	Nonlinear	2500	93,81	7,680	19200,00	1,50
6000	0,99	Nonlinear	2500	196,90	4,200	10500,00	0,82
8000	1,11	Nonlinear	2500	339,60	2,560	6400,00	0,50

 Table E-24: Critical buckling loads and stresses for 2D curved models with $G = 10$ MPa (case B – 2nd solution strategy).

2D curved models- Case B - G = 10 MPa							
Length model L_b	Ratio $f_{g,k}/\bar{\sigma}$	Type of buckling analysis	Applied load P_0	Limit displacement δ_{lim}	New buckling load factor BLF	Critical buckling load $N_{cr,FEA}$	Critical buckling stress $\sigma_{cr,FEA}$
(mm)	(-)	(-)	(N)	(mm)	(-)	(N)	(MPa)
2000	0,89	Nonlinear	2500	20,56	24,400	61000,00	4,78
4000	0,98	Nonlinear	2500	81,12	9,400	23500,00	1,84
6000	1,00	Nonlinear	2500	182,71	4,650	11625,00	0,91
8000	1,00	Nonlinear	2500	325,07	2,710	6775,00	0,53

Case C :

 Table E-25: Section modulus and effective thickness for bending stress for 2D curved models with $G = 0,01$ MPa (case C).

2D curved models - Case C - G = 0,01 MPa					
Model type & case study	Width model b	Length model L_b	Area of laminated glass A_{full}	Effective thickness $h_{ef,\sigma,i}$	Section modulus $W(h_{ef,\sigma,i})$
(-)	(mm)	(mm)	(mm ²)	(mm)	(mm ³)
2D_C	500	2000	14760	19,94	33133,63
	500	4000	14760	20,32	34408,53
	500	6000	14760	20,90	36400,83
	500	8000	14760	21,59	38844,01

Table E-26: Section modulus and effective thickness for bending stress for 2D curved models with $G = 0,1$ MPa (case C).

2D curved models - Case C - $G = 0,1$ MPa					
Model type & case study	Width model b	Length model L_b	Area of laminated glass A_{full}	Effective thickness $h_{ef,\sigma,i}$	Section modulus $W(h_{ef,\sigma,i})$
(-)	(mm)	(mm)	(mm ²)	(mm)	(mm ³)
2D_C	500	2000	14760	21,01	36785,01
	500	4000	14760	23,29	45202,01
	500	6000	14760	25,21	52962,01
	500	8000	14760	26,50	58520,83

Table E-27: Section modulus and effective thickness for bending stress for 2D curved models with $G = 1$ MPa (case C).

2D curved models - Case C - $G = 1$ MPa					
Model type & case study	Width model b	Length model L_b	Area of laminated glass A_{full}	Effective thickness $h_{ef,\sigma,i}$	Section modulus $W(h_{ef,\sigma,i})$
(-)	(mm)	(mm)	(mm ²)	(mm)	(mm ³)
2D_C	500	2000	14760	25,45	53975,21
	500	4000	14760	28,03	65473,41
	500	6000	14760	28,79	69072,01
	500	8000	14760	29,10	70567,50

Table E-28: Section modulus and effective thickness for bending stress for 2D curved models with $G = 10$ MPa (case C).

2D curved models - Case C - $G = 10$ MPa					
Model type & case study	Width model b	Length model L_b	Area of laminated glass A_{full}	Effective thickness $h_{ef,\sigma,i}$	Section modulus $W(h_{ef,\sigma,i})$
(-)	(mm)	(mm)	(mm ²)	(mm)	(mm ³)
2D_C	500	2000	14760	28,86	69408,30
	500	4000	14760	29,34	71736,30
	500	6000	14760	29,44	72226,13
	500	8000	14760	29,47	72373,41

Table E-29: Calculation of true buckling stress for 2D curved models with $G = 0,01$ MPa (case C).

2D curved models - Case C - $G = 0,01$ MPa						
Length model L_b	Type of buckling analysis	Applied load P_0	Maximum displacement δ_{max}	Basic imperfection e_0	$(\delta_{max} + e_0)$	True buckling stress $\bar{\sigma}$
(mm)	(-)	(N)	(mm)	(mm)	(mm)	(MPa)
2000	Nonlinear	2500	29,81	15,94	45,75	36,94
4000	Nonlinear	2500	110,24	19,03	129,27	34,42
6000	Nonlinear	2500	251,63	23,29	274,92	35,82
8000	Nonlinear	2500	430,03	28,20	458,23	35,68

 Table E-30: Calculation of true buckling stress for 2D curved models with $G = 0,1$ MPa (case C).

2D curved models - Case C - $G = 0,1$ MPa						
Length model L_b	Type of buckling analysis	Applied load P_0	Maximum displacement δ_{max}	Basic imperfection e_0	$(\delta_{max} + e_0)$	True buckling stress $\bar{\sigma}$
(mm)	(-)	(N)	(mm)	(mm)	(mm)	(MPa)
2000	Nonlinear	2500	39,09	15,94	55,03	45,74
4000	Nonlinear	2500	124,35	19,03	143,38	43,90
6000	Nonlinear	2500	246,75	23,29	270,04	44,56
8000	Nonlinear	2500	400,68	28,20	428,88	45,58

 Table E-31: Calculation of true buckling stress for 2D curved models with $G = 1$ MPa (case C).

2D curved models - Case C - $G = 1$ MPa						
Length model L_b	Type of buckling analysis	Applied load P_0	Maximum displacement δ_{max}	Basic imperfection e_0	$(\delta_{max} + e_0)$	True buckling stress $\bar{\sigma}$
(mm)	(-)	(N)	(mm)	(mm)	(mm)	(MPa)
2000	Nonlinear	2500	30,13	15,94	42,45	45,06
4000	Nonlinear	2500	99,19	19,03	115,32	50,71
6000	Nonlinear	2500	222,09	23,29	243,08	55,60
8000	Nonlinear	2500	379,77	28,20	406,09	55,65

Table E-32: Calculation of true buckling stress for 2D curved models with $G = 10$ MPa (case C).

2D curved models - Case C - $G = 10$ MPa						
Length model L_b	Type of buckling analysis	Applied load P_0	Maximum displacement δ_{max}	Basic imperfection e_0	$(\delta_{max} + e_0)$	True buckling stress $\bar{\sigma}$
(mm)	(-)	(N)	(mm)	(mm)	(mm)	(MPa)
2000	Nonlinear	2500	25,69	15,94	38,01	54,15
4000	Nonlinear	2500	94,63	19,03	110,76	56,41
6000	Nonlinear	2500	201,01	23,29	225,00	55,70
8000	Nonlinear	2500	348,38	28,20	374,70	53,76

Table E-33: Critical buckling loads and stresses for 2D curved models with $G = 0,01$ MPa (case C – 2nd solution strategy).

2D curved models- Case C - $G = 0,01$ MPa							
Length model L_b	Ratio $f_{g,k} / \bar{\sigma}$	Type of buckling analysis	Applied load P_0	Limit displacement δ_{lim}	New buckling load factor BLF	Critical buckling load $N_{cr,FEA}$	Critical buckling stress $\sigma_{cr,FEA}$
(mm)	(-)	(-)	(N)	(mm)	(-)	(N)	(MPa)
2000	1,22	Nonlinear	2500	36,32	10,890	27225,00	1,84
4000	1,31	Nonlinear	2500	144,12	3,740	9350,00	0,63
6000	1,26	Nonlinear	2500	316,16	1,917	4792,50	0,32
8000	1,26	Nonlinear	2500	542,32	1,224	3060,00	0,21

Table E-34: Critical buckling loads and stresses for 2D curved models with $G = 0,1$ MPa (case C – 2nd solution strategy).

2D curved models- Case C - $G = 0,1$ MPa							
Length model L_b	Ratio $f_{g,k} / \bar{\sigma}$	Type of buckling analysis	Applied load P_0	Limit displacement δ_{lim}	New buckling load factor BLF	Critical buckling load $N_{cr,FEA}$	Critical buckling stress $\sigma_{cr,FEA}$
(mm)	(-)	(-)	(N)	(mm)	(-)	(N)	(MPa)
2000	0,98	Nonlinear	2500	38,46	12,90	32250,00	2,18
4000	1,03	Nonlinear	2500	127,47	5,660	14150,00	0,96
6000	1,01	Nonlinear	2500	249,18	3,540	8850,00	0,60
8000	0,99	Nonlinear	2500	395,58	2,490	6225,00	0,42

Table E-35: Critical buckling loads and stresses for 2D curved models with $G = 1$ MPa (case C – 2nd solution strategy).

2D curved models- Case C - G = 1 MPa							
Length model L_b	Ratio $f_{g,k}/\bar{\sigma}$	Type of buckling analysis	Applied load P_0	Limit displacement δ_{lim}	New buckling load factor BLF	Critical buckling load $N_{cr,FEA}$	Critical buckling stress $\sigma_{cr,FEA}$
(mm)	(-)	(-)	(N)	(mm)	(-)	(N)	(MPa)
2000	1,00	Nonlinear	2500	30,09	23,000	57500,00	3,90
4000	0,89	Nonlinear	2500	88,02	11,280	28200,00	1,91
6000	0,81	Nonlinear	2500	179,76	6,250	15625,00	1,06
8000	0,81	Nonlinear	2500	307,11	3,877	9692,50	0,66

 Table E-36: Critical buckling loads and stresses for 2D curved models with $G = 10$ MPa (case C – 2nd solution strategy).

2D curved models- Case C - G = 10 MPa							
Length model L_b	Ratio $f_{g,k}/\bar{\sigma}$	Type of buckling analysis	Applied load P_0	Limit displacement δ_{lim}	New buckling load factor BLF	Critical buckling load $N_{cr,FEA}$	Critical buckling stress $\sigma_{cr,FEA}$
(mm)	(-)	(-)	(N)	(mm)	(-)	(N)	(MPa)
2000	0,83	Nonlinear	2500	21,35	35,400	88500,00	6,00
4000	0,80	Nonlinear	2500	75,49	14,040	35100,00	2,38
6000	0,81	Nonlinear	2500	164,81	7,030	17575,00	1,19
8000	0,84	Nonlinear	2500	291,60	4,200	10500,00	0,71

F. DESIGN BUCKLING CURVES BASED ON EC3: CALCULATIONS

This annex presents all the calculations necessary to plot the design buckling curves for laminated glass members in compression, based on the Eurocode 3 framework.

Annealed glass (ANG) :

Table F-1: Nondimensional slenderness and buckling reduction factors for annealed glass (case A).

3D models- Case A - G = 0,01 MPa							
Length model	Critical buckling load	Charact. bending strength	Critical buckling load	Nondim. slenderness	Buckling parameter	Buckling reduction factor	Buckling reduction factor (FEM)
L_b	$N_{cr,FEA}$	$f_{g,k}$	$N_{cr,LG}$	$\bar{\lambda}$	Φ	χ	χ_{FEM}
(mm)	(N)	(MPa)	(N)	(-)	(-)	(-)	(-)
2000	13000	45	14811,83	5,718	18,662	0,0275	0,0268
4000	3660	45	4018,27	10,977	64,434	0,0078	0,0076
6000	2000	45	2006,13	15,536	126,482	0,0040	0,0041
8000	1330	45	1287,74	19,391	195,175	0,0026	0,0027

Table F-2: Nondimensional slenderness and buckling reduction factors for annealed glass (case A).

3D models- Case A - G = 0,1 MPa							
Length model	Critical buckling load	Charact. bending strength	Critical buckling load	Nondim. slenderness	Buckling parameter	Buckling reduction factor	Buckling reduction factor (FEM)
L_b	$N_{cr,FEA}$	$f_{g,k}$	$N_{cr,LG}$	$\bar{\lambda}$	Φ	χ	χ_{FEM}
(mm)	(N)	(MPa)	(N)	(-)	(-)	(-)	(-)
2000	16140	45	18434,74	5,125	15,239	0,0338	0,0333
4000	6150	45	6939,75	8,353	38,138	0,0133	0,0127
6000	3900	45	4186,37	10,755	61,935	0,0081	0,0081
8000	2730	45	2864,97	13,000	89,406	0,0056	0,0056

Table F-3: Nondimensional slenderness and buckling reduction factors for annealed glass (case A).

3D models- Case A - G = 1 MPa							
Length model	Critical buckling load	Charact. bending strength	Critical buckling load	Nondim. slenderness	Buckling parameter	Buckling reduction factor	Buckling reduction factor (FEM)
L_b	$N_{cr,FEA}$	$f_{g,k}$	$N_{cr,LG}$	$\bar{\lambda}$	Φ	χ	χ_{FEM}
(mm)	(N)	(MPa)	(N)	(-)	(-)	(-)	(-)
2000	28630	45	39146,01	3,517	7,720	0,0685	0,0591
4000	11950	45	14372,67	5,804	19,192	0,0267	0,0247
6000	6460	45	7149,34	8,230	37,072	0,0137	0,0133
8000	4030	45	4205,49	10,730	61,664	0,0082	0,0083

Table F-4: Nondimensional slenderness and buckling reduction factors for annealed glass (case A).

3D models- Case A - G = 10 MPa							
Length model	Critical buckling load	Charact. bending strength	Critical buckling load	Nondim. slenderness	Buckling parameter	Buckling reduction factor	Buckling reduction factor (FEM)
L_b	$N_{cr,FEA}$	$f_{g,k}$	$N_{cr,LG}$	$\bar{\lambda}$	Φ	χ	χ_{FEM}
(mm)	(N)	(MPa)	(N)	(-)	(-)	(-)	(-)
2000	48750	45	64987,70	2,730	4,981	0,1093	0,1007
4000	14530	45	17451,77	5,267	16,029	0,0321	0,0300
6000	7560	45	7866,90	7,845	33,847	0,0150	0,0156
8000	4240	45	4447,43	10,434	58,427	0,0086	0,0088

Table F-5: Nondimensional slenderness and buckling reduction factors for annealed glass (case B).

3D models- Case B - G = 0,01 MPa							
Length model	Critical buckling load	Charact. bending strength	Critical buckling load	Nondim. slenderness	Buckling parameter	Buckling reduction factor	Buckling reduction factor (FEM)
L_b	$N_{cr,FEA}$	$f_{g,k}$	$N_{cr,LG}$	$\bar{\lambda}$	Φ	χ	χ_{FEM}
(mm)	(N)	(MPa)	(N)	(-)	(-)	(-)	(-)
2000	21250	45	25443,68	4,751	13,257	0,0390	0,0370
4000	6000	45	6797,93	9,191	45,783	0,0110	0,0104
6000	3210	45	3329,44	13,132	91,180	0,0055	0,0056
8000	2160	45	2098,68	16,541	142,960	0,0035	0,0038

Table F-6: Nondimensional slenderness and buckling reduction factors for annealed glass (case B).

3D models- Case B - G = 0,1 MPa							
Length model	Critical buckling load	Charact. bending strength	Critical buckling load	Nondim. slenderness	Buckling parameter	Buckling reduction factor	Buckling reduction factor (FEM)
L_b	$N_{cr,FEA}$	$f_{g,k}$	$N_{cr,LG}$	$\bar{\lambda}$	Φ	χ	χ_{FEM}
(mm)	(N)	(MPa)	(N)	(-)	(-)	(-)	(-)
2000	25370	45	30499,76	4,339	11,241	0,0463	0,0442
4000	9720	45	11005,73	7,223	28,938	0,0176	0,0169
6000	6030	45	6585,80	9,337	47,196	0,0107	0,0105
8000	4280	45	4534,29	11,253	67,599	0,0074	0,0074

Table F-7: Nondimensional slenderness and buckling reduction factors for annealed glass (case B).

3D models- Case B - G = 1 MPa							
Length model	Critical buckling load	Charact. bending strength	Critical buckling load	Nondim. slenderness	Buckling parameter	Buckling reduction factor	Buckling reduction factor (FEM)
L_b	$N_{cr,FEA}$	$f_{g,k}$	$N_{cr,LG}$	$\bar{\lambda}$	Φ	χ	χ_{FEM}
(mm)	(N)	(MPa)	(N)	(-)	(-)	(-)	(-)
2000	46500	45	61611,00	3,053	6,031	0,0890	0,0810
4000	18520	45	23187,60	4,976	14,435	0,0357	0,0323
6000	10270	45	11709,17	7,003	27,292	0,0186	0,0179
8000	6370	45	6936,97	9,098	44,904	0,0113	0,0111

Table F-8: Nondimensional slenderness and buckling reduction factors for annealed glass (case B).

3D models- Case B - G = 10 MPa							
Length model	Critical buckling load	Charact. bending strength	Critical buckling load	Nondim. slenderness	Buckling parameter	Buckling reduction factor	Buckling reduction factor (FEM)
L_b	$N_{cr,FEA}$	$f_{g,k}$	$N_{cr,LG}$	$\bar{\lambda}$	Φ	χ	χ_{FEM}
(mm)	(N)	(MPa)	(N)	(-)	(-)	(-)	(-)
2000	67000	45	106599,2 1	2,321	3,804	0,1467	0,1167
4000	27100	45	28970,61	4,452	11,777	0,0441	0,0472
6000	11930	45	13093,10	6,622	24,566	0,0207	0,0208
8000	7010	45	7408,89	8,803	42,163	0,0120	0,0122

Table F-9: Nondimensional slenderness and buckling reduction factors for annealed glass (case C).

3D models- Case C - G = 0,01 MPa							
Length model	Critical buckling load	Charact. bending strength	Critical buckling load	Nondim. slenderness	Buckling parameter	Buckling reduction factor	Buckling reduction factor (FEM)
L_b	$N_{cr,FEA}$	$f_{g,k}$	$N_{cr,LG}$	$\bar{\lambda}$	Φ	χ	χ_{FEM}
(mm)	(N)	(MPa)	(N)	(-)	(-)	(-)	(-)
2000	32600	45	40242,88	4,063	9,982	0,0524	0,0491
4000	9130	45	10639,15	7,901	34,307	0,0148	0,0137
6000	4920	45	5139,18	11,368	68,944	0,0073	0,0074
8000	3270	45	3194,75	14,419	109,358	0,0046	0,0049

Table F-10: Nondimensional slenderness and buckling reduction factors for annealed glass (case C).

3D models- Case C - G = 0,1 MPa							
Length model	Critical buckling load	Charact. bending strength	Critical buckling load	Nondim. slenderness	Buckling parameter	Buckling reduction factor	Buckling reduction factor (FEM)
L_b	$N_{cr,FEA}$	$f_{g,k}$	$N_{cr,LG}$	$\bar{\lambda}$	Φ	χ	χ_{FEM}
(mm)	(N)	(MPa)	(N)	(-)	(-)	(-)	(-)
2000	31630	45	46968,91	3,760	8,693	0,0605	0,0476
4000	13950	45	16369,57	6,370	22,836	0,0223	0,0210
6000	8890	45	9700,73	8,275	37,459	0,0135	0,0134
8000	6240	45	6699,56	9,957	53,392	0,0094	0,0094

Table F-11: Nondimensional slenderness and buckling reduction factors for annealed glass (case C).

3D models- Case C - G = 1 MPa							
Length model	Critical buckling load	Charact. bending strength	Critical buckling load	Nondim. slenderness	Buckling parameter	Buckling reduction factor	Buckling reduction factor (FEM)
L_b	$N_{cr,FEA}$	$f_{g,k}$	$N_{cr,LG}$	$\bar{\lambda}$	Φ	χ	χ_{FEM}
(mm)	(N)	(MPa)	(N)	(-)	(-)	(-)	(-)
2000	63500	45	90748,58	2,705	4,907	0,1111	0,0956
4000	26980	45	34789,22	4,369	11,384	0,0457	0,0406
6000	15350	45	17807,98	6,107	21,104	0,0242	0,0231
8000	9550	45	10621,51	7,908	34,361	0,0147	0,0144

Table F-12: Nondimensional slenderness and buckling reduction factors for annealed glass (case C).

3D models- Case C - G = 10 MPa							
Length model	Critical buckling load	Charact. bending strength	Critical buckling load	Nondim. slenderness	Buckling parameter	Buckling reduction factor	Buckling reduction factor (FEM)
L_b	$N_{cr,FEA}$	$f_{g,k}$	$N_{cr,LG}$	$\bar{\lambda}$	Φ	χ	χ_{FEM}
(mm)	(N)	(MPa)	(N)	(-)	(-)	(-)	(-)
2000	92500	45	162354,04	2,023	3,051	0,1875	0,1393
4000	34350	45	44633,34	3,858	9,097	0,0577	0,0517
6000	17600	45	20223,19	5,731	18,743	0,0273	0,0265
8000	10600	45	11454,15	7,615	31,984	0,0159	0,0160

Fully tempered glass (FTG) :

Table F-13: Nondimensional slenderness and buckling reduction factors for fully tempered glass (case A).

3D models- Case A - G = 0,01 MPa							
Length model	Critical buckling load	Charact. bending strength	Critical buckling load	Nondim. slenderness	Buckling parameter	Buckling reduction factor	Buckling reduction factor (FEM)
L_b	$N_{cr,FEA}$	$f_{b,k}$	$N_{cr,LG}$	$\bar{\lambda}$	Φ	χ	χ_{FEM}
(mm)	(N)	(MPa)	(N)	(-)	(-)	(-)	(-)
2000	15960	120	14811,83	9,337	47,188	0,0107	0,0124
4000	5220	120	4018,27	17,926	167,317	0,0030	0,0040
6000	2590	120	2006,13	25,370	331,107	0,0015	0,0020
8000	1760	120	1287,74	31,665	512,873	0,0010	0,0014

Table F-14: Nondimensional slenderness and buckling reduction factors for fully tempered glass (case A).

3D models- Case A - G = 0,1 MPa							
Length model	Critical buckling load	Charact. bending strength	Critical buckling load	Nondim. slenderness	Buckling parameter	Buckling reduction factor	Buckling reduction factor (FEM)
L_b	$N_{cr,FEA}$	$f_{b,k}$	$N_{cr,LG}$	$\bar{\lambda}$	Φ	χ	χ_{FEM}
(mm)	(N)	(MPa)	(N)	(-)	(-)	(-)	(-)
2000	18660	120	18434,74	8,369	38,279	0,0132	0,0145
4000	9450	120	6939,75	13,640	98,159	0,0051	0,0073
6000	4380	120	4186,37	17,562	160,736	0,0031	0,0034
8000	3010	120	2864,97	21,229	233,166	0,0021	0,0023

Table F-15: Nondimensional slenderness and buckling reduction factors for fully tempered glass (case A).

3D models- Case A - G = 1 MPa							
Length model	Critical buckling load	Charact. bending strength	Critical buckling load	Nondim. slenderness	Buckling parameter	Buckling reduction factor	Buckling reduction factor (FEM)
L_b	$N_{cr,FEA}$	$f_{b,k}$	$N_{cr,LG}$	$\bar{\lambda}$	Φ	χ	χ_{FEM}
(mm)	(N)	(MPa)	(N)	(-)	(-)	(-)	(-)
2000	34870	120	39146,01	5,743	18,818	0,0272	0,0270
4000	13540	120	14372,67	9,478	48,570	0,0104	0,0105
6000	7400	120	7149,34	13,439	95,360	0,0053	0,0057
8000	5050	120	4205,49	17,522	160,021	0,0031	0,0039

Table F-16: Nondimensional slenderness and buckling reduction factors for fully tempered glass (case A).

3D models- Case A - G = 10 MPa							
Length model	Critical buckling load	Charact. bending strength	Critical buckling load	Nondim. slenderness	Buckling parameter	Buckling reduction factor	Buckling reduction factor (FEM)
L_b	$N_{cr,FEA}$	$f_{b,k}$	$N_{cr,LG}$	$\bar{\lambda}$	Φ	χ	χ_{FEM}
(mm)	(N)	(MPa)	(N)	(-)	(-)	(-)	(-)
2000	57290	120	64987,70	4,457	11,804	0,0440	0,0444
4000	18880	120	17451,77	8,602	40,334	0,0125	0,0146
6000	10400	120	7866,90	12,811	86,900	0,0058	0,0081
8000	6920	120	4447,43	17,039	151,498	0,0033	0,0054

Table F-17: Nondimensional slenderness and buckling reduction factors for fully tempered glass (case B).

3D models- Case B - G = 0,01 MPa							
Length model	Critical buckling load	Charact. bending strength	Critical buckling load	Nondim. slenderness	Buckling parameter	Buckling reduction factor	Buckling reduction factor (FEM)
L_b	$N_{cr,FEA}$	$f_{b,k}$	$N_{cr,LG}$	$\bar{\lambda}$	Φ	χ	χ_{FEM}
(mm)	(N)	(MPa)	(N)	(-)	(-)	(-)	(-)
2000	25160	120	25443,68	7,758	33,131	0,0153	0,0164
4000	6980	120	6797,93	15,008	118,237	0,0042	0,0046
6000	3790	120	3329,44	21,445	237,848	0,0021	0,0025
8000	2410	120	2098,68	27,011	374,677	0,0013	0,0016

Table F-18: Nondimensional slenderness and buckling reduction factors for fully tempered glass (case B).

3D models- Case B - G = 0,1 MPa							
Length model	Critical buckling load	Charact. bending strength	Critical buckling load	Nondim. slenderness	Buckling parameter	Buckling reduction factor	Buckling reduction factor (FEM)
L_b	$N_{cr,FEA}$	$f_{b,k}$	$N_{cr,LG}$	$\bar{\lambda}$	Φ	χ	χ_{FEM}
(mm)	(N)	(MPa)	(N)	(-)	(-)	(-)	(-)
2000	28720	120	30499,76	7,085	27,904	0,0182	0,0188
4000	11150	120	11005,73	11,795	74,038	0,0068	0,0073
6000	6730	120	6585,80	15,248	121,950	0,0041	0,0044
8000	4810	120	4534,29	18,376	175,657	0,0029	0,0031

Table F-19: Nondimensional slenderness and buckling reduction factors for fully tempered glass (case B).

3D models- Case B - G = 1 MPa							
Length model	Critical buckling load	Charact. bending strength	Critical buckling load	Nondim. slenderness	Buckling parameter	Buckling reduction factor	Buckling reduction factor (FEM)
L_b	$N_{cr,FEA}$	$f_{b,k}$	$N_{cr,LG}$	$\bar{\lambda}$	Φ	χ	χ_{FEM}
(mm)	(N)	(MPa)	(N)	(-)	(-)	(-)	(-)
2000	55620	120	61611,00	4,985	14,483	0,0356	0,0363
4000	22040	120	23187,60	8,126	36,189	0,0140	0,0144
6000	11620	120	11709,17	11,435	69,731	0,0072	0,0076
8000	6980	120	6936,97	14,857	115,926	0,0043	0,0046

Table F-20: Nondimensional slenderness and buckling reduction factors for fully tempered glass (case B).

3D models- Case B - G = 10 MPa							
Length model	Critical buckling load	Charact. bending strength	Critical buckling load	Nondim. slenderness	Buckling parameter	Buckling reduction factor	Buckling reduction factor (FEM)
L_b	$N_{cr,FEA}$	$f_{b,k}$	$N_{cr,LG}$	$\bar{\lambda}$	Φ	χ	χ_{FEM}
(mm)	(N)	(MPa)	(N)	(-)	(-)	(-)	(-)
2000	92140	120	106599,2 1	3,790	8,814	0,0596	0,0602
4000	27160	120	28970,61	7,270	29,295	0,0173	0,0177
6000	12870	120	13093,10	10,814	62,600	0,0080	0,0084
8000	7480	120	7408,89	14,376	108,726	0,0046	0,0049

Table F-21: Nondimensional slenderness and buckling reduction factors for fully tempered glass (case C).

3D models- Case C - G = 0,01 MPa							
Length model	Critical buckling load	Charact. bending strength	Critical buckling load	Nondim. slenderness	Buckling parameter	Buckling reduction factor	Buckling reduction factor (FEM)
L_b	$N_{cr,FEA}$	$f_{b,k}$	$N_{cr,LG}$	$\bar{\lambda}$	Φ	χ	χ_{FEM}
(mm)	(N)	(MPa)	(N)	(-)	(-)	(-)	(-)
2000	39160	120	40242,88	6,634	24,649	0,0207	0,0221
4000	11240	120	10639,15	12,903	88,107	0,0057	0,0063
6000	5380	120	5139,18	18,565	179,201	0,0028	0,0030
8000	3580	120	3194,75	23,546	285,851	0,0018	0,0020

Table F-22: Nondimensional slenderness and buckling reduction factors for fully tempered glass (case C).

3D models- Case C - G = 0,1 MPa							
Length model	Critical buckling load	Charact. bending strength	Critical buckling load	Nondim. slenderness	Buckling parameter	Buckling reduction factor	Buckling reduction factor (FEM)
L_b	$N_{cr,FEA}$	$f_{b,k}$	$N_{cr,LG}$	$\bar{\lambda}$	Φ	χ	χ_{FEM}
(mm)	(N)	(MPa)	(N)	(-)	(-)	(-)	(-)
2000	44250	120	46968,91	6,141	21,322	0,0240	0,0250
4000	16270	120	16369,57	10,402	58,080	0,0087	0,0092
6000	9890	120	9700,73	13,512	96,376	0,0052	0,0056
8000	6850	120	6699,56	16,260	138,247	0,0036	0,0039

Table F-23: Nondimensional slenderness and buckling reduction factors for fully tempered glass (case C).

3D models- Case C - G = 1 MPa							
Length model	Critical buckling load	Charact. bending strength	Critical buckling load	Nondim. slenderness	Buckling parameter	Buckling reduction factor	Buckling reduction factor (FEM)
L_b	$N_{cr,FEA}$	$f_{b,k}$	$N_{cr,LG}$	$\bar{\lambda}$	Φ	χ	χ_{FEM}
(mm)	(N)	(MPa)	(N)	(-)	(-)	(-)	(-)
2000	81260	120	90748,58	4,418	11,614	0,0447	0,0459
4000	33460	120	34789,22	7,135	28,276	0,0180	0,0189
6000	17340	120	17807,98	9,973	53,558	0,0094	0,0098
8000	10620	120	10621,51	12,913	88,249	0,0057	0,0060

Table F-24: Nondimensional slenderness and buckling reduction factors for fully tempered glass (case C).

3D models- Case C - G = 10 MPa							
Length model	Critical buckling load	Charact. bending strength	Critical buckling load	Nondim. slenderness	Buckling parameter	Buckling reduction factor	Buckling reduction factor (FEM)
L_b	$N_{cr,FEA}$	$f_{b,k}$	$N_{cr,LG}$	$\bar{\lambda}$	Φ	χ	χ_{FEM}
(mm)	(N)	(MPa)	(N)	(-)	(-)	(-)	(-)
2000	145860	120	162354,04	3,303	6,914	0,0770	0,0824
4000	43840	120	44633,34	6,299	22,365	0,0228	0,0248
6000	19780	120	20223,19	9,359	47,401	0,0107	0,0112
8000	11280	120	11454,15	12,435	82,018	0,0061	0,0064

Heat strengthened glass (HSG) :

Table F-25: Nondimensional slenderness and buckling reduction factors for heat strengthened glass (case A).

3D models- Case A - G = 0,01 MPa					
Length model	Charact. bending strength	Critical buckling load	Nondim. slenderness	Buckling parameter	Buckling reduction factor
L_b	$f_{b,k}$	$N_{cr,LG}$	$\bar{\lambda}$	Φ	χ
(mm)	(MPa)	(N)	(-)	(-)	(-)
2000	70	14811,83	7,131	28,244	0,0180
4000	70	4018,27	13,691	98,869	0,0051
6000	70	2006,13	19,377	194,890	0,0026
8000	70	1287,74	24,185	301,324	0,0017

Table F-26: Nondimensional slenderness and buckling reduction factors for heat strengthened glass (case A).

3D models- Case A - G = 0,1 MPa					
Length model	Charact. bending strength	Critical buckling load	Nondim. slenderness	Buckling parameter	Buckling reduction factor
L_b	$f_{b,k}$	$N_{cr,LG}$	$\bar{\lambda}$	Φ	χ
(mm)	(MPa)	(N)	(-)	(-)	(-)
2000	70	18434,74	6,392	22,985	0,0222
4000	70	6939,75	10,418	58,252	0,0087
6000	70	4186,37	13,413	95,007	0,0053
8000	70	2864,97	16,214	137,493	0,0036

Table F-27: Nondimensional slenderness and buckling reduction factors for heat strengthened glass (case A).

3D models- Case A - G = 1 MPa					
Length model	Charact. bending strength	Critical buckling load	Nondim. slenderness	Buckling parameter	Buckling reduction factor
L_b	$f_{b,k}$	$N_{cr,LG}$	$\bar{\lambda}$	Φ	χ
(mm)	(MPa)	(N)	(-)	(-)	(-)
2000	70	39146,01	4,386	11,465	0,0453
4000	70	14372,67	7,239	29,059	0,0175
6000	70	7149,34	10,264	56,607	0,0089
8000	70	4205,49	13,383	94,587	0,0053

Table F-28: Nondimensional slenderness and buckling reduction factors for heat strengthened glass (case A).

3D models- Case A - G = 10 MPa					
Length model	Charact. bending strength	Critical buckling load	Nondim. slenderness	Buckling parameter	Buckling reduction factor
L_b	$f_{b,k}$	$N_{cr,LG}$	$\bar{\lambda}$	Φ	χ
(mm)	(MPa)	(N)	(-)	(-)	(-)
2000	70	64987,70	3,404	7,291	0,0728
4000	70	17451,77	6,570	24,199	0,0211
6000	70	7866,90	9,785	51,632	0,0098
8000	70	4447,43	13,014	89,585	0,0056

Table F-29: Nondimensional slenderness and buckling reduction factors for heat strengthened glass (case B).

3D models- Case B - G = 0,01 MPa					
Length model	Charact. bending strength	Critical buckling load	Nondim. slenderness	Buckling parameter	Buckling reduction factor
L_b	$f_{b,k}$	$N_{cr,LG}$	$\bar{\lambda}$	Φ	χ
(mm)	(MPa)	(N)	(-)	(-)	(-)
2000	70	25443,68	5,925	19,943	0,0257
4000	70	6797,93	11,463	70,053	0,0072
6000	70	3329,44	16,379	140,238	0,0036
8000	70	2098,68	20,630	220,411	0,0023

Table F-30: Nondimensional slenderness and buckling reduction factors for heat strengthened glass (case B).

3D models- Case B - G = 0,1 MPa					
Length model	Charact. bending strength	Critical buckling load	Nondim. slenderness	Buckling parameter	Buckling reduction factor
L_b	$f_{b,k}$	$N_{cr,LG}$	$\bar{\lambda}$	Φ	χ
(mm)	(MPa)	(N)	(-)	(-)	(-)
2000	70	30499,76	5,412	16,851	0,0305
4000	70	11005,73	9,009	44,064	0,0115
6000	70	6585,80	11,646	72,234	0,0070
8000	70	4534,29	14,035	103,763	0,0048

Table F-31: Nondimensional slenderness and buckling reduction factors for heat strengthened glass (case B).

3D models- Case B - G = 1 MPa					
Length model	Charact. bending strength	Critical buckling load	Nondim. slenderness	Buckling parameter	Buckling reduction factor
L_b	$f_{b,k}$	$N_{cr,LG}$	$\bar{\lambda}$	Φ	χ
(mm)	(MPa)	(N)	(-)	(-)	(-)
2000	70	61611,00	3,808	8,887	0,0591
4000	70	23187,60	6,206	21,751	0,0235
6000	70	11709,17	8,734	41,529	0,0122
8000	70	6936,97	11,347	68,695	0,0073

Table F-32: Nondimensional slenderness and buckling reduction factors for heat strengthened glass (case B).

3D models- Case B - G = 10 MPa					
Length model	Charact. bending strength	Critical buckling load	Nondim. slenderness	Buckling parameter	Buckling reduction factor
L_b	$f_{b,k}$	$N_{cr,LG}$	$\bar{\lambda}$	Φ	χ
(mm)	(MPa)	(N)	(-)	(-)	(-)
2000	70	106599,21	2,895	5,504	0,0982
4000	70	28970,61	5,553	17,674	0,0290
6000	70	13093,10	8,259	37,329	0,0136
8000	70	7408,89	10,980	64,464	0,0078

Table F-33: Nondimensional slenderness and buckling reduction factors for heat strengthened glass (case C).

3D models- Case C - G = 0,01 MPa					
Length model	Charact. bending strength	Critical buckling load	Nondim. slenderness	Buckling parameter	Buckling reduction factor
L_b	$f_{b,k}$	$N_{cr,LG}$	$\bar{\lambda}$	Φ	χ
(mm)	(MPa)	(N)	(-)	(-)	(-)
2000	70	40242,88	5,067	14,923	0,0345
4000	70	10639,15	9,855	52,342	0,0096
6000	70	5139,18	14,179	105,842	0,0047
8000	70	3194,75	17,983	168,374	0,0030

Table F-34: Nondimensional slenderness and buckling reduction factors for heat strengthened glass (case C).

3D models- Case C - G = 0,1 MPa					
Length model	Charact. bending strength	Critical buckling load	Nondim. slenderness	Buckling parameter	Buckling reduction factor
L_b	$f_{b,k}$	$N_{cr,LG}$	$\bar{\lambda}$	Φ	χ
(mm)	(MPa)	(N)	(-)	(-)	(-)
2000	70	46968,91	4,690	12,951	0,0400
4000	70	16369,57	7,945	34,666	0,0146
6000	70	9700,73	10,320	57,204	0,0088
8000	70	6699,56	12,418	81,805	0,0061

Table F-35: Nondimensional slenderness and buckling reduction factors for heat strengthened glass (case C).

3D models- Case C - G = 1 MPa					
Length model L_b	Charact. bending strength $f_{b,k}$	Critical buckling load $N_{cr,LG}$	Nondim. slenderness $\bar{\lambda}$	Buckling parameter Φ	Buckling reduction factor χ
(mm)	(MPa)	(N)	(-)	(-)	(-)
2000	70	90748,58	3,374	7,177	0,0740
4000	70	34789,22	5,450	17,071	0,0301
6000	70	17807,98	7,617	32,001	0,0159
8000	70	10621,51	9,863	52,425	0,0096

Table F-36: Nondimensional slenderness and buckling reduction factors for heat strengthened glass (case C).

3D models- Case C - G = 10 MPa					
Length model L_b	Charact. bending strength $f_{b,k}$	Critical buckling load $N_{cr,LG}$	Nondim. slenderness $\bar{\lambda}$	Buckling parameter Φ	Buckling reduction factor χ
(mm)	(MPa)	(N)	(-)	(-)	(-)
2000	70	162354,04	2,523	4,364	0,1262
4000	70	44633,34	4,811	13,569	0,0381
6000	70	20223,19	7,148	28,369	0,0179
8000	70	11454,15	9,498	48,760	0,0104